

DECLARATION

u
EVALUATION OF GEOLOGICAL
SUITABILITY OF KISERIAN
DAM SITE, KAJIADO)

BY

DOUGLAS MUTHAURA ABUURU

THIS THESIS HAS BEEN ACCEPTED FOR
THE DEGREE OF M.Sc (1989)
AND A COPY MAY BE PLACED IN THE
UNIVERSITY LIBRARY.

*A thesis submitted to the Department of Geology
in partial fulfillment of the requirements
for the degree of Master of
Science (Geology).*

[University of Nairobi]
1989

DECLARATION

This thesis is my original work and has not been presented for a degree in any other University.

Abuuru

.....
D.M. ABUURU

This thesis has been submitted for examination with our approval as University Supervisors.

B.A. Okech

.....
Dr. B.A. OKECH
Dept. of Geology
University of Nairobi.

E.W. Dindi

.....
E.W. DINDI
Dept. of Geology
University of Nairobi.



Plate 1. Panoramic view of the Ngong hills from the left abutment of the dam site facing NW. The dam-axis is shown by the dashed line.

ABSTRACT

This thesis presents the results of geological investigations carried out at the Kiserian dam site, Kajiado district. The study was undertaken with the aim of obtaining information that could help in the design and construction of the proposed dam. The main parameters to be determined were, the structure, lithostratigraphical sequence, hydrogeological conditions and the depth to the bedrock.

Field investigations were conducted by way of an integrated approach. The methods used included photo-interpretation, geological mapping, seismic refraction, electrical sounding, electrical profiling and core-logging.

The dam site is underlain by the Ngong Basalts. Seismic refraction results suggest a highly irregular bedrock surface. There is a substantial variation in velocity within the overburden as well as in the sound rock. These variations are explained in terms of fracturing and weathering of the rocks. Geoelectrical sections revealed a low resistive zone below the foundation bed. This is attributed to a weathered zone. Core-logs show that the overburden materials are underlain by fresh basalts, weathered basalts, agglomeratic zone and residual soils resulting from weathering.

The seismic and resistivity results allowed interpolation of the bedrock surface between drill holes with much more confidence than would otherwise have been possible. On the basis of the results obtained, it is recommended that the overburden be excavated to depths of 1.5 m to 2 m. Grout cap should be used to seal off the fractures. This will strengthen the fractured foundation. A deep cut-off or grout curtain is recommended at the heel of the dam to provide a better anchorage which will increase resistance to sliding.

ACKNOWLEDGEMENTS

I wish to thank the Deans Committee for awarding me a University of Nairobi scholarship for the academic year 1986/87 to study the Master of Science degree course at the University of Nairobi.

It is my pleasure to acknowledge my gratitude to my research supervisors, Dr. B. A Okech and Mr. E. W. Dindi of the Department of Geology. Their untiring encouragement and friendly guidance in the ways of research made the work a rare academic and practical experience. I sincerely thank the Chairman of the Department of Geology, Prof. I.O.Nyambok, Dr.S. J. Gaciri, Dr J. Anyumba and other members of staff for their assistance and the facilities accorded to me in the department.

Acknowledgements go to the Ministry of Water Development (M.O.W.D) for according me varied support and availing the terrameter used in this project. I would also like to express my appreciation to the staff of M.O.W.D for their co-operation and generous assistance. To Mr. Trojanow, Head of Conservation Division, Mr. Thienpoint, Mr. Obath and their colleagues. Similar acknowledgements go to Mr. Mwai, Chief Geologist; Mr. Majanga, Mr. Kinya, Mr. Karanga and Mr. Ituli. Thanks go to the drilling crew from the Materials Branch for their assistance in transport and personnel during the field work.

I am grateful for the advice and encouragement from Prof. Dr. Wohlenberg. I am equally indebted to fellow post-graduate colleagues for their company and encouragement. I acknowledge Mr. Macharia, Mr. Kimani and Susan for typing the thesis using word processing and Mr. Keza for cartographically retracing the figures. Lastly, I appreciate the understanding and encouragement from relatives and friends; and especially my parents for their unflagging patience and support.

CONTENTS

	Page
ABSTRACT	iv
ACKNOWLEDGEMENTS	v
CHAPTER 1	<u>INTRODUCTION</u>
1.1	General Introduction
1.2	Location of the area
1.3	Physiography
1.4	Statement of the problem
<p><i>Dams must stand. Not all of them do, and there are all degrees of uncertainty about them. Reservoirs must hold water. Not all of them do, and there are many ways by which water may be lost. The work must be done safely as a construction job. Not all of them are, and there are many sources of danger. The whole structure must be permanent and the work has a right to be done within the original estimates. Not all of them are, and there are many reasons for their failure or excess cost. Most of them are geologic or geologic dependence.</i></p>	
2.1	Geological History
2.2	By Charles P. Berkey (1929).
CHAPTER 3	<u>THEORY OF GEOPHYSICAL METHODS</u>
3.1	Introduction
3.2	Seismic Refraction
3.3	Resistivity
CHAPTER 4	<u>FIELD WORK</u>
4.1	General Organization
4.2	Refraction Measurements
4.2.1	Equipment
4.2.2	Field Measurements
4.2.3	Limitations and Data Quality
4.3	Resistivity Measurements
4.3.1	Equipment
4.3.2	Field Measurements
4.3.3	Limitations and Data Quality
4.4	Geological Correlating

		<u>CONTENTS</u>	Page
CHAPTER 5	<u>INTERPRETATION OF GEOPHYSICAL DATA</u>		48
5.1	Seismic Refraction		48
5.1.1	ABSTRACT		iv
5.1.2	ACKNOWLEDGEMENTS		v
CHAPTER 1	<u>INTRODUCTION</u>		1
1.1	General Introduction		1
1.2	Location of the area		3
1.3	Physiography		3
1.4	Statement of the problem		9
1.5	Objectives		11
1.6	Methodology		11
5.2	Limitations in the VES curves		
CHAPTER 2	<u>GEOLOGY</u>		13
2.1	Introduction		13
2.2	Rock formations		14
2.3	Geological structures & Seismicity		18
2.4	Geological History		20
2.5	Hydrogeology		22
CHAPTER 3	<u>THEORY OF GEOPHYSICAL METHODS</u>		25
3.1	Introduction		25
3.2	Seismic Refraction		25
3.3	Resistivity		30
CHAPTER 4	<u>FIELD WORK</u>		35
4.1	General Organization		35
4.2	Refraction Measurements		35
4.2.1	Equipment		35
4.2.2	Field Measurements		37
4.2.3	Limitations and Data Quality		40
4.3	Resistivity Measurements		42
4.3.1	Equipment		35
4.3.2	Field Measurements		43
4.3.3	Limitations and Data Quality		44
4.4	Geological Core-logging		45

CHAPTER 5	<u>INTERPRETATION OF GEOPHYSICAL DATA</u>	48
5.1	Seismic Refraction	48
5.1.1	Method of Interpretation	48
5.1.2	Limitations in the Seismic Refraction Data Interpretation	55
5.1.3	Results of Interpretations	56
5.2	Resistivity	57
5.2.1	Method of Interpretation	57
APPEND 5.2.1.1	Visual Interpretation	58
5.2.1.2	Master Curves	60
5.2.1.3	Computer Modelling	61
5.2.2	Limitations in the VES curves Interpretation	62
5.2.3	Results of Interpretation	64
5.2.3.1	VES Data	64
APPEND 5.2.3.2	Profiling Data	65
5.1	Geometrical constants (K) for	
CHAPTER 6	<u>GEOLOGICAL INTERPRETATIONS OF THE RESULTS</u>	68
6.1	Seismic Refraction	68
6.2	Vertical Electrical Sounding	71
6.2.1	River Course	72
6.2.2	Spillway	74
6.2.3	Dam-axis	76
APPEND 6.3	Core logs	78
6.3.1	River course	79
6.3.2	Spillway	81
APPEND 6.3.3	Dam-axis	83
6.4	Correlation of Geoelectrical and Geological Sections	83
6.5	Discussions of Results	87
CHAPTER 7	<u>EVALUATION OF THE DAM SITE IN TERMS OF GEOLOGY</u>	93

CHAPTER 8	<u>CONCLUSION AND RECOMMENDATIONS</u>	98
8.1	Conclusions	98
8.2	Recommendations	99
	<u>REFERENCES</u>	100
	<u>APPENDICES</u>	104
APPENDICES A	<u>SEISMIC REFRACTION</u>	
A.1	The Plus-Minus method of seismic refraction data interpretation. (A&B)	27
A.2	Seismic refraction data. (N&N)	31
A.3	Interpreted seismic refraction depth section along BH1 profile.	36
APPENDICES B	<u>RESISTIVITY</u>	
B.1	Geometrical constants (k) for schlumberger array.	42
B.2	Horizontal Profiling data.	52
B.3	Field data and curve for VES S7.	54
B.4	Computer model and curve for VES S7.	58
B.5	Computer model and curve for VES S15.	68
APPENDIX C	<u>GEO-HYDRAULICS</u>	
C	Packer (Pump-in) tests data.	87
APPENDIX D	<u>WEATHERING GRADES</u>	
D	Weathering Grades.	89
	Interpreted geoelectrical cross-section along the river course profile	97
	Interpreted geoelectrical cross-section across the spillway profile	75

FIGURES

1.1	Map showing Location of the study area	4
1.2	Dam site plan	7
2.1	Geological map of the Kiserian area	16
2.2	Seismic Zoning map of Kenya	19
3.1	Raypaths and Time-distance curve for two layers separated by Horizontal interface	26
3.2	Ray paths and travel-time curves for an inclined interface	27
3.3	Arrangement of current electrodes (A&B) and potential electrodes (M&N)	31
4.1	Pocket-seis Engineering Seismograph	36
4.2	Dam site plan showing seismic refraction and resistivity profiles along the boreholes	38
4.3	SAS 300 Terrameter controls and terminals	42
5.1	Time-distance graph of reversed seismic data spread A-B and the time-depths	52
5.2	Types of apparent resistivity curves at Kiserian Dam site	58
5.3	Resistivity profile across the dam-axis Separation $a=4$ m and $a=10$ m	66
5.4	Resistivity profile across the dam-axis separation $a=25$ m and $a=40$ m	67
6.1	Interpreted seismic refraction depth-section along the river course profile	69
6.2	Interpreted seismic refraction depth-section along the dam-axis	70
6.3	Interpreted geoelectrical cross-section along the river course profile	73
6.4	Interpreted geoelectrical cross-section across the spillway profile	75

6.5	Interpreted geoelectrical cross-section across the dam-axis	77
6.6	Geological cross-section along the river course	80
6.7	Geological cross-section along the Spillway	82
6.8	Geological cross-section along the dam-axis	84
6.9	Comparison between lithostratigraphical column and interpreted resistivity curve (D5) next to BH3	85

PLATES

1	Panoramic view of the Ngong Hills from the dam-site facing NW.....	iii
1.1	Panoramic view of the Ngong Hills from the Pipeline road facing NW	5
1.2	Panoramic view of the plateau covering the southern section of the Kiserian area	6
1.3	Photograph of the dam-site taken near BH2 facing upstream	8
1.4	Photograph of the dam-site taken from BH5 facing north	9
2.1	The Ngong Basalts exposed along a road cutting on the hill slopes	15
2.2	Agglomerates exposed on the sides of an old murram pit	17
4.1	Core-drilling in progress at BH2	47

CHAPTER 1

xii

TABLES

5.1	Layer parameters of VES data at S7, from curve matching and computer Interpretation.	64
6.1	Layer parameters of the model obtained for sounding S15.	86
6.2	Summary of the core-logging, seismic refraction and resistivity sounding results.	88
6.3	Summary of the first geoelectrical layer depths and top soil depths obtained from core-logs of the 9 test-boreholes.	90

CHAPTER 1

INTRODUCTION

1.1 General Introduction

The development of an area is to a large extent hinged on the existence of reliable sources of water preferably in close proximity. Water is required for among other uses, industrial, agricultural, construction and domestic uses. It is therefore inevitable that the development of an area should go hand in hand with the development of its water resources. Measures to ensure adequate water supply include development of aquifers, conservation of rain water through roof catchment and construction of dams; and conservation of catchment areas through implementation of afforestation programs and strict land use management.

The Government of Kenya embarked on programs aimed at conserving water after the creation of the Ministry of Water Development (M.O.W.D). Since then, several water conservation projects have been successfully completed throughout the republic. Several other such projects are in the implementation stages while others are planned for future implementation. The present project falls within the latter category. It is estimated that through development of aquifers and intensification of water conservation measures Kenya should be self sufficient in water by the year 2000.

The present study was conducted on a water conservation project planned for the Kiserian area of Kajiado District.

The area is dry and hence its groundwater potential is very low. It is however known that the Ngong Hills which constitute its catchment have an unusually high precipitation for most part of the year. The area receives an average rainfall of 790 mm per annum. The task has been therefore, to find a suitable site within the area where the runoff from the Ngong Hills can be dammed and eventually used for the purposes mentioned earlier. A possible site had been located before the onset of this study.

The dam site is situated in Kiserian area of Kajjado District. It lies some 2 Km to the SE of Kiserian market. The Selection of the possible site was done purely on the basis of topographical considerations. The M.O.W.D surveyors did the surface survey. Essential information such as location of dam-axis, spillway, extent of the embankment and location of test-boreholes were then incorporated on the topographical contour map, (Fig 1.2 and 4.2)

Since the identification of the site had been based purely on topographical considerations, further site investigations were necessary to gain knowledge on the nature of the subsurface. These further investigations were to be two-fold. One aspect was to involve the study of the engineering properties of the subsurface rocks, while the other entailed a study of the subsurface geology. Test boring and investigations into the engineering properties was done by the staff of the Ministry of Transport and communication, (MOTC). At that time, the task of looking into the geology of the subsurface had not been assigned to any person or group. Since the author had an interest in this aspect of dam site investigation, he offered to conduct the study. Both the MOWD and MOTC offered to assist the author with logistics.

The main objective of the geological and geophysical investigations were to determine the lithological and structural set-up of the subsurface.

The information was then to be used to make recommendations on the suitability of the site. Apart from contributing towards the success of the conservation project, the study by the author was also to constitute part of his studies at the University of Nairobi.

1.2 Location of the Area

The Kiserian dam site is situated in Kiserian area of Kajiado District. It lies some 2 Km to the SE of Kiserian market. The area of study is however not restricted to the dam site but extends to cover the catchment area of the dam, (Fig 1.2). The area of study is therefore bound by latitudes $1^{\circ}26'S$ and $1^{\circ}30'S$ and longitudes $36^{\circ}38'E$ and $36^{\circ}42'E$. This covers an area of about 60 Km^2 and lies within Ngong sheet (148/3) of the survey of Kenya.

The area is well served by roads and tracks most of which are passable even during the heavy rain season. The Nairobi-Magadi road which traverses the area in a NE-SW direction is the principal line of communication. A complimentary road joins Kiserian market and Ngong town which lies to the North of the area. A loose surface road commonly known as the 'Pipeline Road' located to the south of Kiserian market connects the area to Kajiado town. The road passes within 2 Km of the dam site.

1.3 Physiography

The Kiserian area lies at an altitude of about 1800 m above sea level. This high altitude contributes to its relatively fine climate. The area forms part of the eastern flank of the Rift Valley. Closest to the rift, are the Ngong Hills (Fig.1.2) which constitute the main catchment for the area.

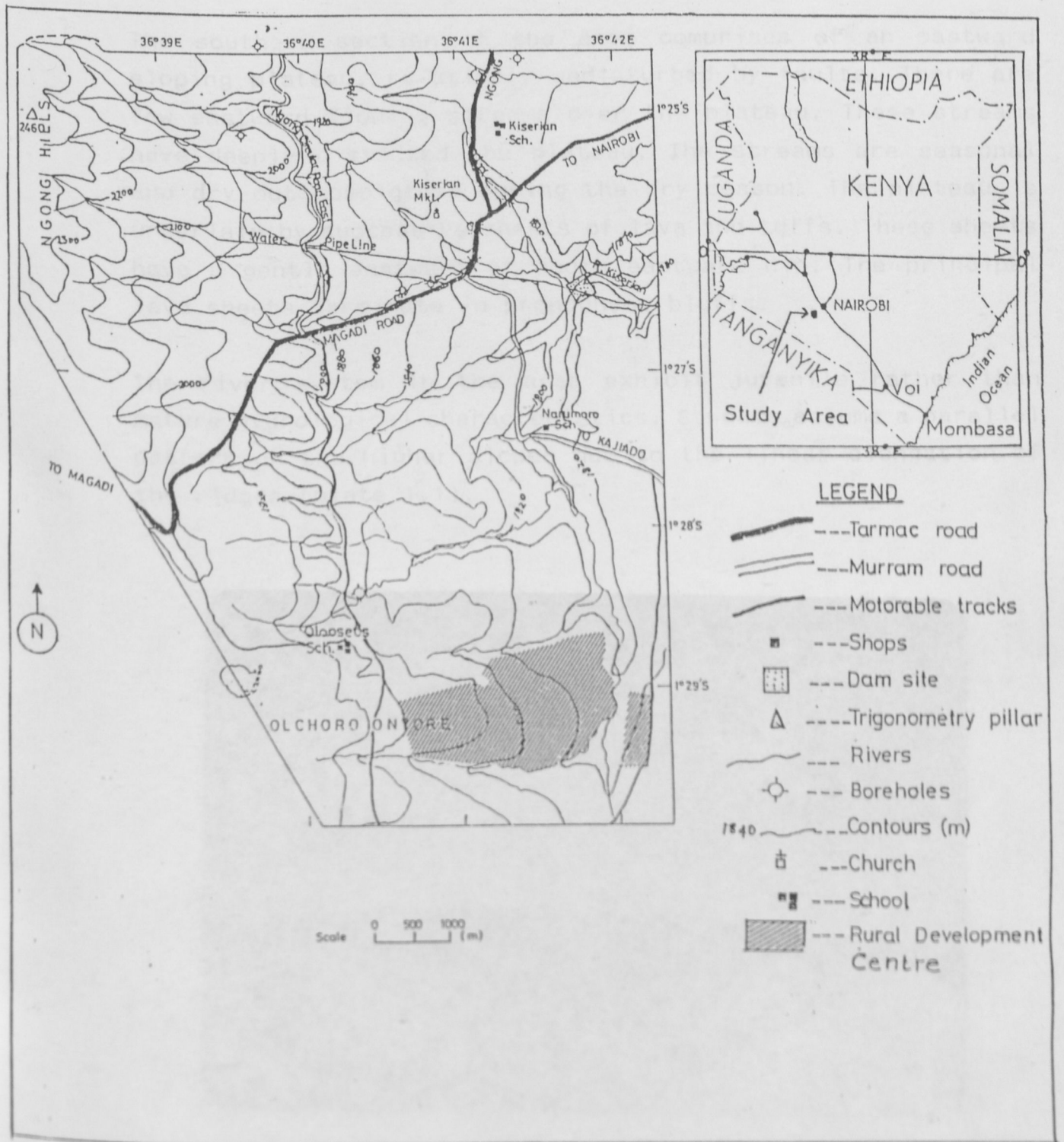


Fig. 1.1 MAP SHOWING LOCATION OF THE STUDY AREA

The southern section of the area comprises of an eastward sloping plateau, relatively undisturbed by faults. There are few eastward flowing streams over the plateau. These streams have deeply dissected the plateau. The streams are seasonal and dry out completely during the dry season. The plateau is underlain by successive sheets of lava and tuffs. These sheets have a gentle eastward or south eastward dip. The principal lava sheets terminate in pronounced bluffs.

The river system in the area exhibit juvenile rather than mature hydrological characteristics. Streams assume a parallel pattern on the higher slopes due to the linear elongation of the ridges (plate 1.1).



Plate 1.1 Panoramic View of the Ngong Hills from the Pipeline road facing NW. Note the rugged slopes which are dissected by east flowing streams.

One set of streams converge to form the tributary which flows southward to the main confluence, (Fig 1.2).

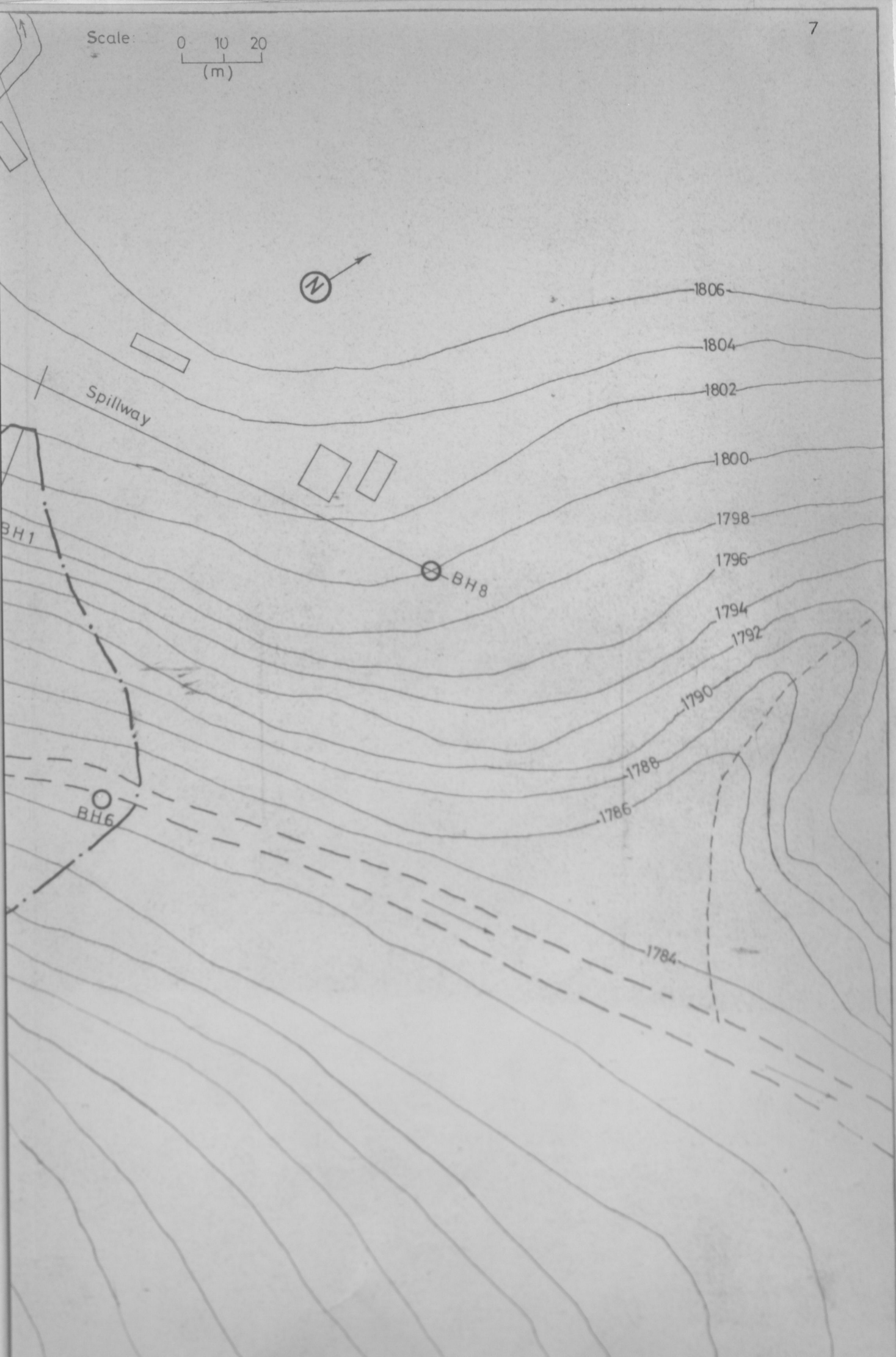
A tributary from Olchoro Onyore flows in a NNE-SSW direction and collects waters from the east flowing streams emanating from the relatively flat plateau, (Plate 1.2). The two tributaries converge just before the dam site to form the Kiserian river. The Kiserian river then flows in a W-E direction across a ridge. The gorge cut by the river in this ridge constitutes the dam site.



Plate 1.2 Panoramic view of the plateau covering the southern section of Kiserian area. Note the gentle slope of the plateau from the southern end of the Ngong Hills. The stream flowing in NNE-SSW direction is shown with arrows.

The dam site consists of a cut in valley, 150 m wide, with scarps 18 m high, (Plate 1.3). The valley is flat at the bottom, but rises gently towards the upland. West of the confluence is a vertical cliff 8 m high trending in a N-S direction, (Fig 1.3).

Scale: 0 10 20 (m)



Another cliff having a similar trend occurs some 700 m south of the confluence, and extends southward for another 300 m.



Plate 1.3

Photograph of the dam site taken near BH2, facing upstream. Note the napier grass along the stream course which deviates to the right to follow north bound tributary at the confluence (marked with an arrow). The slopes on both sides of the valley constitute the abutments.

The Southern part of the dam site is hilly and rugged, and reaches an elevation of 80 m above the level of the valley. The ridge continues north of the dam site. In this section it attains an average of 100 m above the valley. It extends northwards past the Nairobi-Kiserian road, (plate 1.4).



Plate 1.4 Photograph of the dam site taken from BH5 facing north. The dam-axis is indicated with the dashed line. Note the exposed boulderly basalts covering the right abutment. The ridge rises to 100 m above the elevation of the valley at the far horizon next to Nairobi-Kiserian road.

1.4 Statement of the Problem

The development of the Kenya Rift Valley was accompanied by faulting, tectonic movements and volcanicity. These events affected both the floor and shoulders of the Rift. The shoulders were therefore affected by faulting, fracturing and eventual intense weathering along the fault zones and fractures.

The Kiserian area shows these characteristics. Since these can be detrimental to a dam, the area should be evaluated to formulate a general model of the geology at the site. It is also essential to identify any potential problems to aid in the design and construction of the dam. Location of faults also need to be identified.

Varying series of lava flows emerged from different episodes of volcanicity. As a result, the layered sequence is accordingly varied. It is therefore essential to determine the type of layering and identify location of the bedrock; which if used will ensure a stable foundation. Joints and fractures which occurred during the cooling and crystallization of lava are often pervious. These need to be investigated to ascertain their water tightness by determining the uniformity of the foundation and the abutments.

Decomposition and disintegration is reported to have preceded the deposition of succeeding lavas, (Sikes, 1939). Such zones if present below the foundation can induce substantial displacement leading to weakening of the foundation. Their presence should be investigated and remedies be undertaken. Subsurface weathering has reduced some lavas to clay. Since the effect is gradational, it has resulted in varying thickness of the overburden. There is need therefore to determine depth to the bedrock at several points to obtain some average working value.

It is well known that if a dam foundation is located above the water table and the rocks are pervious, impounded water may leak to the lower levels. It is therefore important to determine the position and depth of any groundwater bodies and to assess the suitability of the site from this point of view.

1.5 Objectives:

The aims of the present project were:-

- (i) To establish the rock formations in the area and look into their state of weathering at the dam site.
- (ii) To establish the stratigraphical sequence at the dam site.
- (iii) To locate and map faults and joints occurring in the vicinity of the dam site.
- (iv) To determine the thickness of the overburden and map all the weathered zones.
- (v) To delineate an aquifer if any, below the dam site.
- (vi) To use the information gained from the study to assess the suitability of the site and make recommendations on any special remedial measure to be undertaken to enhance the suitability of the site.

1.6 Methodology

Several methods were used in this study. These include photo-interpretation, reconnaissance geological mapping, geophysical investigations and core-boring. A brief outline of the applications of these methods follows:

Photo-interpretation involves studying of aerial photographs and landsat imagery to obtain the major and minor linearments in the project area. These are also useful for delineating the various geological formations.

Geological mapping in dam site investigations involves examination of outcrops and structural features in the project area. Boundaries of geological formations are delineated and presence of any deleterious minerals or zones noted. Results are presented in form of geological maps and sections.

Geophysical methods are useful in dam site investigations mainly to obtain information on lithology of the underlying strata and its structural features. Seismic refraction and resistivity have been known to be the most effective. Seismic refraction yields data on seismic velocities, geometry of the various formations and depth to the bedrock. Structures such as faults are easily recognized from refraction depth sections. The resistivity method in addition to determining the depth to the bedrock can also isolate the weathered layers. This is done on the basis of resistivities. Thickness of layers are easily determined and weathered layers at depth easily identified.

Core drilling is normally conducted to obtain cores which are tested for different geotechnical properties. Geological logging of the cores provide information on the stratification at the site. Since core drilling is expensive and time consuming the usual practice is to use the least possible number of test-boreholes.

The use of the various methods is generally dictated by the effectiveness in the field area to be investigated, as well as the cost and time. Where conditions permit an integrated approach is usually recommended as it offers a means of checking the interpretations. Geophysical methods have the advantage of being cheap and fast in subsurface investigations. Since they can best establish continuity from point to point at the site, they are widely used. It is however important to note that they also have limitations. They can therefore, only complement but not substitute geological mapping and core-drilling. In this study all the methods mentioned above were used. The study was therefore an integrated one.

CHAPTER 2

GEOLOGY

2.1 Introduction:

The only detailed geological works covering the present area of study are those by Saggerson, (1961-67). Unfortunately, his works have so far not been compiled into a report. Only the geological map exists and is at a scale of 1:125,000. Other works touching on the area are of regional significance so that their coverage of the area is rather sketchy. Among these, are works by Gregory(1921), Sikes (1926, 1934,1939), Fairburn (1963), Geaverts (1964), Hunter (1965), Matheson (1966), and Loupekine (1971).

In view of the above limitations, an authoritative description of the rock types and structures in the Kiserian area is lacking. Since such detailed descriptive information was required for this project, it became necessary for the author to carry out spot checks in the area. Identification of structures and description of rocks was done prior to the geophysical investigations. Further investigations into the rock types and structures was done during the test-drilling phase. The review of the geology given here, therefore includes information from existing reports as well as contributions from the author. In order to emphasize on information relevant to the present project, the review is treated under four sub-headings. These are rock formations, tectonic structures and seismicity, geological history and hydrogeology.

2.2 Rock Formations

The study area is underlain by two main rock types. These are designated as the Ngong Basalts and the Ol Doinyo Narok Agglomerates by Sikes, (1939). The Ngong Basalts comprise of basic lavas, tuffs and agglomerates. The Doinyan Agglomerates are coarse rocks containing lava blocks which vary considerably in size and composition. The lava fragments include coarse to fine grained phonolites and trachytes from the older rocks, which distinguish Ol Doinyo Narok Agglomerates from other agglomerates and tuffs associated with later volcanicity. The sequences have been affected by post-deposition tilting so that the original dip is not readily visible. Observations made in deep gorges however show that the dip is towards the east.

The Ngong Basalts cover the dam site and most of the North and North Western parts of the area. Exposures are however rare as the basalts are usually overlain by a thin layer of soil. Good exposures can be found in gorges, hilltops and along road cuttings. The rock is usually highly fractured and in places occurs as highly fragmented boulders. Fresh basalts are bluish-black, dense and invariably porphyritic. The phenocrysts vary in quantity and size but are mainly of augites. On weathering, the basalts assume dark to yellow brown colouration, (Plate 2.1). In the extremely weathered cases, the basalts have been reduced to residual soils.

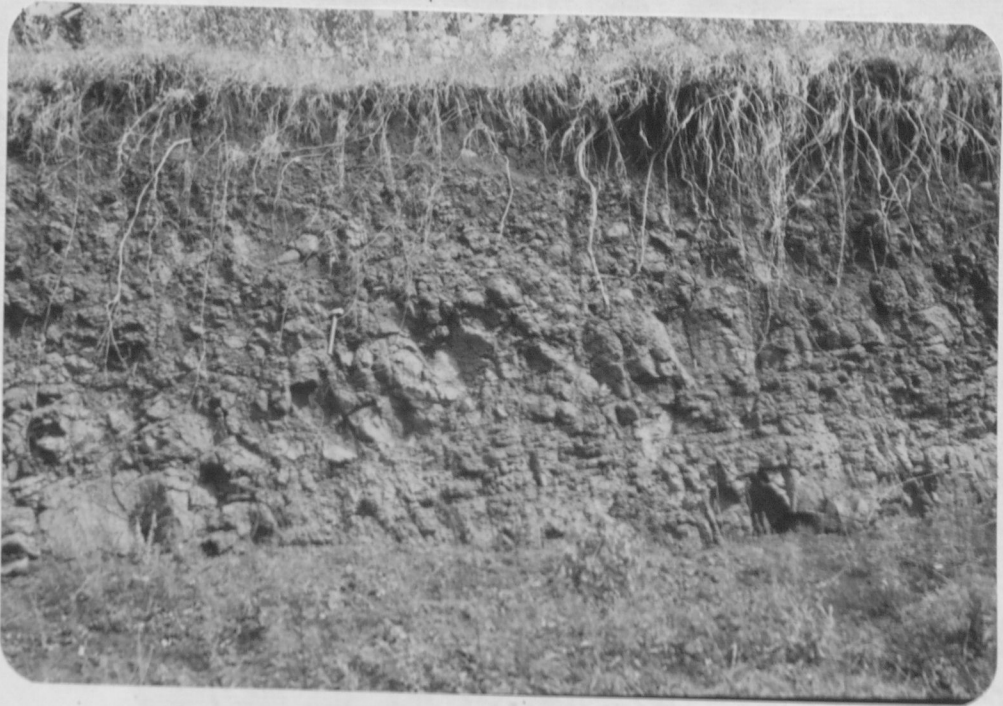


Plate 2.1 The Ngong Basalts exposed along a road cutting on the hill slopes. Weathered basalts are in contact with the red top soils. Note the blue-black fresh basalt patches on the middle-right hand side of the photograph.

The Southern part of the area is underlain by agglomerates referred to as the Ol-Doinyo Narok agglomerates. These underlie the basalts. The Agglomerates are generally light coloured, tending to greyish with shades of yellowish brown, (Plate 2.2). Rock fragments of varied origin can be identified in the agglomerates. These include phonolites, phonolitic trachytes and obsidian debris. The fragments are contained within a tuffaceous matrix. The Agglomerates become more tuffaceous northwards grading into tuffs at Naru Moro school, (fig 2.1). Unlike the Basalts, the Agglomerates rarely show fracturing. On weathering they assume grey-yellowish or dark colouration.

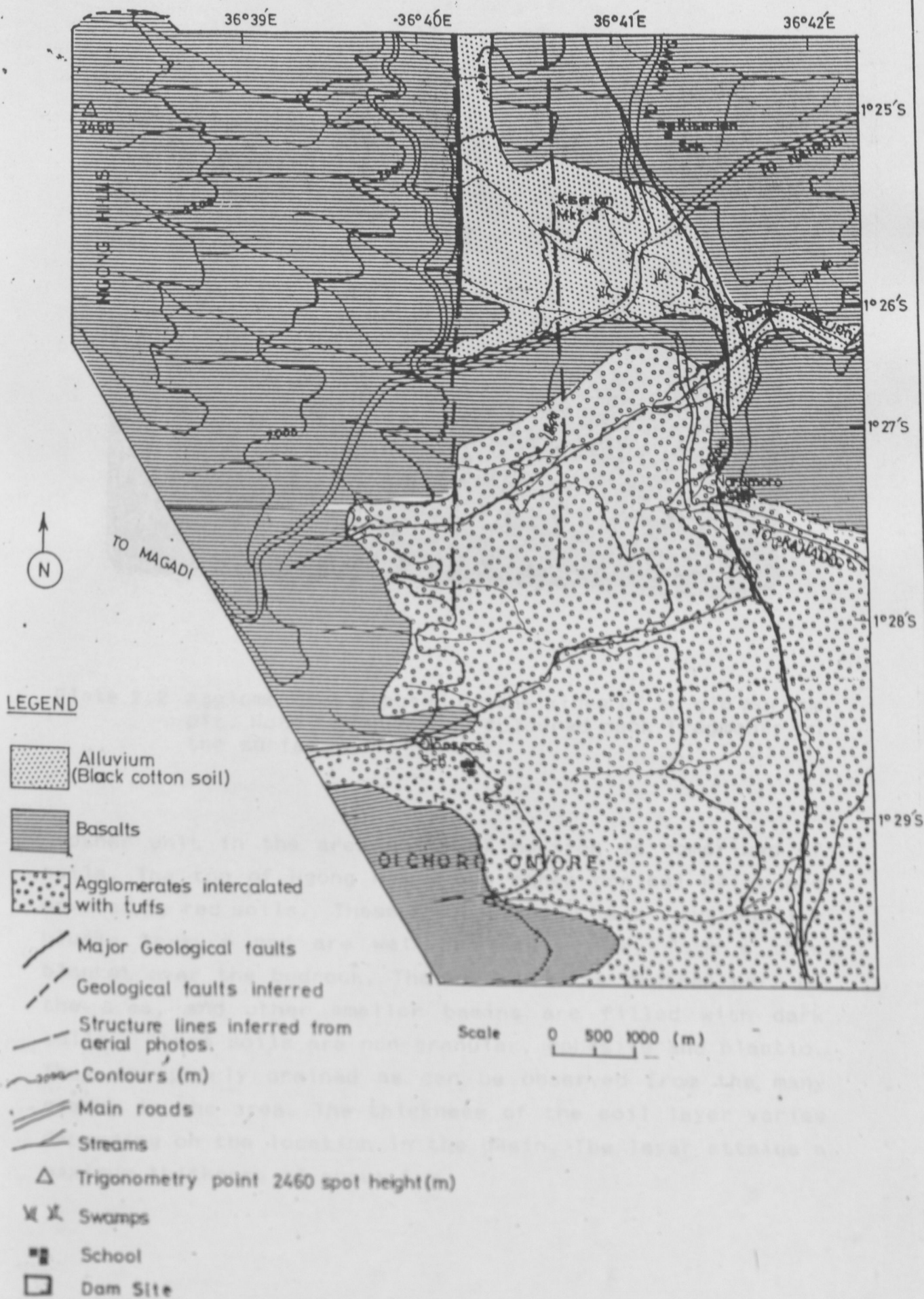


Fig. 2.1 GEOLOGICAL MAP OF KISERIAN AREA



Plate 2.2 Agglomerates exposed on the sides of an old murram pit. Note the numerous coloured rock fragments on the surface.

Another unit in the area worth of mention is comprised of soils. The top of Ngong Hills and other conical hills are covered by red soils. These soils usually have a sub-angular blocky texture and are well drained. They form a thin blanket over the bedrock. The basin in the central part of the area, and other smaller basins are filled with dark soils. These soils are non-granular, cohesive and plastic. They are poorly drained as can be observed from the many swamps in the area. The thickness of the soil layer varies depending on the location in the basin. The layer attains a maximum thickness of about 5 m.

2.3 Geological Structures and Seismicity:

Location of the Kiserian area on the flank of the Rift Valley made it prone to the subsequent movements during the formation of the Rift Valley. The geological structures found in the area are therefore a result of the rift movements and volcanism. Structures encountered are mainly faults having a north-south trend. Evidence for existence of faults is abundant but mostly indirect. This is in the form of linear cliffs oriented in the same direction, rectilinear alignment of stream segments, sharp contacts between basalts and agglomerates, well defined tonal variations on aerial photographs and marked linear trends on satellite imageries. Figure 2.1 shows the four major faults and transverse structural lineaments in the area. Although other minor faults exist, they are considered insignificant and have therefore been omitted from the map.

Evidence for joints also exist. The drainage on the slopes of the Ngong Hills is subparallel and is characteristic of volcanic areas. Numerous parallel gullies formed by incision into the slopes occur. The incisions seem to have followed lines of least resistance caused by tectonic dislocations such as fractures and joints.

The seismicity of the area is related to contemporary earth movements within the Rift Valley. Generally the movements in the area are slight and infrequent. Loupekine (1971) used the only existing catalogue of felt earthquakes to produce a seismic zoning map of Kenya. The map, Fig. 2.2 shows the maximum expected intensities of future earthquakes. The Kiserian area is listed in the range VIII-IX, (modified Mercalli scale). The possible damage on a dam or a reservoir within this scale would range from slight to considerable depending on its design.

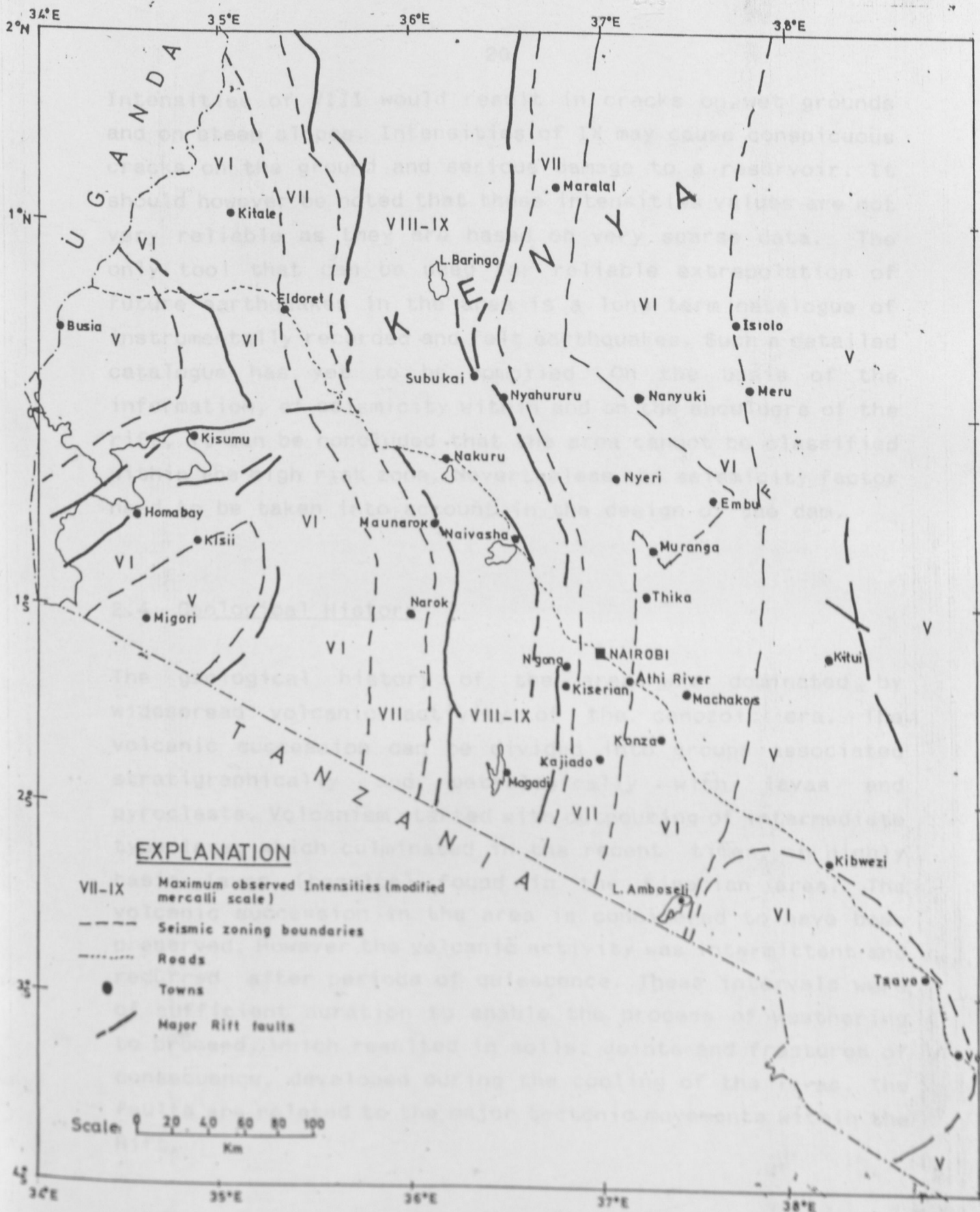


Fig. 2.2 Seismic zoning map of Kenya showing maximum observed intensities, (1892-1969). After Loupekine (1971).

Intensities of VIII would result in cracks on wet grounds and on steep slopes. Intensities of IX may cause conspicuous cracks on the ground and serious damage to a reservoir. It should however be noted that these intensities values are not very reliable as they are based on very sparse data. The only tool that can be used for reliable extrapolation of future earthquakes in the area is a long term catalogue of instrumentally recorded and felt earthquakes. Such a detailed catalogue has yet to be compiled. On the basis of the information, of seismicity within and on the shoulders of the rift, it can be concluded that the area cannot be classified within the high risk zone. Nevertheless the seismicity factor need to be taken into account in the design of the dam.

The Kiserian Phonolites have been referred to as the basal phonolites. Most of these phonolites originated from N-S

2.4 Geological History

The geological history of the area was dominated by widespread volcanic activity of the cenozoic era. The volcanic succession can be divided into groups associated stratigraphically and petrologically with lavas and pyroclasts. Volcanism started with outpouring of intermediate type lava, which culminated in the recent times, in highly basic lavas (basalts) found in the Kiserian area. The volcanic succession in the area is considered to have been preserved. However the volcanic activity was intermittent and recurred after periods of quiescence. These intervals were of sufficient duration to enable the process of weathering to proceed, which resulted in soils. Joints and fractures of consequence, developed during the cooling of the lavas. The faults are related to the major tectonic movements within the Rift.

The outbreak of volcanic activity in the area began with discharge of the Kapiti Phonolites. These also cover other areas of Kenya. The chronology of the succession is rather conjectural. Nevertheless, the Kapiti Phonolites are known to be of tertiary age, (Matheson, 1966). They rest directly on the folded precambrian rocks.

5. Kapiti Phonolite

The next division to erupt was the Doinyan series. These seem to have been less fluid and hence tended to build mountains. The division includes flows of phonolites which terminated in phonolitic trachytes. These flows are generally more basic than the Kapiti Phonolite. The phonolites of this division designated the Doinyan phonolites, (Sikes, 1939) and the Kapitian Phonolites have been referred to as the basal phonolites. Most of these phonolites originated from N-S trending fissures. The phonolitic trachytes are represented in the Kiserian area by the so called the Mbagathi Phonolitic trachytes. These are occasionally vesicular and have a distinctive flow oriented feldspar laths within a grey-brown matrix. The Ol Doinyo Narok agglomerates were later deposited and overlie the phonolitic trachytes in the area. The Agglomerates are typical of volcanic tuffs and breccia of sub-aerial origin. These seem to overlap into the Ngong basic lavas (basalts) in the study area.

Characteristics

Later there were eruptions of basic lavas and associated pyroclastics. The eruption of this group discharged a varied series of lavas which consisted mainly of basalts, basanites and tephrites; and were more basic than the lower groups. The lower part of this group is represented in the area by the Ngong Basalts.

The sequence of volcanism can therefore be represented (starting from the youngest to the oldest) as follows.

1. Ngong Basalts
2. Ol Doinyo Narok Agglomerates
3. Mbagathi Phonolitic Trachytes
4. Ol Doinyo Phonolite
5. Kapiti Phonolite
6. Precambrian rocks

A detailed description of the succession at the dam site is given in chapter 6.

2.5 Hydrogeology

As was mentioned in chapter 1, the Ngong Hills constitute the main catchment for the present area. Most of the precipitated waters runoff in the eastward direction in conformity with the topographic gradient. The volcanics and soils on account of their porosity and degree of fracturing and jointing allow a substantial amount of water to infiltrate into them. Although a detailed investigation into the groundwater in the area has not been done, data from the few existing productive wells give some clue of the general characteristics.

The solid lava-rocks transmit water through anastomosing joints and fractures along fault planes and cracks, (Sikes, 1934). The tuffs and agglomerates being compact and without joints are usually too argillaceous to transmit water readily. In the Ngong basalt formation, the main aquifers are struck by deep boreholes which penetrate through the fresh fractured volcanics into the weathered zone. Large quantities of groundwater occur on, or below the old land surface of disintegrated weathered rocks.

It is observed from the data on water struck levels of the wells in the area, that the main aquifer in the central basin region is shallower than those sited on the slopes of the hilly ground. This tends to suggest that water accumulates in this zone before moving eastwards.

In the agglomerates, only one borehole data was available for use, (Fig 1.2). The aquifer was struck in a zone within the agglomerates where spheroidal weathering had resulted in a diversity of structures. Because of these structures agglomerates tended to be pervious at this zone. Elsewhere, compact tuffs and agglomerates are relatively retentive and inhibit the infiltration of water beyond the weathered zone.

The Ngong Basalt formation at the abutment showed a top soil cover of about 1 m. This thickens to about 3 m at the valley bottom. The dark soils at the site are soft and argillaceous so that they soak water but do not transmit it readily. Swampy conditions prevail during the rain season and ponds continue to retain water even after the stream has ceased flowing. At the dam site the soils are underlain by a weathered zone of the Ngong Basalts. The zone is highly fractured and invariably filled with soils. The presence of soils in the fractures tend to check any downward migration of the waters. The water struck levels obtained from the well data show that the main aquifer is at depths in excess of 40 m. The maximum depth drilled during the test-boring operation was 30 m. At this depth, there exists a highly weathered basalt zone containing no water.

Surface water infiltrating from the streams and held by clayey layer was at less than 3 m in BH3, BH6, and BH7. These boreholes are about 2 m from the stream.

On the whole it can be said that because of the fracturing and faulting the groundwater flow regime is fairly complicated. Since some of the faults in the area are likely to be deep, chances of striking reliable aquifers for large scale water supply are rather slim.

3.1 Introduction

The theory of the two geophysical methods used is well documented in several standard texts of geophysics. These include Dobrin (1976), Grant and West (1965), Keller et al (1962), Musgrave (1967), Parasnis (1979), Telford et al (1980) and Zohdy (1980). The purpose of this chapter is therefore not to give details of the theory but rather to outline and emphasize the various factors and conditions that tend to invalidate the theoretical assumptions. This approach has been considered necessary as the structural set up of the area of study is far from ideal. In order to appreciate the types of geophysical responses expected from non-ideal conditions an understanding of those from the ideal needs to be essential. It is in this context that a brief outline of the theory is presented.

3.2 Seismic Refraction

The seismic refraction method involves the timing of arrivals of artificially generated pulses of elastic energy propagated through the ground and picked by the geophones. It is assumed that the earth is layered and that the various layers are horizontally homogeneous. It is further assumed that the earth is a plane surface. Where the structure of the ground is close to these ideal conditions, and the layering is horizontal, values of the elastic wave velocity and the thickness of the various layers are easily determined. (Fig 3.1)

CHAPTER 3

THEORY OF THE GEOPHYSICAL METHODS

3.1 Introduction

The theory of the two geophysical methods used is well documented in several standard texts of geophysics. These include Dobrin (1976), Grant and West (1965), Keller et al (1982), Musgrave (1967), Parasnis (1979), Telford et al (1980) and Zohdy (1980). The purpose of this chapter is therefore not to give details of the theory but rather to outline and emphasize the various factors and conditions that tend to invalidate the theoretical assumptions. This approach has been considered necessary as the structural set up of the area of study is far from ideal. In order to appreciate the types of geophysical responses expected from non-ideal conditions an understanding of those from the ideal cases is essential. It is in this context that a brief outline of the theory is presented.

3.2 Seismic Refraction

The seismic refraction method involves the timing of artificially generated pulses of elastic energy propagated through the ground and picked by the geophones. It is assumed that the earth is layered and that the various layers are homogeneous. It is further assumed that the datum is a plane surface. Where the structure of the ground is close to these ideal conditions, and the layering is horizontal, values of the elastic wave velocity and the thicknesses of the various layers are easily determined, (Fig 3.1).

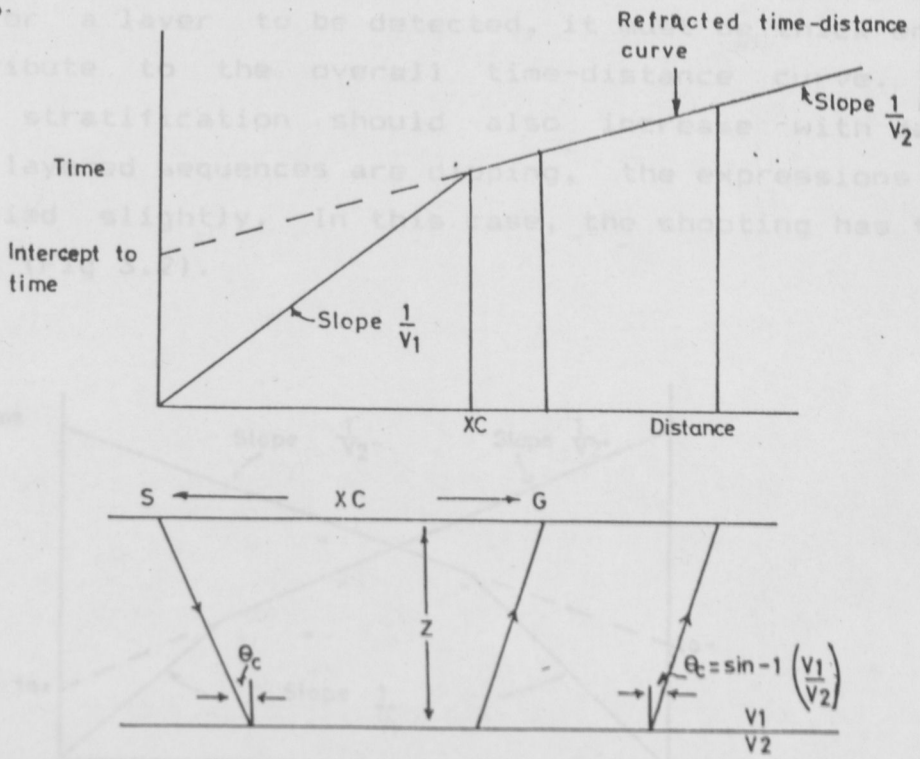


Fig 3.1 RAYPATHS AND TIME-DISTANCE CURVE FOR TWO LAYERS SEPARATED BY HORIZONTAL INTERFACE,

The velocities of the various layers are got from the slope of the time-distance graph, while the thicknesses are got from the intercept times. The general expression used is given as

$$t = \frac{x}{v_n} + \sum_l \left(\frac{2z_l \cos \theta_c}{v_l} \right) \dots\dots\dots 3.1$$

where $\theta_c = \sin^{-1} \frac{v_1}{v_n} \dots\dots\dots 3.2$

- t is the arrival time.
- x is the offset distance.
- θ_c is the critical angle of the refracted wave at the nth layer.
- z_l is the thickness of the ith layer.
- v_l is the velocity of the ith layer.
- v_n is the velocity of the deepest layer.
- v_1 is the velocity of the first layer.
- n is the number of layers.

The expression can be applied to any number of layers. However for a layer to be detected, it must be thick enough to contribute to the overall time-distance curve. The velocity stratification should also increase with depth. When the layered sequences are dipping, the expressions used are modified slightly. In this case, the shooting has to be reversed, (Fig 3.2).

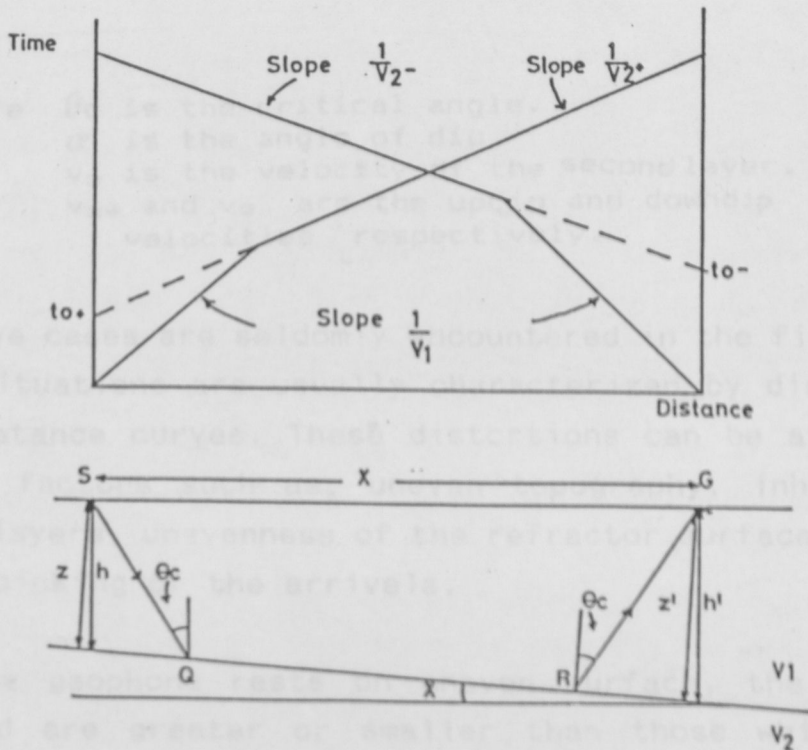


Fig 3.2 RAYPATHS AND TRAVELTIME CURVES FOR A INCLINED INTERFACE.

In the single refractor case, the velocity of the second layer will have to be computed from apparent velocities. The depths are again calculated from the intercept times.

The expressions used for a dipping refractor are:

$$\theta_c = \left[\sin^{-1} \frac{v_1}{v_{2+}} + \sin^{-1} \frac{v_2}{v_{2-}} \right] \dots\dots\dots 3.3$$

$$\alpha = \left[\sin^{-1} \frac{v_1}{v_{2+}} - \sin^{-1} \frac{v_2}{v_{2-}} \right] \dots\dots\dots 3.4$$

where θ_c is the critical angle.
 α is the angle of dip.
 v_2 is the velocity of the second layer.
 v_{2+} and v_{2-} are the updip and downdip velocities respectively.

The above cases are seldomly encountered in the field. Actual field situations are usually characterized by distortions of time-distance curves. These distortions can be attributed to various factors such as; uneven topography, inhomogeneities within layers, unevenness of the refractor surface, and errors in the picking of the arrivals.

When the geophone rests on uneven surface, the traveltimes obtained are greater or smaller than those which would be obtained if the surface was plane. This error has an effect not only on the intercept time but also on the calculated velocities of the refractor. In such cases, depth computations using the calculated velocities will also be in error. Elevation of the shotpoint and geophone positions should therefore be measured accurately for subsequent data reduction.

The effect of shooting along a sloping ground surface is analogous to that of a dipping refractor below a horizontal surface. In both cases the path length of rays in the upper medium varies with horizontal distance.

Unlike the dipping refractor case, the slope of the ground is known before shooting and corrections can be applied to the observed travel-times.

Even if the velocity increases with depth, not all velocity layers are recognizable as first breaks. This happens where there is a large velocity contrast between the refractor and an overlying thin layer. If second arrivals are recorded, then the headwave from the thin layer might be seen on the seismogram. When digital seismic timers are used, where the arrival of a single pulse of energy is all that is recorded, the hidden layer cannot be unveiled. The error due to the hidden bed makes the computed depth too shallow, as the overburden is assumed to be less than what it actually is, (Soskei, 1958).

It is usually assumed that each layer is thick enough to produce a separate branch of the travelttime curve. When the refractor is overlain by thin layers of no discrete velocities, they approximate to one group with a continuous velocity increase with depth. In such a case the overburden has velocity-depth relationship which is continuous. This results in a curved raypath of the upper medium.

If segments of the time-distance curves that are too short are used, errors in the determination of the slope of the straight line may be made. This error has an effect on the intercept time and in the calculation of the velocity of the refractor. The depth computed with such velocities will also be in error.

Incorrect picking of the inception of the energy at the geophone may occur at large offset distances. The possibility of this error occurring increases with offset distances.

The amplitude of the signal decreases and the higher frequency components attenuate more rapidly as the offset distance increases. This results in a large period of the signal. Thus the magnitude of the error is a function of the offset distance. The error affects both depth and dip determination.

3.3 Resistivity

In the application of electrical methods in geophysical exploration, two parameters are of primary importance. These are the ability of rocks to conduct an electric current and the polarization which occurs when an electric current is passed through them. Electric conduction in most rocks is essentially electrolytic. This is through interstitial water hence the resistivity of a formation depends on the effective porosity and the degree of saturation of the fluids present. In crystalline rocks with low porosity, conduction takes place mainly along cracks, fissures or fractures. Conductivity of earth materials can be studied by measuring the electrical potential distribution produced at the earth's surface by an electric current passed through the earth.

The resistivity method is an effective method in providing a quantitative measure of the conducting properties of the subsurface. Irregularities in the conductivity below the surface affect the relationship between the current and the potential drop on the surface. This can be employed to obtain corresponding layer distribution and hence reveal the subsurface structure.

The method can be illustrated by assuming a semi-infinite medium which is the simplest earth model of uniform resistivity

ρ .

If a current is introduced through electrodes A and B placed on the surface, (Fig 3.3) and potential difference V, associated with the current is measured across potential electrodes M and N on the same surface,

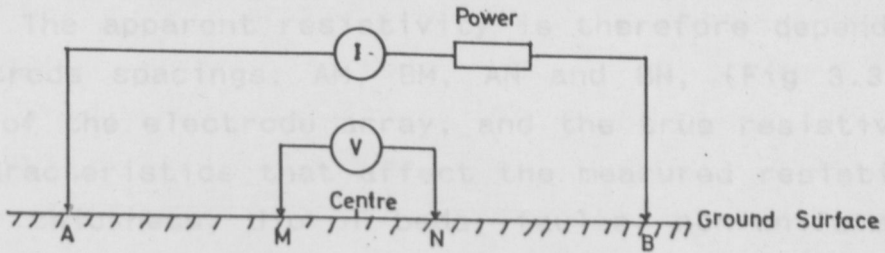


Fig 3.3 ARRANGEMENT OF CURRENT ELECTRODES (A&B) AND POTENTIAL ELECTRODES (M&N)

the measured resistivity P is given by

$$\rho = \frac{V}{I} \left[\frac{2\pi}{\frac{1}{AM} - \frac{1}{BM} - \frac{1}{AN} + \frac{1}{BN}} \right] \dots\dots\dots 3.5$$

This can be expressed as

$$\rho = k \frac{V}{I} \dots\dots\dots 3.6$$

where k is the geometric factor of the electrode arrangement., (Appendix B.1).

AB and MN are the distances between the current and potential electrodes respectively.

V is the potential difference measured across the potential electrodes.

In the field conditions the medium is never a semi-infinite space of homogeneous and isotropic material, hence resistivity is variable throughout the medium.

The effective resistivity calculated from equation 3.6 is therefore not the true resistivity but the apparent resistivity, ρ_a of the depth under investigation. Furthermore the layer interpretation theory is based on a purely horizontal stratified model while in practice this assumption is rarely achieved. The apparent resistivity is therefore dependent on the electrode spacings: AM, BM, AN and BN, (Fig 3.3), the geometry of the electrode array, and the true resistivities. Other characteristics that affect the measured resistivities are layer thickness, dip of beds, faults, non-uniformity of beds, rugged topography and anisotropy.

The basis of conducting an electrical sounding is that the larger the current electrode separation, the greater the amount of current that penetrates to a given depth. Therefore the greater the current electrode separation, the deeper the probing.

Several electrode configurations are used for the current and potential electrode arrangement. Constant electrode array is used in investigating the lateral variations in resistivity (horizontal profiling). The arrangement whereby the current electrode separation is expanded after every measurement is used for depth investigation surveys (vertical electrical sounding). In the Schlumberger sounding arrangements the distance between the potential electrodes is assumed to be infinitely short compared to the current electrode separation. In this respect it can be shown that, when the ratio $MN/AB = 1/3$, it may cause an error of about 10% whereas the ratio $MN/AB = 1/5$ the error does not exceed 2%, (Chyba, 1986) which is less than the standard error of the measured data.

The conventional interpretation methods of resistivity data are based on simple models such as multiple layers separated from one another by horizontal interfaces. The rock formation rarely exhibit such simple stratification of electrical properties. Resistivity variations are therefore much more complex in both the lateral and vertical directions. Electrical soundings conducted over laterally inhomogeneous ground results in a shift of the whole or a part of the sounding curve, by a constant on the logarithmic scale. Lateral resistivity variations are those caused by inhomogeneities and anisotropy other than the presumed horizontal beds, (Kunetz, 1966). Presence of lateral inhomogeneity is indicated by the formation of cusps on the sounding curves. This is well developed whenever the sounding line makes an azimuth angle close to 90° with the surface of the vertical plane boundary, (Zohdy, 1980). A shift on the sounding curve when measurements are made with different MN spacings is also attributed to inhomogeneous ground. Sounding conducted over steeply dipping geological structures result in large orientation variations. This is attributed to resistivity contrast between constituent layers or from anisotropy within beds, (Matias, 1986).

A given electrical sounding curve can correspond to a variety of subsurface distributions of resistivities and layer thicknesses. Thus the layer parameters obtained from the interpreted sounding curves may not provide a unique layer model for a particular case. If either the transverse or longitudinal conductance of two geoelectrical sections are equal, the resulting sounding curves for both sections will practically be identical, (Zohdy, 1980).

When a sounding is carried out with a spread parallel to the strike of a vertical or inclined contacts, the sounding curve obtained can be quite similar to that obtained over sections with horizontal contacts only. Those problems are attributed to the so called principle of equivalence, (Van Overmeeren, 1989).

The thickness and resistivity of a layer, relative to the overlying and underlying layers, also plays an important role in the detectability of the layer on the sounding curve. If the ratio of the bed thickness to its depth of burial (relative thickness) is small, its effect on the sounding curve might be so small that the presence of the thin layer is suppressed. In such a case, a sounding curve obtained over a four-layer section may be nearly equivalent to one obtained over a three-layer section. This problem is attributed to the so called principle of suppression.

A typical field day started at 8 a.m. and ended at 3 p.m. The equipments were checked and serviced in the evening and kept ready for the following day's work. Trips to Nairobi were made only when extremely necessary.

In the following sections, details of the field work involving geophysical investigation and soil drilling are given. Details on geological investigations and core logging are dealt with elsewhere.

4.2 Geophysical Investigations

4.2.1 Introduction

A tripod drill socket type resistivity sounding recording unit was used for the investigation. It is designed to probe the subsurface features in the foundation studies.

CHAPTER 4

FIELD WORK

4.1 General Organization

Field work in the study area was done between October, 1987 and January, 1988. It involved geological and geophysical investigations as well as the logging of the drilled cores. The field crew consisted of eighteen men. The author was involved in nearly all the aspects of the investigations. Since these were going on almost concurrently, a tight time schedule was inevitable. In order to maximise on the time in the field, a camp was established very close to the site. Thus no time was wasted travelling to and from the camp. The weather was also quite favourable and there were very few delays due to bad weather. A typical field day started at 7 a.m and ended at 3 p.m. The equipments were checked and serviced in the evening and kept ready for the following days' work. Trips to Nairobi were made only when extremely necessary.

In the following sections, details of the field work involving geophysical investigation and test drilling are given. Details on geological investigations and core-logging are dealt with elsewhere.

4.2 Seismic Refraction Measurements

4.2.1 Equipment

A "Nimbus ES-1A" pocket type seismic refraction recording unit was used for the investigation. It is designed to probe shallow subsurface features in the foundation studies.

It comprises of a counting circuit capable of measuring times in the interval of 0.1 milliseconds (ms) and 999.9 ms. The other components are the start and stop plugs, a reset switch, light emitting diode (LED), display screen and a polarity selector.



Fig 4.1 POCKET-SEIS ENGINEERING SEISMOGRAPH.

The pocket-seis is powered by four 1.5V dry cells (Size AA) and a 9V dry cell. The 9V dry cell can be utilised for 15 hours and the 1.5V cells are replaced after 5 hours of continuous use. Other accessories which go with the equipment are one geophone, a 30 m extension cable, a sledge hammer and a switch cable.

During the field operation, the start switch is clamped on the top side of the handle near the head of the hammer. The former is connected to the extension cable which traverses over the whole spread to the start plug of the equipment. The geophone on the other hand is connected to the stop plug. The counting circuit is started by the closing of the start switch as the hammer strikes the ground. The circuit continues to count as the seismic wave travels through the earth towards the geophone. A small voltage generated when the seismic wave strikes the geophone stops the counting circuit and the total count is displayed on the LED readout in milliseconds and tenths of milliseconds. On noting the reading, the reset switch is depressed and returns the counting circuit to zero.

4.2.2 Field Measurements

The survey lines were laid out to coincide with the test-boreholes on a straight path along the profiles (Fig 4.2). Spreads were set intercrossing and continuous along each profile. A 30 m measuring tape was spread along the survey line and the hammer position, (shotpoint) placed at one geophone position inside the preceding spread. The geophone spacing was 1.5 m. Surveys were carried out by moving the geophone to the next position with the hammer position, (shotpoint) stationary. The gain was adjusted to a point slightly below where background noise stopped the timer. This was achieved by turning up the gain knob until a zero appeared on the LED display. The gain knob was then turned down while pressing the reset until the highest gain setting was attained where normal background noise did not cause a zero to appear.

Scale 0 10 20
(m)



LOCATION OF THE SEISMIC REFRACTION AND RESISTIVITY PROFILES

Starting with the geophone position nearest to the hammer, the ground was struck with the hammer continuously until a reasonably consistent time was recorded. Four or five arrival times which were the same or close were sufficient.

The readings and the average data computed where necessary were entered on the data sheet, (Appendix A.2). The average reading was then plotted on a field time-distance graph to evaluate the trend of the curve. If a deviation from the rest of the plotted curve was noted and the point was not a cross-over point, the geophone position was shifted to another position whose distance was noted. The new reading was taken and plotted. The geophone was then moved to the next position and the readings taken the same way until the end of the spread.

The hammer position was then moved to the opposite end of the spread and the measurement repeated. These were plotted on the same graph as before but using the end of the forward spread as the origin, (Fig 3.2). The next spread was conducted on the same azimuth with the hammer position one geophone inside the preceding spread. Once sufficient spreads were made to cover a profile, another profile was carried out along a line coinciding with another test-borehole on about the same orientation.

Six seismic refraction profiles consisting of a number of spreads were conducted at the dam site. The profiles were along the spillway, BH1, BH2, BH4, BH5 and along the river course, (Fig 4.2). These comprised a total of 750 m of seismic refraction line-length covering an area of about 0.02 Km². Most profiles had a general SW-NE orientation parallel to the river course. However, this was not strictly maintained because the traverses were planned to follow the contour, in cases of sudden changes in the topography of the valley.

Starting with the geophone position nearest to the hammer, the ground was struck with the hammer continuously until a reasonably consistent time was recorded. Four or five arrival times which were the same or close were sufficient.

The readings and the average data computed where necessary were entered on the data sheet, (Appendix A.2). The average reading was then plotted on a field time-distance graph to evaluate the trend of the curve. If a deviation from the rest of the plotted curve was noted and the point was not a cross-over point, the geophone position was shifted to another position whose distance was noted. The new reading was taken and plotted. The geophone was then moved to the next position and the readings taken the same way until the end of the spread.

The hammer position was then moved to the opposite end of the spread and the measurement repeated. These were plotted on the same graph as before but using the end of the forward spread as the origin, (Fig 3.2). The next spread was conducted on the same azimuth with the hammer position one geophone inside the preceding spread. Once sufficient spreads were made to cover a profile, another profile was carried out along a line coinciding with another test-borehole on about the same orientation.

Six seismic refraction profiles consisting of a number of spreads were conducted at the dam site. The profiles were along the spillway, BH1, BH2, BH4, BH5 and along the river course, (Fig 4.2). These comprised a total of 750 m of seismic refraction line-length covering an area of about 0.02 Km². Most profiles had a general SW-NE orientation parallel to the river course. However, this was not strictly maintained because the traverses were planned to follow the contour, in cases of sudden changes in the topography of the valley.

Starting with the geophone position nearest to the hammer, the ground was struck with the hammer continuously until a reasonably consistent time was recorded. Four or five arrival times which were the same or close were sufficient.

The readings and the average data computed where necessary were entered on the data sheet, (Appendix A.2). The average reading was then plotted on a field time-distance graph to evaluate the trend of the curve. If a deviation from the rest of the plotted curve was noted and the point was not a cross-over point, the geophone position was shifted to another position whose distance was noted. The new reading was taken and plotted. The geophone was then moved to the next position and the readings taken the same way until the end of the spread.

The hammer position was then moved to the opposite end of the spread and the measurement repeated. These were plotted on the same graph as before but using the end of the forward spread as the origin, (Fig 3.2). The next spread was conducted on the same azimuth with the hammer position one geophone inside the preceding spread. Once sufficient spreads were made to cover a profile, another profile was carried out along a line coinciding with another test-borehole on about the same orientation.

Six seismic refraction profiles consisting of a number of spreads were conducted at the dam site. The profiles were along the spillway, BH1, BH2, BH4, BH5 and along the river course, (Fig 4.2). These comprised a total of 750 m of seismic refraction line-length covering an area of about 0.02 km². Most profiles had a general SW-NE orientation parallel to the river course. However, this was not strictly maintained because the traverses were planned to follow the contour, in cases of sudden changes in the topography of the valley.

The profile along the river course was carried out on the valley bottom along the longitudinal axis of the dam. The profile was extended to the reservoir area and across the eroded southern section of the scarp on the western side of the site. The profiles were 20-30 m apart. This happens to be the separation of the test-boreholes which were located on the dam-axis.

The 1.5V dry cells were replaced when display became dim and the 9V dry cell replaced during the third replacement of the former. Care was taken to make sure that the cells were attached to the proper connections. Longer lifespan of the cells was attained by turning off the pocket-seis or resetting after every reading. The cells were removed when the pocket-seis was not in use for extended period of time to prevent damage from leakage.

4.2.3 Limitations and Data Quality

The refraction data collected in the field area cannot be considered to be perfect. Like any field data, it had several limitations. The limitations in this study can be attributed partly to the type of equipment used and partly to the complex structural setup of the lithologies at the dam site. In this section, these limitations are highlighted.

The depth investigated by the use of the pocket-seis was limited by the amount of energy produced using a sledge hammer and the length of extension cable. By rule of thumb, it is estimated that the distance between the source and detector should be about four to five times the depth of probe. In this case, the maximum separation was 30 m. This implies that the depth of penetration was generally less than 8 m. Where the overburden was thick, few or no refraction arrivals were detected.

Because of the variation in the amplitude of the first arrival, it was found necessary to use both positive and negative polarities of the first arrival to estimate the arrival times. The first positive arrival is normally detected before the first negative. On the other hand, the first negative arrival has a higher amplitude. It was therefore found convenient to use the negative polarity under noisy conditions. The slope of the plotted line in such instances was not necessarily parallel to the line plotted from the first positive arrivals. This can be attributed to lack of an averaging facility in the instrument used. The negative polarity was also used to confirm if the positive arrival displayed was actually the first wave. This is easily checked since the first negative wave arrives within a travel time between the first and second positive waves.

At some geophone position the first arrival emanating from the bedrock was not detected due to faint signal amplitude. In such cases, surface waves were registered. These were recognised from their high travel times. This problem was also encountered where the headwaves surfaced beyond the end of the spread. In such circumstances, the time-distance graph had no cross-over points. Data collected on such spreads was improved where possible by placing the geophone off the survey line to countercheck the reading.

Despite the fact that the data is limited in depth of penetration, it was found good enough for this study. This is mainly because the zone of interest was shallow and therefore within the range of the instrument used. Limitations associated with lithological and structural setup are difficult to assess. However, the use of resistivity and core-logging data in addition to refraction provided a means of assessing the effects of these factors. This point will be discussed further in later chapters.

4.3 Resistivity Measurements

4.3.1 Equipment

The equipment used for all the resistivity data acquisition was ABEM SAS 300 Terrameter, (Fig 4.3).

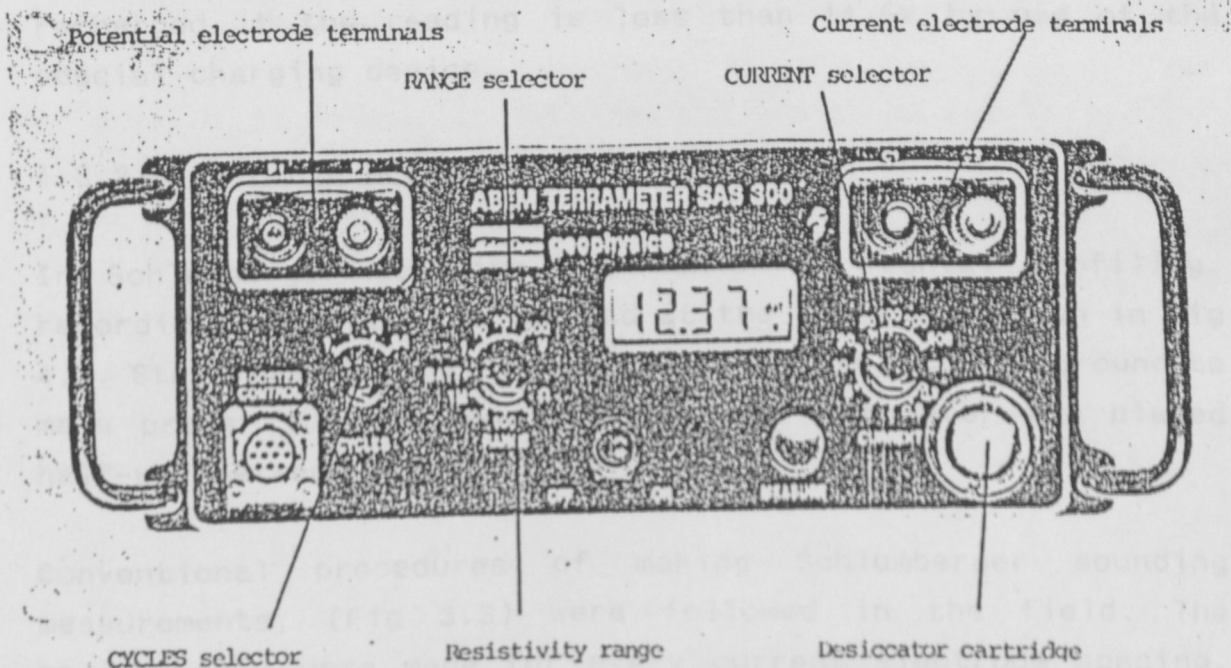


Fig 4.4 SAS 300 TERRAMETER CONTROLS AND TERMINALS

It contains three main units all housed in a single casing: the transmitter, the receiver and the microprocessor. The battery pack is attached on the bottom of the whole component. The transmitter sends out well defined and regulated signal currents. The receiver discriminates noise and measures voltages correlated with the transmitted signal current. The microprocessor monitors and controls all the measurements to ensure optimal accuracy and sensitivity. It also makes certain that the instrument is used correctly by sending warnings and information comprising of beeper and simple error codes, (ABEM Manual). The battery powered resistivity meter has an output sufficient for a current electrode separation of 2000 m.

The voltage to current ratio (dV/I) is automatically calculated and displayed digitally in Kilo-ohms, ohms and milliohms. The overall range extends from 0.5 milliohms to 1999 kilo-ohms.

The equipment is powered by a battery which when properly charged, displays a voltage of 12.5-15V. The battery is recharged if the reading is less than 11.5V by use of the special charging device.

4.3.2 Field Measurements

In Schlumberger sounding and Wenner horizontal profiling, recording stations were located at the positions shown in Fig 4.2. Stainless steel electrodes were driven into the ground to make proper contacts and the SAS 300 Terrameter was placed half-way between the electrodes.

Conventional procedures of making Schlumberger sounding measurements, (Fig 3.3) were followed in the field. The measurements were made for every current electrode spacing, ($AB/2$). Repeat readings were taken for the same $AB/2$ where the potential electrode spacing was increased. Measurements were also repeated where the values of the measured apparent resistivity deviated from the trend of the earlier readings in the same spread.

A total of 27 vertical electrical soundings (VES) were made utilising Schlumberger probe configuration. Seven of these had an electrode spacing of $AB/2 = 250$ m, and the other twenty, had an $AB/2 = 100$ m. The VES measurements were made along the same six profiles where the seismic refraction surveys were conducted. The recording stations of the measurements in the same profile were 45 m to 50 m apart, (Fig.4.2).

Nine horizontal profiles using the Wenner probe configuration were made, at Wenner separations of $a = 4, 10, 25$ and 40 m. The centre positions were at the test-boreholes along the dam-axis while the others were at the spillway and the SE section of the dam-axis.

During the field operation, meticulous care was taken in the arrangement of the cables and electrodes. This was to minimize any current leakage. Current leakage and creep substantially reduce the attainable accuracy and sensitivity; and thus the depth of penetration. Care was always taken to connect the cables to the correct polarities, because wrong connections caused negative resistivity readings. The electrodes were always driven deep into the ground to ensure good contact. Loose contacts resulted in the display of consecutive unsteady readings.

Other errors such as loose connections, voltage range setting and interferences during measurements were registered on the display by error codes which were rectified as per the instructions set in the ABEM instruction manual.

4.3.3 Limitation and Data Quality

The main limitation experienced during the execution of the resistivity surveys was the terrain effect. Large topographical differences between the current electrodes and recording station caused anomalous values of the measured apparent resistivities. This problem was encountered where the measuring stations was close to the valley. When the current electrodes were placed on the sloping surface of the valley, high resistivity readings were registered. The readings reached a maximum at the valley bottom. After crossing the valley the value of the readings started reducing (normalising).

The original shape of the apparent resistivity curve was obtained once the surface elevation on the other side of the valley was the same as the former side. A repeat of the measurements yielded the same condition in all the spreads where the current electrodes were placed on sloping surface, (discussed in section 5.2.2).

Warnings and information comprising of beeper signals and simple error codes minimized operational errors by advising on the right parameters and checks of the circuits. This improved the overall data obtained by use of the SAS 300 Terrameter.

The Self Averaging System (SAS) in the equipment ensured continuous averaging of all the measurements for every reading. This made the field data acquisition exercise fast and accurate. In most cases, the measurements were steady and rarely required repeat readings.

The SAS 300 Terrameter has an overall system accuracy of $\pm 2\%$ of the reading. This accuracy added to that assumed for the Schlumberger sounding when $MN/AB > 1/5$ which theoretically is less than 2%, showed that the field data had an overall error of less than 4%. Generally the data obtained was of good quality and adequate for the intended interpretations.

4.4 Geological Core-Logging

A skid mounted rotary drill was used in the test-drilling exercise. The soft overburden materials were recovered by using air as the flushing medium. Once the hard rock was reached, water was used as the flushing medium. The rate of drilling was determined by the degree of fracturing of the basalts and the number of times drilling was stopped to recover the cores and remove pebbles stuck on the drill-bit.

Under normal drilling conditions about 1.5 m of the core was recovered in an hour.

Once the core was removed, the Parker test was carried out in the drillhole to determine the permeability of a particular zone of the rocks. This was done by sealing off a length of uncased hole with packers and injecting water under pressure into the test section. Single packer test method was used where a 3 m length of the drill hole was sealed by a single packer and tested independently. After the test a further section was then drilled and another test performed.

The recovered cores were generally of good quality. A recovery of 80-100% was achieved in most of the drilled depths. However poor recovery occurred from highly weathered zones. In such cases, the total length of the recovered core to the total length drilled was less than 50%.

The cores were then stored in core-boxes, which were labelled by the borehole number and the position in the borehole from which the material was obtained. Geological core-logging was carried out on the cores in the boxes. Stratigraphical units were delineated to determine the stratal succession at the site. Particular emphasize was placed on the depth of the weathered horizons, the location of bedrock, subsurface voids and the fractured zones. The fractures induced by the drilling process was distinguished from natural fractures in the rock. The weak zones were evaluated soon after the cores were recovered because materials from the highly weathered rocks deteriorated after extraction. Completely weathered rocks and residual soils disintegrated if allowed to dry. The broken as well as the fractured rocks and weathered zones overlapped into the fresh rocks, hence the zonal boundaries were subjective.

A total of nine test-boreholes were sunk at the dam site, (Fig 4.2). Two of these were located along the spillway, five on the dam-axis and two along the river course, (plate 4.1). Those on the abutments were drilled to depths of 10 to 16 m, while those along the river course were sunk to a maximum depth of 30 m.



Plate 4.4 Core drilling in progress at BH2. Note V.E.S. S17 being conducted next to the borehole. The spread is along the flat valley bottom with the steep rise on the right abutment seen on the background.

CHAPTER 5INTERPRETATION OF GEOPHYSICAL DATA5.1 Seismic Refraction5.1.1 Method of Interpretation

Interpretation of seismic refraction data invariably entails determination of thicknesses, velocities and dips associated with a given layering situation. More rigorous interpretation may also involve identification of faults and other structural discontinuities. In dam site investigations, the interest is usually in the determination of the overburden thickness and delineation of the weak zones.

Several methods exist for interpretation of refraction data. Where the layering situation is straight forward, simple formulae or nomographs can effectively be used. However in a complex structural setup, more involving schemes of interpretation have to be used. As tedious mathematical manipulations have to be dealt with in the latter case, computer programmes are commonly used. Several hand methods capable of handling complicated layering situations have however been used in the recent years. These include Delay-time method (Gardener, 1939); Graphical method (Slotnick, 1950); Plus-minus method (Hagedoorn, 1959); Reciprocal method (Hawkins, 1961); Mid-point method (Mcphail, 1967); and Generalised Reciprocal Method (Palmer, 1981). These methods differ in the nature of the approximations made in the field, the computational procedures used, and in the relative or absolute nature of the results obtained. Hence they have their own merits and demerits. An assumption inherent in all refraction interpretation methods is that both the overburden and refractor velocities do not vary in horizontal directions.

The Delay-time method utilises the time difference between the hypothetical time which would be measured, if the refractor was at the surface, and the actual time measured. Horizontal disposition of the refractor is assumed. The method provides only the depths at the two ends of a reverse profile.

The Graphical Method employs the laws of geometrical optics to infer velocities from the time-distance curves. In practice, the accuracy is restricted to an unknown degree by the assumption that the velocity stratification is inferred unambiguously from the time-distance curves. When the number of layers to be considered are many, the method becomes tedious to apply.

The reciprocal method employs the standard inline arrangement of geophones and shotpoints with pairs of corresponding shotpoints bracketing the geophones spread. In addition to the travel-times along the geophone spread, the travel-time between each pair of corresponding shotpoints is also recorded and is termed the reciprocal time. Determination of depths in this method is based on "time-depth", which is the time delay associated with the critical ray in travelling between the refractor and the surface. In this case the depth is taken normal to the plane of the refractor.

The mid-point method is an analytical method that exploits the simplification in the equations of the time-distance curves when the refracting surfaces are flat. The method provides an approximation of the average depth of the refractor in the interval of the offset distance used for the computation. The method assumes a smooth horizontal surface between the shotpoints.

The Generalized Reciprocal Method (GRM) is a technique for processing and interpreting in-line seismic refraction data consisting of forward and reverse traveltimes. The processing involves use of computer programmes to compute velocity analysis function and generalized time-depth to obtain the velocity and depth of the refractor respectively. The GRM overcomes the ambiguity inherent in intercept time by recording the reciprocal time in the field and incorporating the value into calculations involving the arrival times at the geophones.

The Plus-Minus method is an approximation of Thornburgh's (1930), wave front reconstruction method. It assumes that the individual layers are homogeneous with a large acoustic impedance difference between layers, and that the dip of the slope of the refractor is small. The method employs traveltimes obtained from geophone stations where the first arrivals from both forward and reverse shots have travelled via the same refractor. Simple addition of the two travel-times from the symmetrical shotpoints minus the total travel-time ("plus" values) gives a relative picture of the depths. Simple subtraction of the same pairs of travel times plotted against distance ("minus" value) gives a picture of the refractor velocities.

Thus before deciding which method to use, the author tried out some of the above. This was done in an attempt to pick out the most reliable and efficient for the present problem. The plus-minus method was considered most appropriate due to its simplicity and quickness. The computations involve simple addition and subtraction of traveltimes recorded at geophone stations of interest. This was done manually.

The main applications of the plus-minus method are in shallow investigations, (one interface). Its application is simple and fast to execute manually. The method has a significant advantage over the standard formula interpretation, in that it uses the data collected at each geophone in the interpretation. In a two-layer case, a standard interpretation utilising text formulae, (Dobrin, 1976) would produce a depth to the second layer near each shotpoint. The plus-minus method on the other hand provides depth to the refracting horizon for each geophone that receives a refracted wave from the layer, (Fig. 5.1).

The method uses the principles of intercept time and delay time to determine the depth (z) to the refractor. For a two layer case, (Cummings, 1979).

$$z = (t_1 + t_2 - t_x)k_1 \dots\dots\dots 5.1$$

where $(t_1 + t_2 - t_x)$, defined as the plus time is the equivalent of the intercept time corresponding to different parts of the time-distance graph. The terms t_1 and t_2 are the arrival times at the same geophone from a forward and reverse shotpoint respectively and t_x is the total travel time between the shotpoints, (Fig 5.1).

The term k_1 represents the relation of the velocities for the delay time,

$$k_1 = 0.5 \frac{v_1}{1 - \frac{v_1^2}{v_2^2}} \dots\dots\dots 5.2$$

where v_1 and v_2 are the velocities of the upper and lower layers respectively.

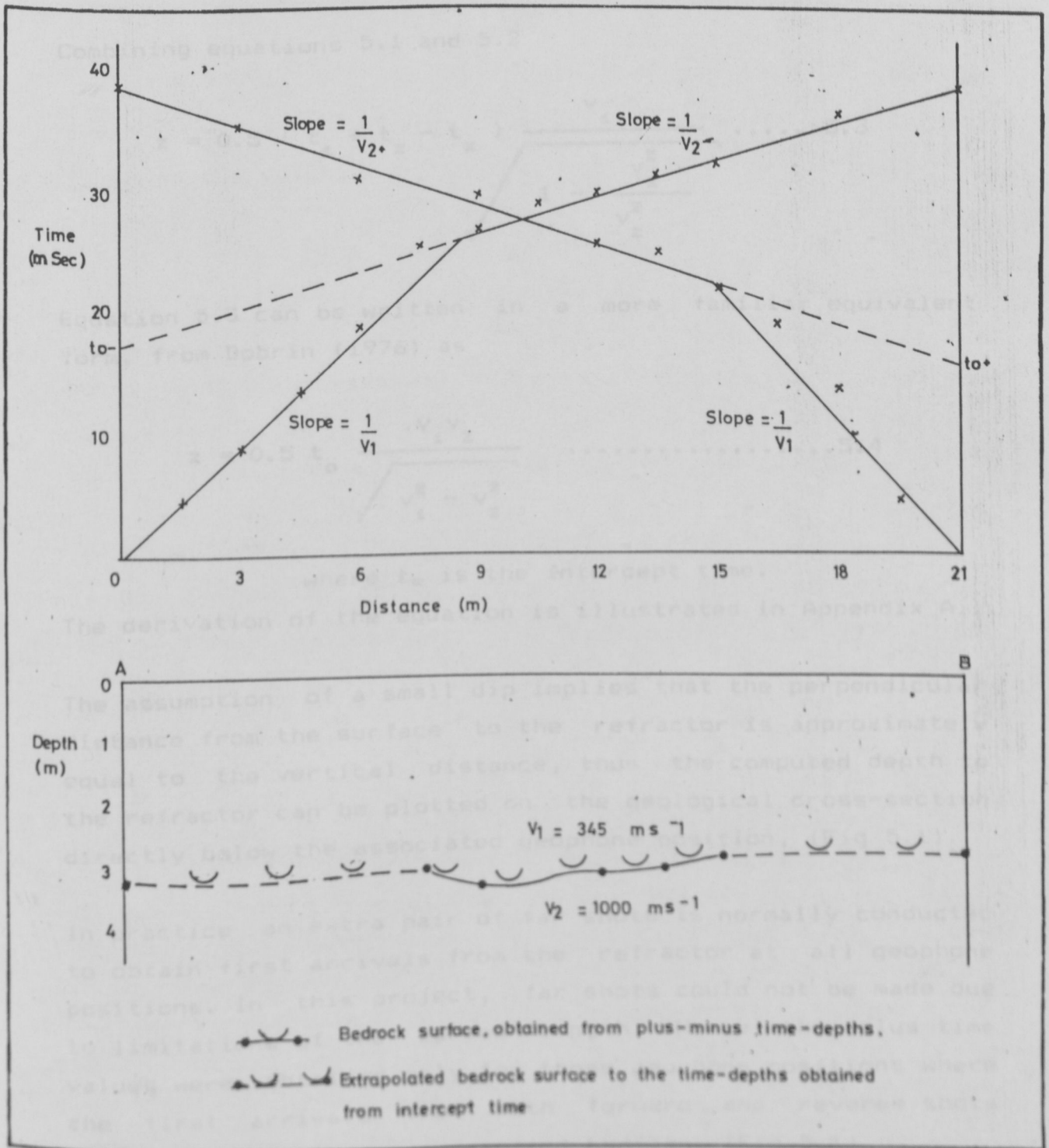


Fig 5.1 TIME-DISTANCE GRAPH OF REVERSED SEISMIC DATA OF SPREAD A-B, AND THE TIME-DEPTHS SHOWING THE GEOLOGICAL INTERPRETATION OF THE IRREGULAR BEDROCK SURFACE.

Combining equations 5.1 and 5.2

$$z = 0.5 (t_1 + t_2 - t_x) \frac{v_1}{1 - \frac{v_1^2}{v_2^2}} \dots\dots 5.3$$

Equation 5.3 can be written in a more familiar equivalent form, from Dobrin (1976) as

$$z = 0.5 t_o \frac{v_1 v_2}{\sqrt{v_1^2 - v_2^2}} \dots\dots\dots 5.4$$

where t_o is the Intercept time.

The derivation of the equation is illustrated in Appendix A.1.

The assumption of a small dip implies that the perpendicular distance from the surface to the refractor is approximately equal to the vertical distance, thus the computed depth to the refractor can be plotted on the geological cross-section directly below the associated geophone position, (Fig 5.1).

In practice an extra pair of far shots is normally conducted to obtain first arrivals from the refractor at all geophone positions. In this project, far shots could not be made due to limitations of the spread length. Hence the plus time values were obtained only for those geophone positions where the first arrivals from both forward and reverse shots travelled via the same refracting horizon, (Fig 5.1).

The velocities were calculated from the traveltime curves by computing the reciprocal of the slope gradients. The first slope provided the velocity v_1 , of the surface waves hence the velocity of the surface layer.

The velocity v_2 of the refracted waves was taken to be the average of the up dip velocity, v_{2+} and downdip velocity, v_{2-} . This was the velocity of the refracting horizon.

The intercept times for the updip end, t_{0+} and downdip end, t_{0-} for every spread was read directly from the time-distance graph by extending the traveltime curve from the cross-over point to the abscissa axis. The total traveltime, t_x between each pair of forward and reverse shot points normally termed as reciprocal time was also obtained from the graph.

The plus time t_b , for each geophone, defined in equation 5.1 is the sum of the travel times, t_1 from a forward shotpoint and t_2 from a reverse shotpoint, minus the total traveltime t_x .

$$\text{Thus } t_b = (t_1 + t_2 - t_x) \dots\dots\dots 5.5$$

In this single interface interpretation t_1 and t_2 were obtained directly from the sections of the curve where the first arrivals were both from the refracting interface. In the example shown in Fig 5.1 plus-minus times from the refracting horizon were obtained between the geophones at 7.5 m and 15 m.

The critical angle θ_c , made by the refracted wave was calculated using equation 3.3. The other variables were obtained as described above, hence the depths h and h' (of the updip and downdip ends of the spread) from the surface to the refractor at the shotpoints were calculated using the standard formula, (equation 5.4).

The plus times t_b for every geophone position were used to calculate depths h_b from the surface to the refractor at the geophone positions.

$$\text{where } h_b = \frac{t_b v_1}{2 \cos \theta_c} \dots \dots \dots 5.6$$

Those provided the depth to the refractor at the shotpoint positions and geophone position. The refractor-depths were then plotted to define the topography of the refractor, (section 6.1).

5.1.2 Limitations in the Seismic Refraction Data Interpretation

Most of the first arrival plots fall on a straight line. A few points were scattered along the general trend of the time-distance curve. Scattering is normally caused by travel time errors, lateral variation in velocity or dip, and intersection of segments representing arrivals from deeper layers. Therefore the critical task in the interpretation was to relate inflection points on time-distance curves to either crossover points or lateral geological changes. The time-distance curves were then constructed for the refracting horizon with the first arrival data on hand.

Inflections corresponding to the crossover points were manifested by a decrease in slope of the time-distance curve with increase in distance from the shotpoint. Changes in the dip or velocity of refracting horizon resulted in crossover point being marked by an increase in slope with increased distance. These were easily recognised from the time-distance curves where gradual change in the dip resulted in different intercept time of the forward and reverse spreads.

In this study, the orientation of the spreads was parallel to the topographical contours. This ensured the same surface elevation for the shot and detector positions. Furthermore the length of the spreads were too short to have any appreciable variation in surface elevation. This was confirmed from the reciprocal times which were the same for the forward and reverse spreads. The first arrivals data obtained was from the shallowest refracting horizons (bedrock). Hence the topsoils and the weathered rocks were interpreted as constituting the overburden. Therefore the weathering correction did not arise in the interpretations.

5.1.3 Results of Interpretations

The interpretations of the time-distance curves was relatively straight forward. The first slope on the curves represented the direct waves while the second slope represented the first arrivals from the refracting horizon. The velocities of the surface layer and refracting horizon were calculated from the slopes. Combination of the intercept time and the plus times allowed the depth to the refracting horizon to be determined.

The overburden materials had generally low velocities whereas the bedrock had higher seismic velocities. Velocities in all the profiles were variable for both surface layer and refracting horizon. The travel-times indicated that the surface layer had an average velocity of 350 m/sec, but ranged from 280 m/sec to 500 m/sec. The main refractor was found to have an average velocity of 1000 m/sec, but ranged from 800 m/sec to 1900 m/sec. The depth of the refractor was also variable in all the profiles ranging between 2 m to 5 m.

The surface velocities in the upstream section were found to be generally lower than those on the downstream section.

Refractor velocities on the river course profile between station k and q ranged from 1500 to 1600 m/sec. The rest had an average velocity of 940 m/sec. The depths to the refractor on this section were also relatively shallow. The average depths on spread u and p were 2 m.

The refractor velocities on the abutments are higher than those at the valley bottom. The higher velocities are attributed to a lesser degree of fracturing of the fresh basalts on the abutments. The depth section across the dam axis show an approximately constant depth to the refractor, which follows the surface topography of the valley. The depth sections calculated from the interpretations are shown in Figs 6.1 and 6.2.

5.2 Resistivity

5.2.1 Methods of Interpretation

The main purpose of carrying out the resistivity sounding was to determine the nature and characteristics of the subsurface (resistivity and thickness of layers). Therefore, the interpretation of the measured resistivity sounding data involved the distinction of the number of layers and their layer parameters. The standard procedure of plotting the results in bi-logarithmic graph was performed, (Appendix B.3). Visual interpretation was carried out in the field by studying the apparent resistivity (ρ_a) curves. The layer parameters were determined using the indirect methods of interpretations by matching the observed ρ_a curves with master curves and by computer modelling. In the Wenner horizontal profiling, ρ_a values were plotted on linear graphs for every wenner separation.

5.2.1.1 Visual Interpretation

The type of apparent resistivity (ρ_a) curves obtained in an area are functions of the resistivities, thickness of the layers and electrode configuration. The ρ_a curves obtained at the dam site are composed of many combinations of the simple H, A, K, and Q type of sounding curves. The curves with the same relationship were classified together for interpretation purpose. The dominant resistivity curves in the whole area were of three types, (Fig 5.2).

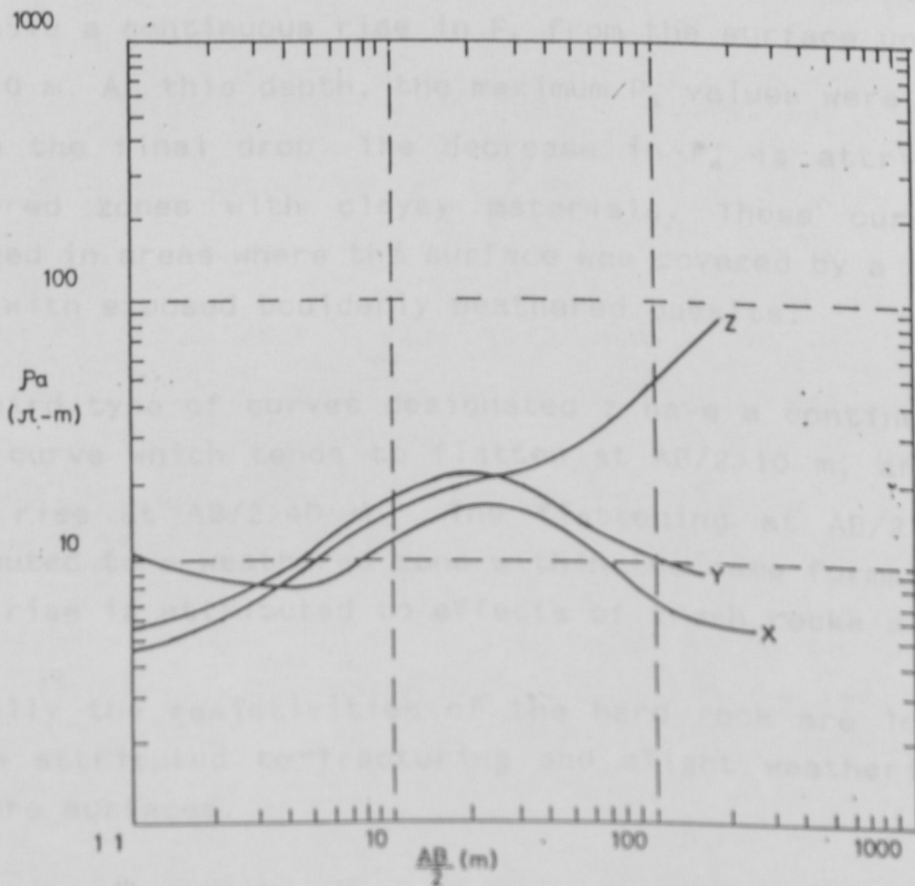


Fig. 5.2 TYPES OF APPARENT RESISTIVITY CURVES AT KISERIAN DAMSITE.

5.2.1.1 Visual Interpretation

The type of apparent resistivity (ρ_a) curves obtained in an area are functions of the resistivities, thickness of the layers and electrode configuration. The ρ_a curves obtained at the dam site are composed of many combinations of the simple H, A, K, and Q type of sounding curves. The curves with the same relationship were classified together for interpretation purpose. The dominant resistivity curves in the whole area were of three types, (Fig 5.2).

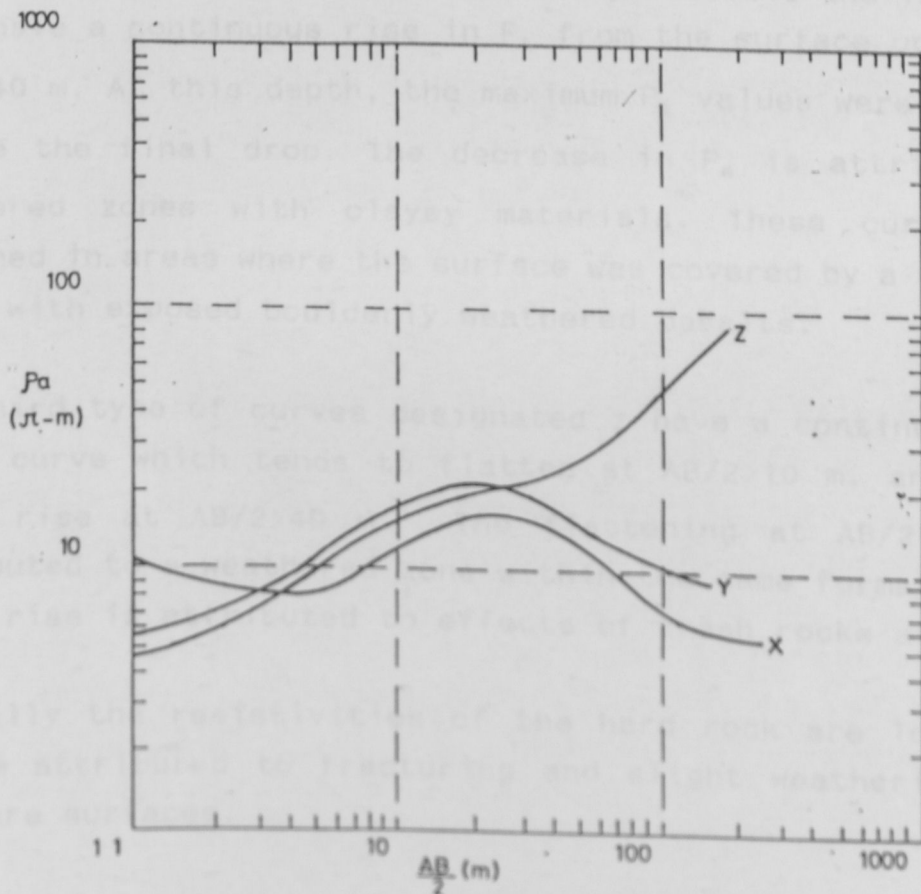


Fig. 5.2 TYPES OF APPARENT RESISTIVITY CURVES AT KISERIAN DAMSITE.

Generally, the p_a curves in the area were characterized by a sharp rise in apparent resistivity between separation $AB/2=4$ m and 10 m. The first type of curves designated x have high apparent resistivities on the surface followed by a gently drop around $AB/2=3$ m and then a rise up to a maximum $AB/2=10$ m. This is followed by a drop of p_a which tends to flatten or rise at $AB/2 > 100$ m. These curves were found in areas where there was topographical depression. These depressions are filled up by thick clayey materials at S18, S19, S8 and D2, (Fig 4.2). The clays contributed to the initial gentle drop in p_a values.

The second type of curves designated y resemble the latter but they have a continuous rise in P_a from the surface up to $AB/2=10$ m. At this depth, the maximum P_a values were attained before the final drop. The decrease in P_a is attributed to weathered zones with clayey materials. These curves were obtained in areas where the surface was covered by a thin clay layer with exposed boulderly weathered basalts.

The third type of curves designated z have a continuous rise of P_a curve which tends to flatten at $AB/2 > 10$ m, and then a final rise at $AB/2 > 40$ m. The flattening at $AB/2 > 10$ m is attributed to a weathered zone within the same formation. The final rise is attributed to effects of fresh rocks at depth.

Generally the resistivities of the hard rock are low, which can be attributed to fracturing and slight weathering along fracture surfaces.

5.2.1.2 Master Curves.

The common method of interpretation is by use of assemblage of theoretical curves (master curves). The master curves are computed apparent resistivity curves plotted on logarithmic co-ordinate system. They are prepared using the generalized expression of apparent resistivity where all the variables occur as dimensionless ratios, (equation 5.7).

$$\frac{\rho_a}{\rho_1} = 1 + 2 \sum_{n=1}^{\infty} \frac{k^n}{\left[1 + 4n^2 \left\{ \frac{h}{a} \right\}^2 \right]^{3/2}} \quad \dots 5.7$$

Where k is the boundary reflection coefficient.

a/h is the thickness of the overburden.

ρ_a/ρ_1 is the resistivity of overburden.

n is the n^{th} layer which assumes a

homogeneous isotropic ground.

The master curves are presented as a plot of apparent resistivity (ρ_a) versus electrode separation ($AB/2$) for the arrangement of electrodes employed in the field. Various thicknesses, specified layering and resistivity ratios are assumed for individual layers. The resistivity and thickness of the first layer is assumed to be unity, which eliminates two parameters in the calculation of the sounding curve for a given earth model. Therefore the theoretical curves have no regard of the units used, absolute values of resistivities, electrode spacing or bed dimensions. This forms the basis of curve-matching interpretation method. The shape of the curve is preserved in logarithmic co-ordinates even when the ordinate, ($AB/2$) and abscissa, (ρ_a) of each point along the curve are multiplied by arbitrary constants, (Keller, 1982).

Three-layer theoretical curves by Rijkwaterstat (1980) were used in the curve matching interpretations. The 3-layer master curves provided the thicknesses and resistivities of the overburden and those of the bedrock which was the objective of the investigations. However auxiliary point method was employed to interpret the deeper layers. Auxiliary curves combined the first two layers into a single fictitious layer so that the portion not interpreted by the 3-layer master curve could be interpreted. This provided the layer parameters of the deeper layers. It was noted that in the 3-layer curve matching interpretation, the resistivity of the third layer was an estimation of the earth model assuming infinite thickness of the layer. Hence the resistivity was unreliable. Therefore the resistivity obtained using the auxiliary point method was more reliable and was the one assigned to the third layer.

5.2.1.3 Computer Modelling

Curve matching using the pre-calculated master curves is limited by the specific parameters of thicknesses and resistivities of the assemblage of the master curves employed. The 2268 standard curves from which selection was made in the curve matching interpretation are just a few of the many possible 3-layer combinations. Hence computer modelling was used to generate the actual curves that could be produced by any model.

Computer interpretations were done by use of Olivetti M24 personal computer. The VES programme designed for interpreting Schlumberger sounding data was used. In this programme the inversion of sounding curves is achieved iteratively using inverse filters, (O'Neil, 1975). The match between field and model curves using the programme is controlled by use of the Root Mean Square (R.M.S) percentage specified to be less than 5%, (Fawzia, et al, 1986).

The data input for the VES programme are the measured field p_a values and the corresponding electrode spacing, $AB/2$. These were stored in a floppy disk where every spread had its own file. The model menu required an input of the layer depths and the corresponding expected resistivity for the specific layer. The computer then computed the O'Neil VES curve to match the model fed by the interpreter. This was adjusted by changing the depths and resistivities parameters until the computed curve on the screen matched the field data points. This procedure was followed to get the correct model for every spread.

The quality of the computer models was improved by starting with the layer parameters from the curve matching interpretation. The VES programme had also facilities for shifting data points on the screen without affecting the stored field measurements. This facilitated the interpretation of the field data obtained from different MN spacing by giving them a uniform shift to fit the left hand section of the resistivity curve.

After retrieving the particular file of the sounding to be interpreted, the whole process of plotting the logarithmic graph, drawing the data points on the screen and the curve to fit the given model took about 20 seconds. The model and the plot were stored in the same file opened for that particular spread and could be retrieved for modification.

5.2.2 Limitations in the VES curve Interpretations

The resistivity method assumes homogeneity and isotropy. In reality these conditions are hardly achieved. Even though the earth may be homogeneous in some instances, it may not necessarily be isotropic.

The determination of the layer parameters in the interpretation thus provide a way of averaging the electrical properties over large volume of rocks, which may not necessarily be homogenous. The geoelectrical section boundaries between layers are also determined by resistivity contrast rather than by the combination of factors used by the geologist in establishing the boundaries between beds.

The field curves were displaced as a result of enlarging the potential electrode spacing after several measurements. Very often the measurements repeated with unchanged current electrode spacing showed a shift in the P_a curve. In such cases the curves were smoothed by shifting the right side of the curve to match the previous section. In the computer interpretations, a shift of a section could be performed on the screen for smoothing and subsequent interpretations.

Lateral inhomogeneities also affected the resistivity measurements which was indicated by formations of cusps on the P_a curves. Field P_a curves were distorted as compared to the theoretical ones. This anomaly was prevalent also in cases where the current electrodes were placed on inclined surfaces on the valley slopes. This resulted in anomalous P_a values which normalised when the surface across the valley reached the elevation of the measuring station on the opposite side. The latter condition was attributed to the topographical effect, which is generally encountered in areas of moderate to strong relief. The ground surface acts as a streamline for the current flow, therefore irregularities in the shape of the ground surface introduces local squeezing together or drawing apart of the equipotential surfaces. This is registered as spurious anomalies. These sections in the curves were smoothed during the interpretations.

Another serious ambiguity in the interpretation of the multilayer sounding curves was caused by the well known principles of equivalence and suppression. Unique layer-model solutions could not be found. Many solutions could be obtained corresponding to a variety of layer thicknesses and resistivities. It was observed (McCann, 1977), that curve matching or computer programmes do not correctly compute the resistivity of an earth model containing a perfectly insulating or perfectly conductive layer. In order to check for the existence of such a condition in the sounding curves, layer models of curves increasing or decreasing rapidly with depth were carefully investigated. This was also for the purpose of ensuring that a small perturbation of the model did not result in a large change of computed resistivity.

5.2.3 Results of Interpretation

5.2.3.1 VES Data

Interpretation of the P_a curves by curve matching and computer modelling provided the subsurface parameters which were used to draw the geoelectrical sections. The two methods of interpretation gave results which compared closely. An example, (Table 5.1) of the interpretation of the sounding curve S7, (Appendix B.4) yielded the following layer parameters.

Layer	Depth(m)		Resistivity(ohm-m)	
	Curve Matching	Computer	Curve Matching	Comp.
1	1.7	1.7	28.0	24.0
2	3.4	3.5	700.0	710.0
3	130.0	9999.0	56.6	43.0
4	"	-	1.7	-

Table 5.1 Layer parameters of VES data at S7, from curve matching and computer interpretation.

The surface geoelectrical layer had resistivities of 4 to 27 ohm-m. The layer has average depths of about 1.3 m. The second geoelectrical layer had resistivities of 52 to 710 ohm-m, and attains a maximum depth of 17 m. The third geoelectrical layer had variable resistivities which were characteristic of the different profiles. The valley bottom had resistivities ranging from 6 to 28 ohm-m, while the abutments had resistivities of 35 to 46 ohm-m. Apparently this layer was thickest at the valley bottom and tended to thin out on the abutments. It was also observed that the layer attains the maximum depths on the downstream section of the site. The deepest geoelectrical layer investigated had resistivities exceeding 50 ohm-m. These corresponded with those of the second geoelectrical layer. The layer is shallow on the abutments and deeper at the valley bottom. The interpreted geoelectrical sections are shown in Figs 6.3, 6.4 and 6.5.

5.2.3.2 Profiling Data

The wenner horizontal profiling data, (Appendix B.2) was plotted on resistivity profiles as shown in Figs. 5.3 and 5.4. Subsurface features are recognised qualitatively from anomalies in P_a at different wenner spacing.

The resistivity profile at wenner spacing $a = 4$ m and $a = 10$ m, (Fig 5.3) reveals the features of the bedrock. The effect of shallow features of the bedrock are suppressed in the profile made with 10 m, whereas the effects of the deeper ones are retained. In the profile made with 4 m, the effects of shallow features are retained and the deeper ones suppressed.

The resistivity profile shows high P_a on the right abutment. The left abutment has high P_a at only station H7. The p_a values show presence of low resistivity materials at the valley bottom and beyond H7 on the left abutment. Generally the bedrock has the same characteristics between the two depths which conforms with the observations obtained from the core-logs.

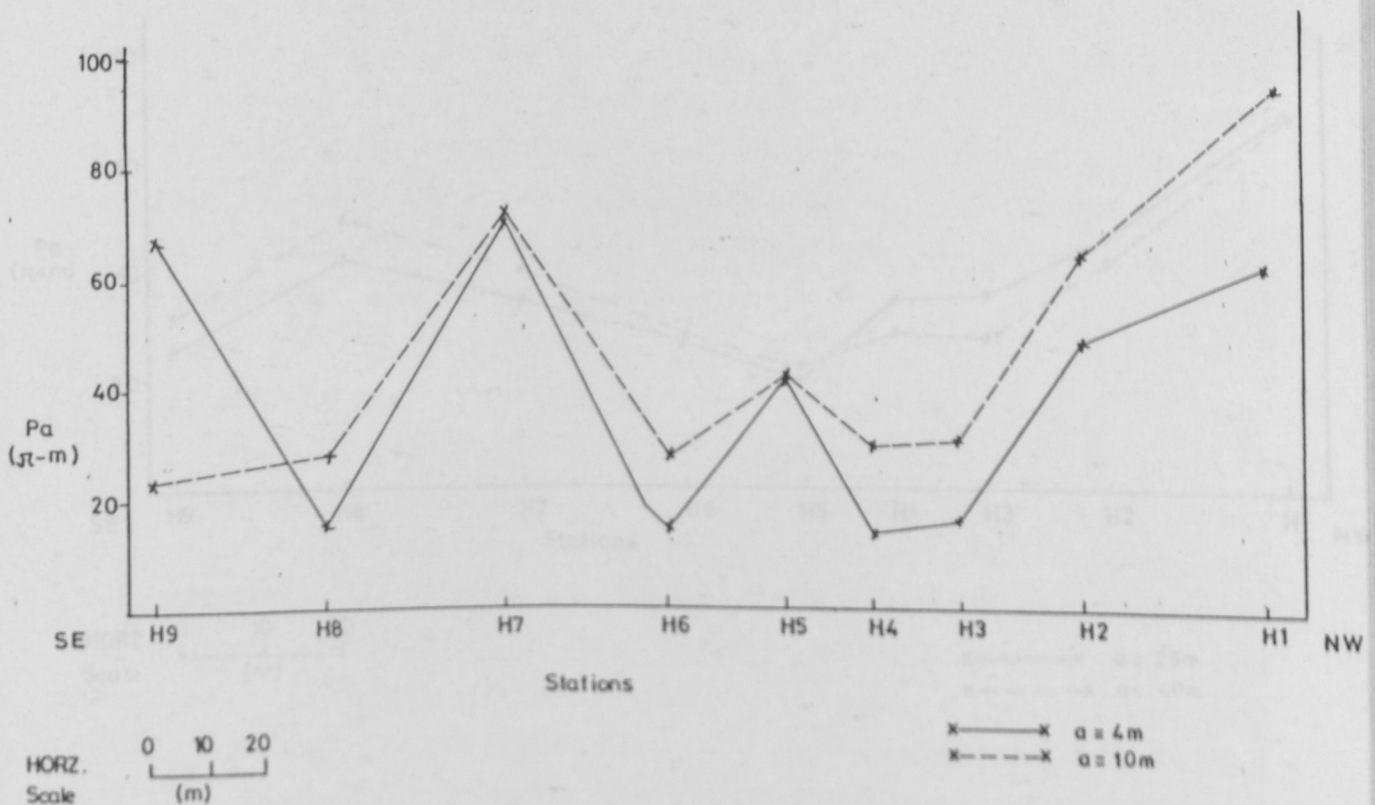


Fig 5-3 RESISTIVITY PROFILING WITH WENNER SPREAD A CROSS THE DAM-AXIS. SEPARATION $a = 4\text{m}$, $a = 10\text{m}$.

Fig. 5.4 shows the resistivity profile at wenner spacing of $a = 25$ m and $a = 40$ m. This was conducted to investigate the weathered zone underlying the bedrock. The P_a values show uniformity between the two depths, across the dams-axis. Low P_a are obtained at the valley bottom while the abutments have higher values.

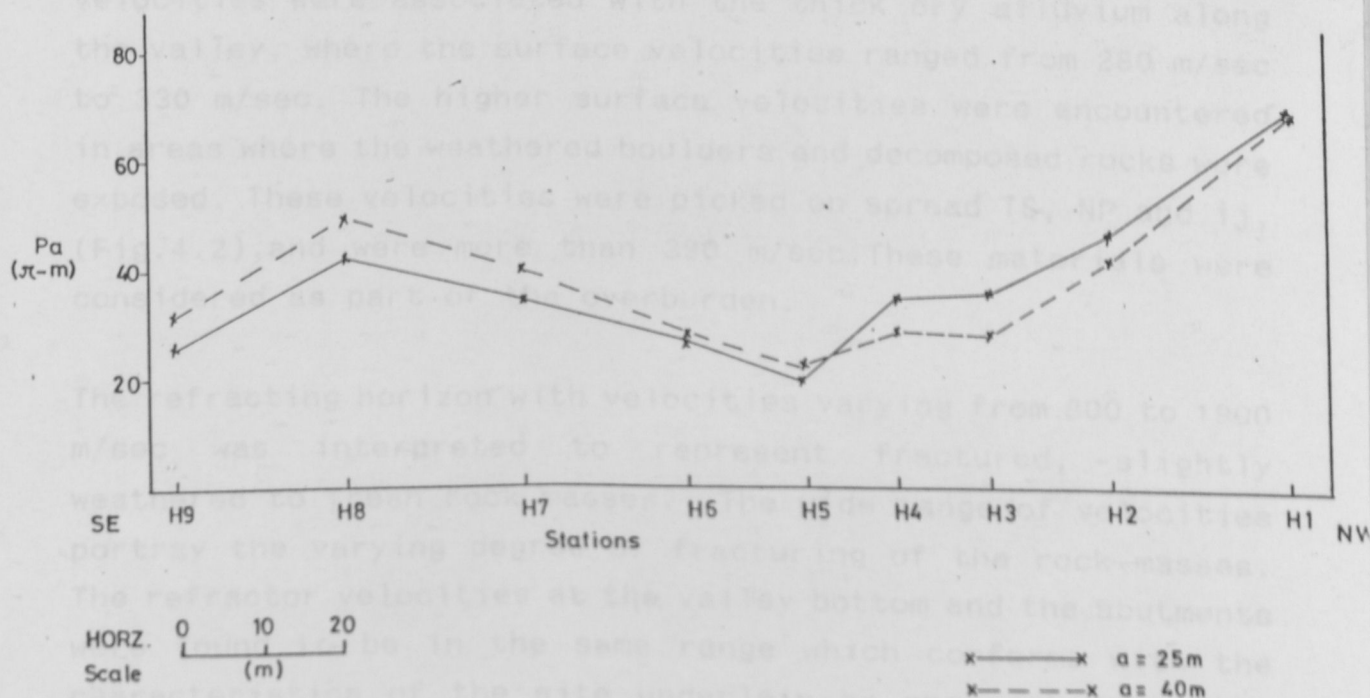


Fig 5.4 RESISTIVITY PROFILE WITH WENNER SPREAD A CROSS THE DAM-AXIS.
SEPARATION $a=25$ m, $a=40$ m.

CHAPTER 6GEOLOGICAL INTERPRETATIONS OF THE RESULTS6.1 Seismic Refraction

The low velocity surface layer was interpreted to represent dry soils occurring with weathered boulderly rocks. These were directly overlying the hard rock, (bedrock). The extremely low velocities were associated with the thick dry alluvium along the valley, where the surface velocities ranged from 280 m/sec to 330 m/sec. The higher surface velocities were encountered in areas where the weathered boulders and decomposed rocks were exposed. These velocities were picked on spread TS, NP and ij, (Fig.4.2), and were more than 390 m/sec. These materials were considered as part of the overburden.

The refracting horizon with velocities varying from 800 to 1900 m/sec was interpreted to represent fractured, slightly weathered to fresh rock masses. The wide range of velocities portray the varying degree of fracturing of the rock masses. The refractor velocities at the valley bottom and the abutments were found to be in the same range which conforms with the characteristics of the site underlain by one rock type. The interpretation therefore postulated that extensive fracturing and not variation of the rock properties was the dominant factor that explains the seismic velocities.

Fig 6.1 shows the interpreted depth section of the interface between the overburden and the irregular bedrock along the longitudinal axis of the dam. Shallow depths to the refractor and high refractor velocities between stations k and q are associated with fresh rocks near the surface.

The valley is constricted at this section, (Fig 4.2) with fresh rocks and boulders extending next to the stream course. The visible surface topography of the dam axis. This postulates Lateral change in seismic velocity between station k and j coincided with a deepening of the surface layer between the two stations. The abrupt contrast between the deeper downstream section and the shallower upstream section was suspected to be caused by a minor fault. The fault could be correlated with the similar deepening of the surface layer in the profiles along BH1, (Appendix A.3). The fault assumes a NNW-SSE direction with a downthrow to the east. Similar deepening of the surface layer on the downstream section was encountered between stations u and q which are next to the scarp on the western side of the dam site, (Fig 4.2).

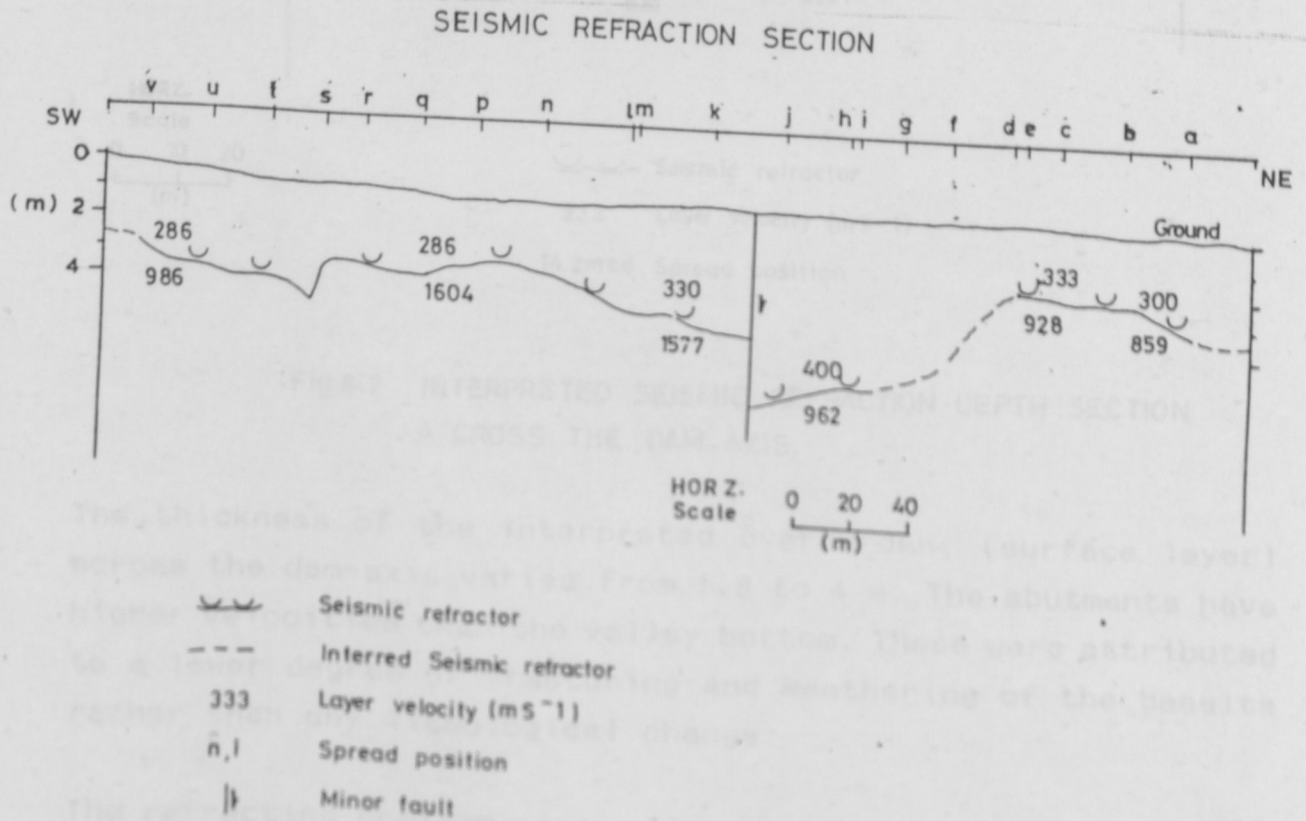


Fig 6.1 INTERPRETED SEISMIC REFRACTION DEPTH SECTION ALONG THE RIVER COURSE PROFILE

Fig 6.2 shows the interpreted depth section across the dam axis. The buried refracting horizon follows extrapolation of the visible surface topography of the dam-axis. This postulates an even surface weathering of the basalts to about the same depths.

SEISMIC REFRACTION SECTION

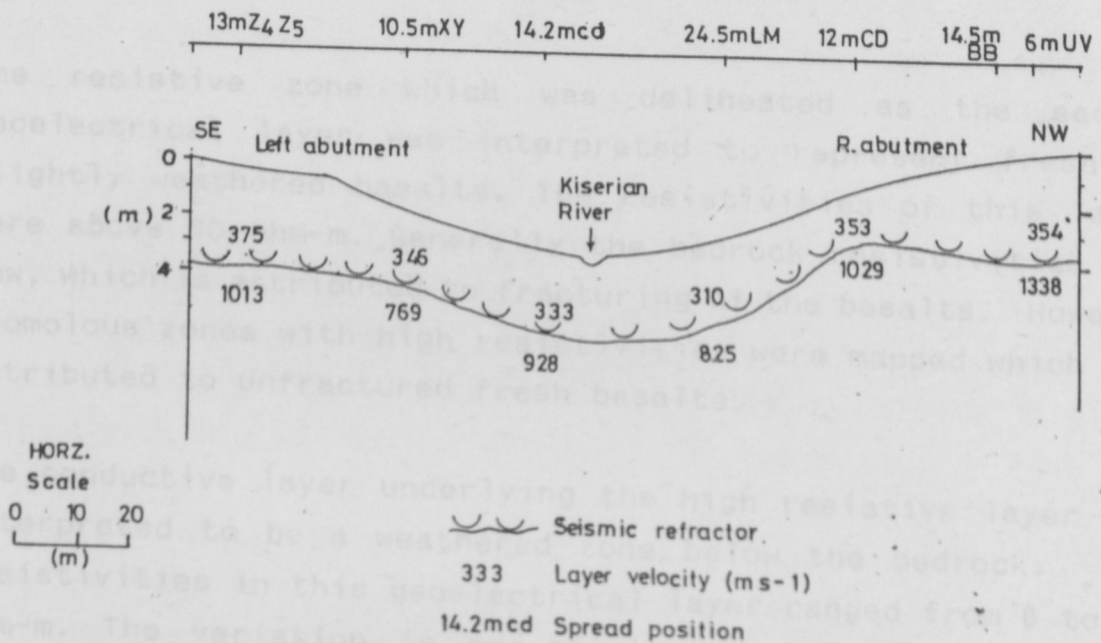


Fig 6.2 INTERPRETED SEISMIC REFRACTION DEPTH SECTION A CROSS THE DAM-AXIS.

The thickness of the interpreted overburden, (surface layer) across the dam-axis varies from 1.8 to 4 m. The abutments have higher velocities than the valley bottom. These were attributed to a lower degree of fracturing and weathering of the basalts rather than any lithological change.

The refracting horizon across the dam-axis was constructed by joining the refractor-depths obtained from the positions where the refraction profiles crossed the dam-axis, (Fig 4.2).

6.2.1 River Course

Fig 6.3 shows the interpreted geoelectrical cross-section drawn along the river course profile. This section reveals four geoelectrical layers decreasing to the three at the SW limits of the profile.

Interpreted resistivities suggest a top layer of clays, which is the conductive zone. This attained a maximum depth of 5.2 m at S18, but the average depth along this profile is 1.3 m. Apparently this geoelectrical layer is controlled by topographical depression as the deepest zones were encountered only where deep clays covered a depression. The resistivities along this profile also reflect variations in soil moisture, due to the infiltration of the water from the stream. The interpreted resistivities of 4 to 11 ohm-m in this layer are therefore attributed to wet clays. Transitional zone with resistivities of 20 to 22 ohm-m were evident at D5 and S15. These correspond to the resistivities of the boulderly surfaces on the abutments. Hence they were attributed to boulders and weathered rock masses within the overburden.

The second geoelectrical layer was interpreted to be the resistive zone with resistivities ranging from 52 to 123 ohm-m. This was associated with the bedrock. This layer was encountered between depths of 1.1 to 17 m. The resistivity variations were attributed to the degree of fracturing of the rock mass which varied from slightly to highly fractured.

The third layer is characterized by resistivities of 6 to 28 ohm-m. This was attributed to highly weathered rock mass resulting in clays (residual soils) which contributed to the low resistivities. The layer is thin upstream at depths of 25 m but becomes thick downstream.

GEOELECTRICAL SECTION

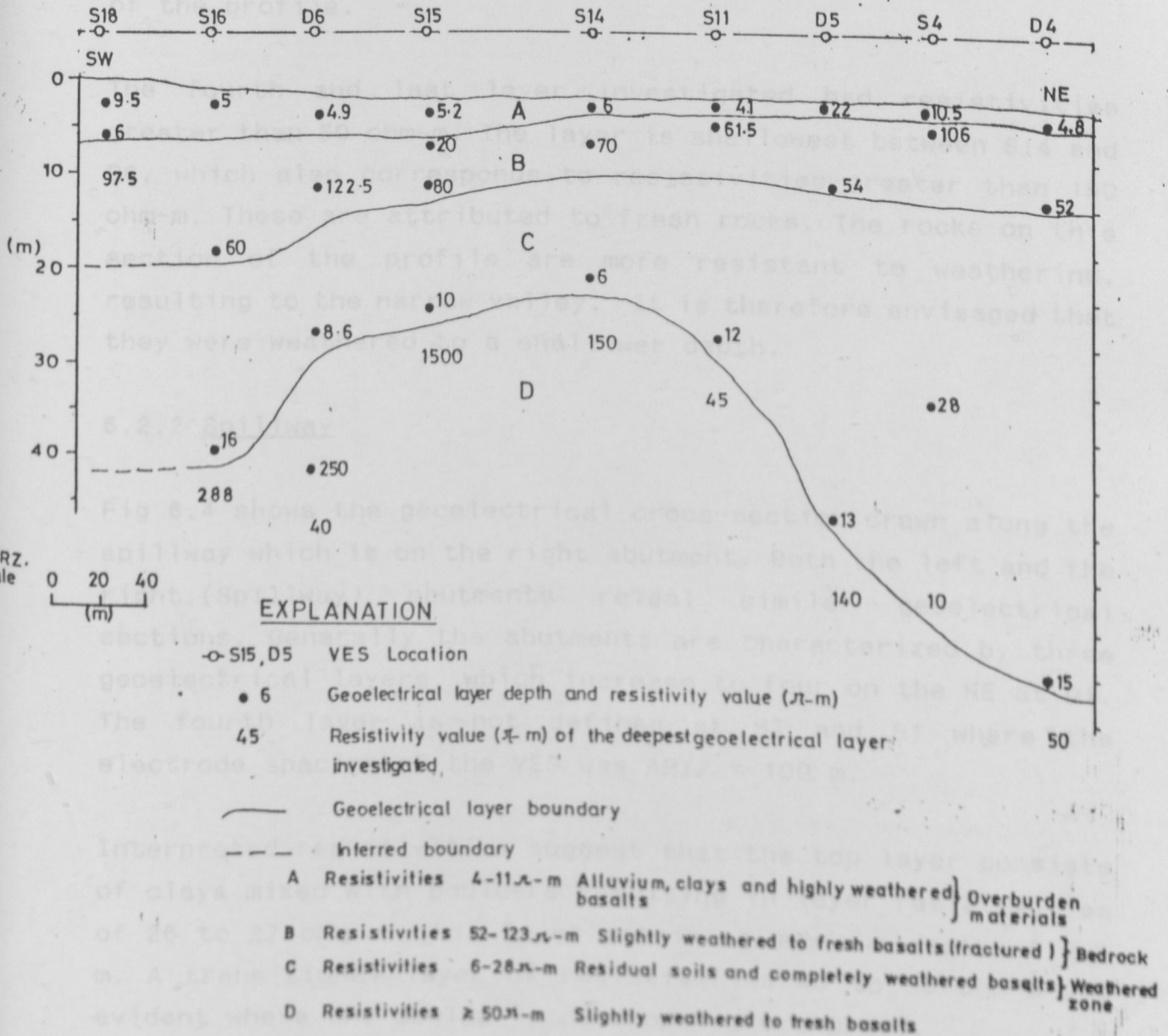


Fig 6.3 INTERPRETED GEOELECTRICAL CROSS SECTION ALONG THE RIVER COURSE PROFILE

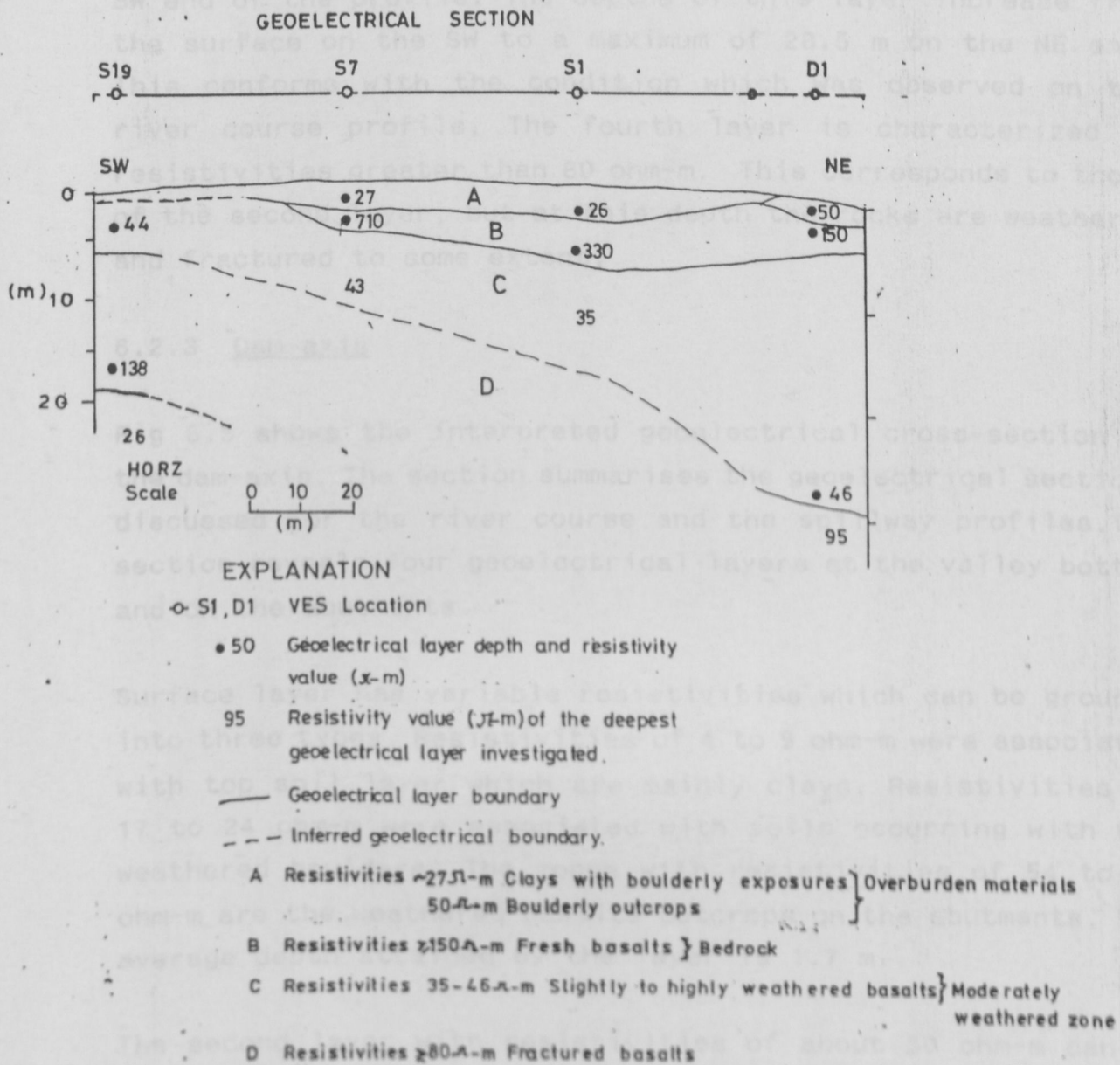


Fig 6.4 INTERPRETED GEOELECTRICAL CROSS SECTION ALONG THE SPILLWAY PROFILE

This layer appears as the second geoelectrical layer on the SW end of the profile. The depths of this layer increase from the surface on the SW to a maximum of 28.5 m on the NE end. This conforms with the condition which was observed on the river course profile. The fourth layer is characterized by resistivities greater than 80 ohm-m. This corresponds to those of the second layer, but at this depth the rocks are weathered and fractured to some extent.

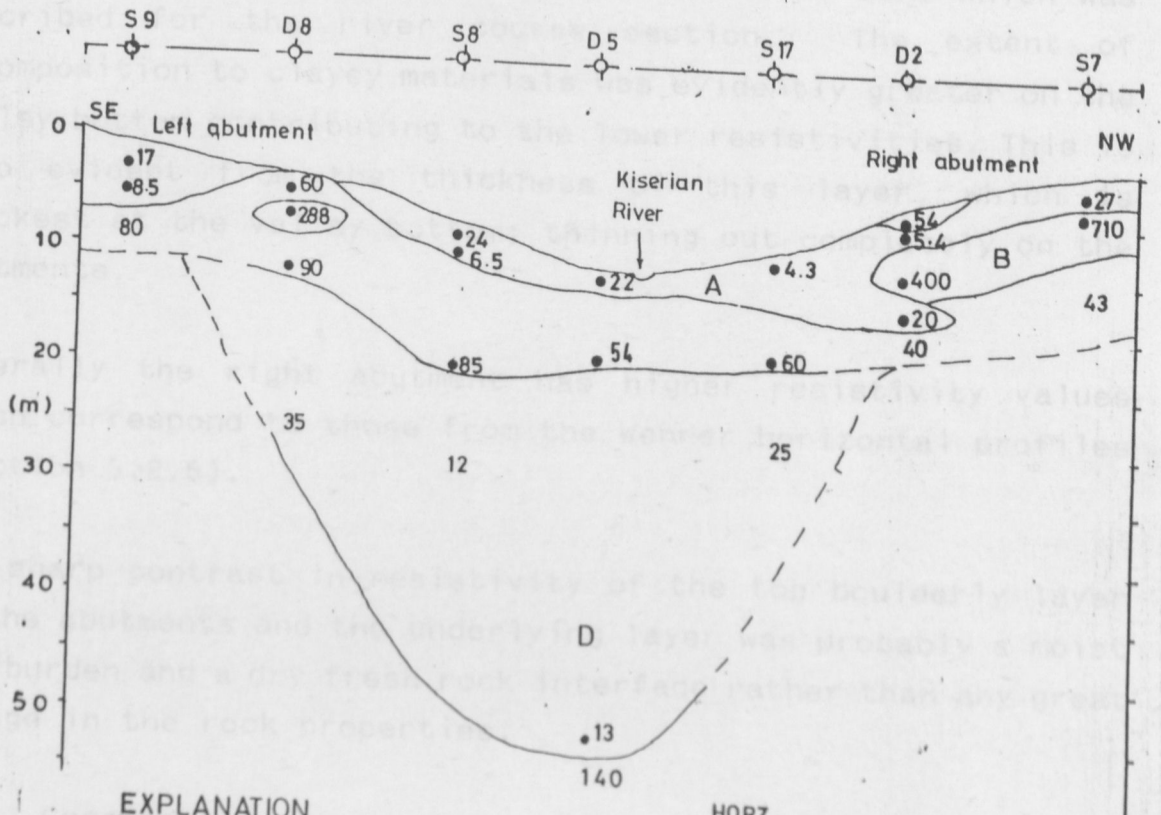
6.2.3 Dam-axis

Fig 6.5 shows the interpreted geoelectrical cross-section of the dam-axis. The section summarises the geoelectrical sections discussed for the river course and the spillway profiles. The section reveals four geoelectrical layers at the valley bottom and on the abutments.

Surface layer has variable resistivities which can be grouped into three types. Resistivities of 4 to 9 ohm-m were associated with top soil layer which are mainly clays. Resistivities of 17 to 24 ohm-m were associated with soils occurring with the weathered boulders. The zones with resistivities of 54 to 60 ohm-m are the weathered basalts outcrops on the abutments. The average depth attained by the layer is 1.7 m.

The second layer with resistivities of about 60 ohm-m can be associated with the slightly weathered and fractured rocks exposed at the abutments. A lensoidal layer of high resistivities which are greater than 280 ohm-m was delineated on the abutments. This was attributed to fresh rocks which are not fractured. The third layer had predominantly low resistivities, which range from 12 ohm-m, on the valley bottom to about 30 ohm-m on the abutments.

GEOELECTRICAL SECTION



EXPLANATION

○ S8, D2 VES Location

• 54 Geoelectrical layer depth and resistivity value (Ω -m)

43 Resistivity value (Ω -m) of the deepest geoelectrical layer investigated.

— Geoelectrical layer boundary

- - - Inferred boundary

A Resistivities 4-9 Ω -m Alluvium and clays (top soils)
 17-24 Ω -m Clays with boulders
 54-60 Ω -m Weathered basalts exposures } Over burden materials

B Resistivities $\geq 300 \Omega$ -m Fresh basalts

C Resistivities 60-90 Ω -m Slightly weathered to fresh basalts (fractured) } Bedrock

D Resistivities 12-30 Ω -m Residual soils and completely weathered basalts } Weathered zone

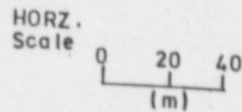


Fig 6.5 INTERPRETED GEOELECTRICAL CROSS SECTION ACROSS DAM AXIS

These were attributed to the highly weathered zone which was described for the river course section. The extent of decomposition to clayey materials was evidently greater on the valley bottom contributing to the lower resistivities. This is also evident from the thickness of this layer, which is thickest at the valley bottom; thinning out completely on the abutments.

6.3.1 River course

Generally the right abutment has higher resistivity values which correspond to those from the Wenner horizontal profiles (section 5.2.5). The top soil layer consists of black cotton soils. Their depths range from 0.6 to 2 m. The test-boreholes were The sharp contrast in resistivity of the top boulderly layer at the abutments and the underlying layer was probably a moist overburden and a dry fresh rock interface rather than any great change in the rock properties.

6.3 Core Logs

The geological boundaries were delineated by the degree of weathering, (Appendix D) owing to the fact that the dam-site was covered by one formation (Ngong basalts). In all the core samples from the site, a thin layer of black cotton soil was recovered, attaining a maximum depth of 2.0 m, but with average depths of 1 m. The soils were underlain by highly weathered broken rocks. These vary from boulderly to highly fractured rocks which were clay filled, on the fracture surfaces.

The fresh basalts occur as slightly to highly fractured rocks. Fractures were horizontal, sub-vertical and vertical but did not show any continuity. Slight weathering was visible along the fracture surfaces discolouring the adjacent rock masses.

The basalt formation was completely weathered in the deeper zones resulting to a completely weathered zone, moderately to slightly weathered zone and residual soils. The top basalt flow is underlain by an agglomerate layer which was subsequently deposited above an earlier basaltic flow. Core logging results are given in the next sections.

6.3.1 River course

Fig 6.6 shows the geological cross-section along the river course. The top soil layer consists of black cotton soils. Their depths range from 0.6 to 2 m. The test-boreholes were bored next to the river course and the infiltrating water rest level from the stream was found to coincide with the interface of the top soils and the highly weathered basalts, (Section 2.5).

The highly weathered basalts layer was deeper upstream (5 m) and shallowest at the dam-axis (2.4 m). These were underlain by the fresh basalts zone. The fresh basalts occur as slightly fractured rocks with slight alterations along the fracture surfaces. The fresh basalts zone is thickest upstream (4.6 m) narrowing to 1 m downstream. A uniform zone of completely weathered basalts underlies the fresh basalts. The thickness of the latter zone increases from 2.6 m upstream to 4.7 m downstream, with an average depth of 9 m from the surface.

An agglomerate layer underlies the completely weathered zone. This has a thickness of 4.4 m upstream increasing to 7.9 m downstream. Generally the lower surface of the agglomerate layer is sloping downstream, which corresponds with the general direction of dip. The agglomerate layer is underlain by a residual soil zone which ranges from 5.7 m thick, upstream to 0.7 m thick, downstream.

Fig 6.6

Geological cross-section

along the river course

Fig 6.6 GEOLOGICAL CROSS-SECTION ALONG THE RIVER COURSE

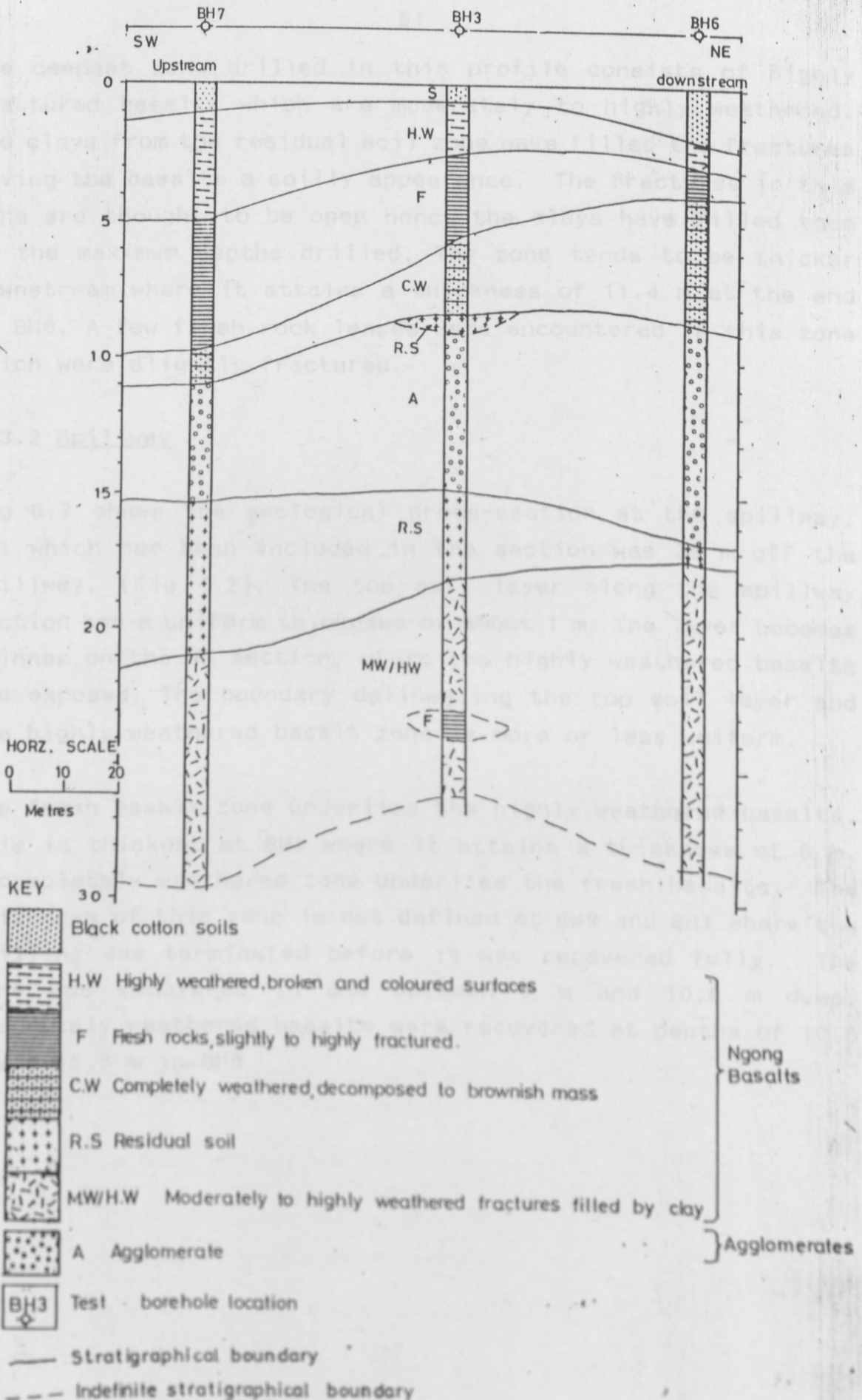


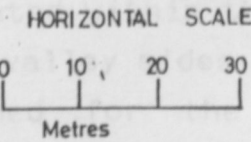
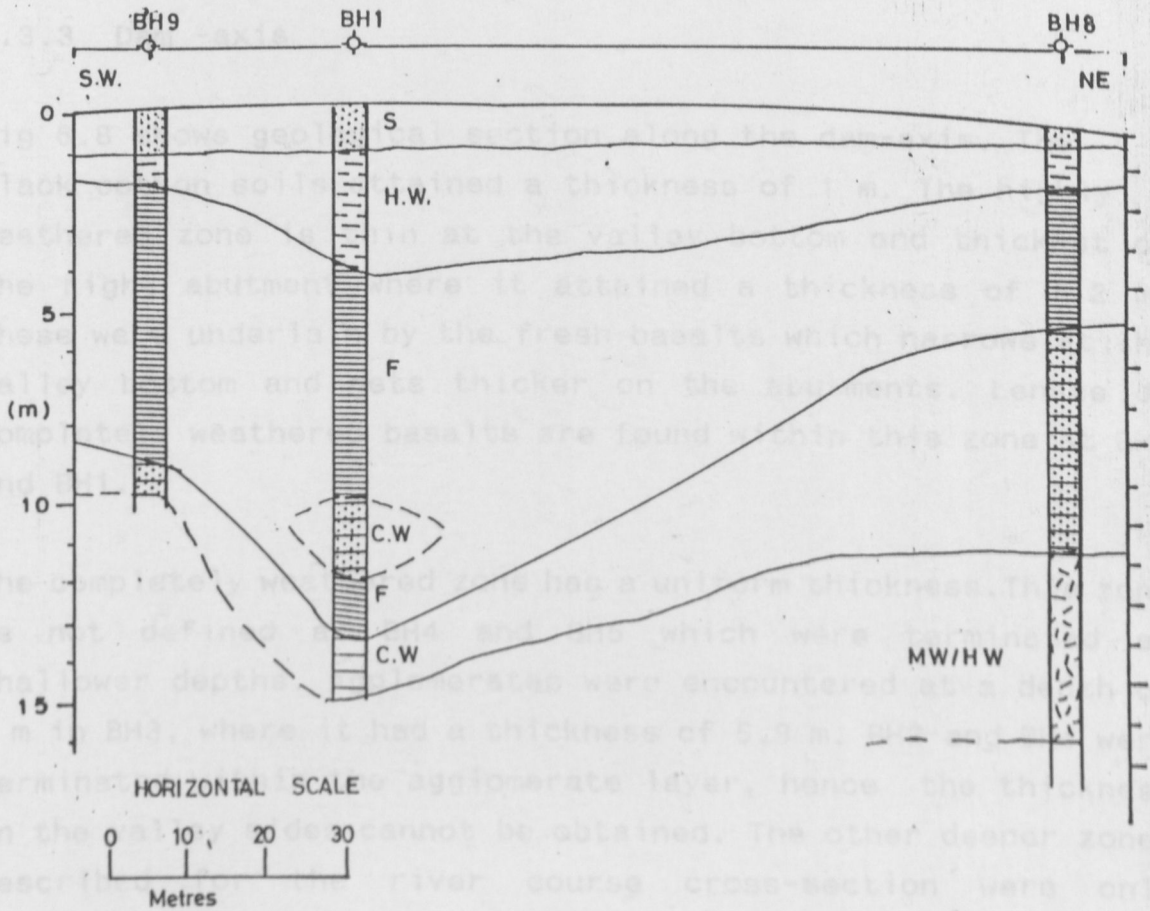
Fig 6.6 GEOLOGICAL CROSS-SECTION ALONG THE RIVER COURSE

The deepest zone drilled in this profile consists of highly fractured basalts which are moderately to highly weathered. The clays from the residual soil zone have filled the fractures giving the basalts a soilly appearance. The fractures in this zone are thought to be open hence the clays have filled them to the maximum depths drilled. The zone tends to be thicker downstream where it attains a thickness of 11.4 m at the end of BH6. A few fresh rock lenses were encountered in this zone which were slightly fractured.

6.3.2 Spillway

Fig 6.7 shows the geological cross-section at the spillway. BH1 which has been included in the section was 32 m off the spillway, (Fig 4.2). The top soil layer along the spillway section has a uniform thickness of about 1 m. The layer becomes thinner on the NE section, where the highly weathered basalts are exposed. The boundary delineating the top soil layer and the highly weathered basalt zone is more or less uniform.

The fresh basalt zone underlies the highly weathered basalts. This is thickest at BH1 where it attains a thickness of 6 m. A completely weathered zone underlies the fresh basalts. The thickness of this zone is not defined at BH9 and BH1 where the drilling was terminated before it was recovered fully. The zone was recovered in BH8 between 5 m and 10.8 m deep. Moderately weathered basalts were recovered at depths of 10.8 m and 15.5 m in BH8.



KEY

-  Black cotton soils
 -  H.W. Highly weathered, broken and coloured surfaces
 -  F Fresh rocks, slightly to highly fractured.
 -  C.W. Completely weathered, decomposed to brownish mass.
 -  R.S. Residual soil
 -  MW/HW Moderately to highly weathered fractures filled by clays.
- } Ngong Basalts
-  BH9 Tested borehole location
 - Stratigraphical boundary
 - - - Indefinite stratigraphical boundary

Fig 6.7 GEOLOGICAL CROSS-SECTION ALONG THE SPILLWAY

6.3.3 Dam -axis

Fig 6.8 shows geological section along the dam-axis. The black cotton soils attained a thickness of 1 m. The highly weathered zone is thin at the valley bottom and thickest on the right abutment where it attained a thickness of 4.2 m. These were underlain by the fresh basalts which narrows at the valley bottom and gets thicker on the abutments. Lenses of completely weathered basalts are found within this zone at BH5 and BH1.

The completely weathered zone has a uniform thickness. This zone is not defined at BH4 and BH5 which were terminated at shallower depths. Agglomerates were encountered at a depth of 9 m in BH3, where it had a thickness of 5.9 m. BH2 and BH4 were terminated within the agglomerate layer, hence the thickness on the valley sides cannot be obtained. The other deeper zones described for the river course cross-section were only recovered in BH3 which was drilled to a depth of 26 m.

6.4 Correlation of Geoelectrical and Geological Sections

Geological core-logs were used as a control to correlate the various geological zones with the geoelectrical layers. A comparison between the lithostratigraphical column and interpreted resistivity curve (D5) next to BH3 is shown as an example. A logarithmic depth scale of the core-log is used to show which lithological layers were resolved for different geoelectrical layers, (Fig 6.9).

The depths of the various lithotypes are given in metres along the column. The abbreviations used (S, H.W, F, A, C.W and R.S) are as explained in the geological cross-section shown in Fig 6.6.

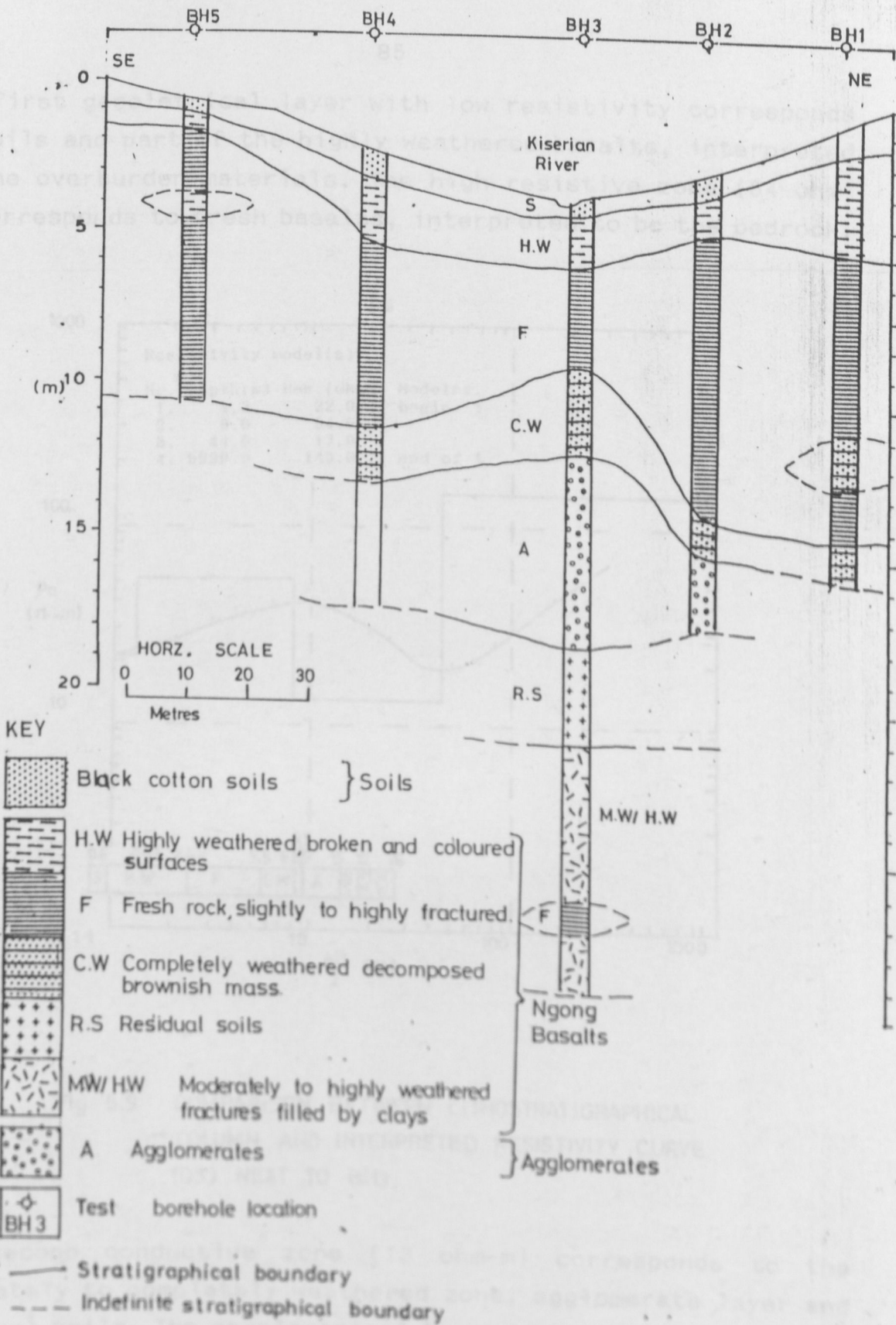


Fig 6.8 GEOLOGICAL CROSS-SECTION ACROSS THE DAM-AXIS

The first geoelectrical layer with low resistivity corresponds to soils and part of the highly weathered basalts, interpreted as the overburden materials. The high resistive zone (54 ohm-m) corresponds to fresh basalts, interpreted to be the bedrock.

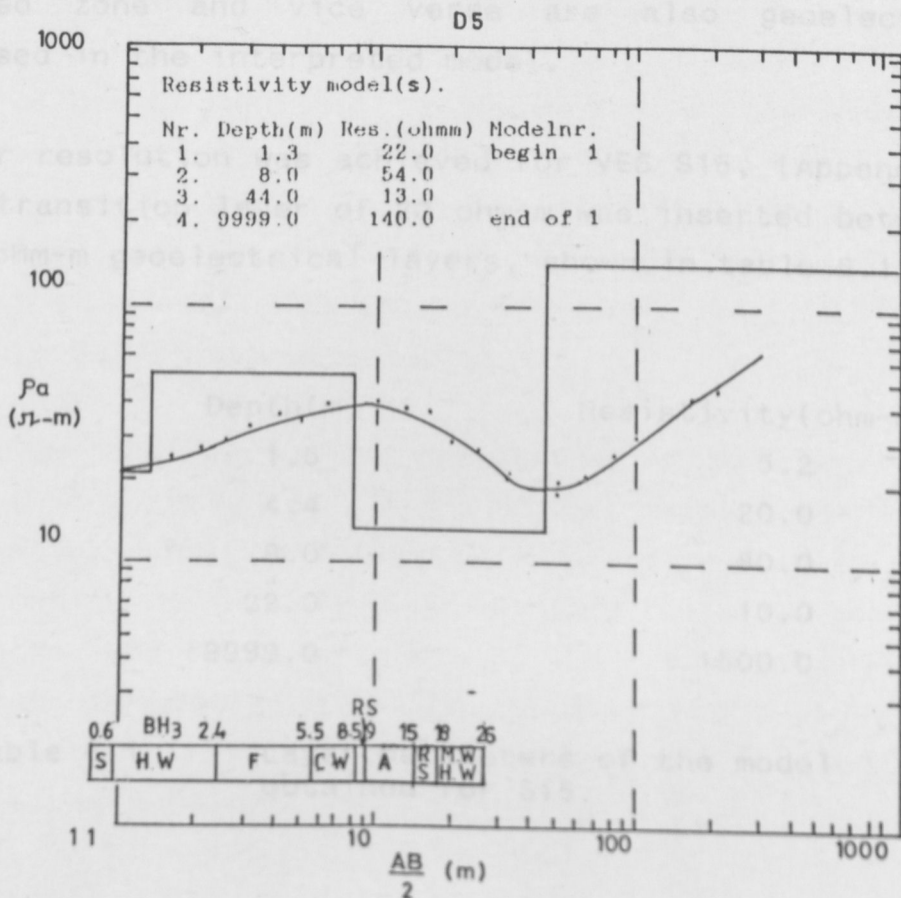


Fig 6.9 COMPARISON BETWEEN LITHOSTRATIGRAPHICAL COLUMN AND INTERPRETED RESISTIVITY CURVE (D5) NEXT TO BH3.

The second conductive zone (13 ohm-m) corresponds to the moderately to completely weathered zone, agglomerate layer and residual soils. The geoelectrical layer boundary for this layer extends up to 44 m, but the drilling was terminated at 26 m.

The relative thicknesses of geological zones in the latter geoelectrical layer are small as compared to their depth of burial. This restricted their individual resolution, hence they were geoelectrically resolved as one layer of resistivity 13 ohm-m. The thin lenses of the fresh basalts within the highly weathered zone and vice versa are also geoelectrically suppressed in the interpreted model.

A better resolution was achieved for VES S15, (Appendix B.5) when a transition layer of 20 ohm-m was inserted between 5.2 and 80 ohm-m geoelectrical layers, shown in table 6.1.

Layer	Depth(m)	Resistivity(ohm-m)
1	1.5	5.2
2	4.4	20.0
3	8.0	80.0
4	22.0	10.0
5	9999.0	1500.0

Table 6.1 Layer parameters of the model obtained for S15.

The model corresponds with the initial interpretation of a top clayey layer of resistivity 5.2 ohm-m reaching a depth of 1.5 m. Then highly weathered basalts (20 ohm-m) to a depth of 4.4 m. The resistive layer with resistivities of 80 ohm-m is the fresh basalts which comprise the bedrock. This extends to a depth of 8 m. The bedrock is underlain by residual soils, completely weathered basalts and agglomerates, which were resolved as one geoelectrical layer of 10 ohm-m.

The relative thicknesses of geological zones in the latter geoelectrical layer are small as compared to their depth of burial. This restricted their individual resolution, hence they were geoelectrically resolved as one layer of resistivity 13 ohm-m. The thin lenses of the fresh basalts within the highly weathered zone and vice versa are also geoelectrically suppressed in the interpreted model.

A better resolution was achieved for VES S15, (Appendix B.5) when a transition layer of 20 ohm-m was inserted between 5.2 and 80 ohm-m geoelectrical layers, shown in table 6.1.

Layer	Depth(m)	Resistivity(ohm-m)
1	1.5	5.2
2	4.4	20.0
3	8.0	80.0
4	22.0	10.0
5	9999.0	1500.0

Table 6.1 Layer parameters of the model obtained for S15.

The model corresponds with the initial interpretation of a top clayey layer of resistivity 5.2 ohm-m reaching a depth of 1.5 m. Then highly weathered basalts (20 ohm-m) to a depth of 4.4 m. The resistive layer with resistivities of 80 ohm-m is the fresh basalts which comprise the bedrock. This extends to a depth of 8 m. The bedrock is underlain by residual soils, completely weathered basalts and agglomerates, which were resolved as one geoelectrical layer of 10 ohm-m.

6.5 Discussion of Results

One problem inherent in all geophysical studies is the ambiguity of any particular geological model to a set of field data. The source of the problem is that geophysical techniques measure physical properties of the earth from the surface to obtain the subsurface information. Several different combinations of earth materials can give the same signal at the surface. Hence geological information from other sources is useful in quantitative interpretation of the data. Geophysical techniques also have a limitation in that the equipments used have their own allowed degree of error. This applies also to the methods of interpretation.

The seismic refraction and resistivity methods which were used in this study have their own setbacks which were discussed in chapter 4. The core-logging also presented a problem in establishing accurately the boundary between the boulderly overburden and the upper parts of the fractured fresh basalts. Therefore the decision making required the evaluation of the quality of the results in the light of all the geological and geophysical results.

The Core-logs were used as a control in the interpretation of the VES and seismic refraction data in terms of stratified layers of definite thicknesses. The results from the three methods were correlated to delineate the overburden from the bedrock, which would be the foundation of the dam.

Table 6.2 summarises the results of the depth to the bedrock of seismic refraction and resistivity soundings next to eight test-boreholes.

Borehole No	Core log Depth(m)	Seismic refraction travel Depths(m)	Geoelectr. layer Depth (m)
BH1	4.2	1.8	2.1
BH2	2.0	2.9	1.2
BH3	2.4	2.6	1.3
BH4	3.2	2.8	2.7
BH5	1.0	3.3	1.2
BH6	3.0	3.0	1.2
BH7	5.0	5.0	1.1
BH9	2.0	3.2	3.4

Table 6.2 Summary of the core logging, seismic refraction and resistivity sounding results of the depth to the bedrock.

The depths of the bedrock obtained from drilling agree with the seismically determined depths at BH6 and BH7. Those of BH3 and BH4 are within the expected uncertainty of $\pm 15\%$ of the seismic refraction method. Differences indicate the complex nature of the bedrock surface which is characterized by boulderly rocks, fractured and weathered surfaces. This was too variable to be resolved accurately by the seismic refraction method. Hatherly et al. (1986) points out that variations in refractor depths can also be caused by travel-time errors, unmapped near surface velocity variations and errors inherent in the conventional interpretation method. Furthermore the refraction depths must vary smoothly to define the boundary properly. This should dissuade users of the results from measuring depths with high precision.

It was difficult to establish the exact boundary between the boulders and the surface of the highly fractured bedrock during the core-logging. The rocks on the top surface of the bedrock occurred as broken pieces. These resembled the discrete boulders in the overburden materials, hence there was no clear distinction between the two.

The above limitation was borne in mind when comparing results from drilling and refraction. In the refraction method, the dry loose materials on the surface layer constituted a problem in determining their velocities. The velocities in this layer were low and relatively small variation in thickness influenced the recorded times. Owing to the fact that the site is underlain by the same formation, the velocities of the surface layer increased uniformly until the fresh basalt zone (refracting horizon) was reached. Hence the refractor-depths were affected by all these factors.

Refraction results are consistent with the drilling results between BH6 and BH7, (Fig 4.2) at the valley bottom. Here the surface is even and not boulderly, hence the refractor was well resolved. The results allowed interpolations of bedrock depths between drill holes with much more confidence than would have been otherwise possible. The boundary of the refracting layer can therefore be used as a basis for estimation of excavation depth of the dam foundation. At this depth, the basalts are slightly to highly fractured and the foundation would require treatment.

Comparison of the core-logs and geoelectrical results in table 6.2 show that the geoelectrical boundaries coincide with core-log boundaries only where there is pronounced change in texture at the boundary. Such contrasts of soils and the hard rock were observed at BH4 and BH5. The geoelectrical boundaries of the bedrock compare well with the refractor depths at BH1, BH4 and BH9 which are on the abutments. Hence the results of the shallow seismic refraction and drilling can be used as the basis for estimation of the required depths of excavation on the valley bottom. The geoelectrical and refractor-depths can guide in excavation depths on the abutments.

The valley bottom is filled by deposits of varying composition. Such surface deposits generally vary in their electrical conductivities because of heterogeneity, variable moisture conditions, and the effects of weathering and erosion. Hence the resistivity results realised at the valley bottom are characteristic of such terrains. Taking into consideration that the least depth of the first geoelectrical layer that can be resolved is 1 m, the results in table 6.3 show that the top soils were well defined by the resistivity method.

Borehole No.	Core log Depth(m)	First Geoelectrical layer Depth(m)
BH1	1.0	1.5
BH2	0.8	1.2
BH3	0.6	1.3
BH4	1.0	1.4
BH5	0.5	1.2
BH6	2.0	1.2
BH7	1.0	1.1
BH8	0.3	1.0
BH9	1.2	3.4

Table 6.3 Summary of the first geoelectrical layer depths and top soil depths obtained from the core logs of nine test-boreholes.

The correlation of the geoelectrical layer depths and drilling lithostratigraphical depths have shown that the former are deeper than the latter. This could be attributed to the effect of anisotropy. Soundings conducted over gently sloping beds such as the lava flows in the area result in large measured resistivities than the longitudinal resistivity by a ratio equal to the coefficient of anisotropy, (Keller et al, 1982).

Consequently, the interpreted thicknesses are greater by the same ratio as observed in the comparison, shown in Table 6.3. This study aimed at delineating the conductive overburden from the resistive bedrock, hence the anisotropy investigations which require a number of cross spreads at every station, (Matias M.J.S. et al 1986) was not necessary.

A minor fault with a downthrow to the east is eminent between spread k and j of the seismic refraction surveys. This had a NNW-SSE trend which is parallel to the major fault west of the dam site. The depression observed between stations u and q, (Fig.4.2), is suspected to be the surface manifestation of the fault. The throw is to the east, but the present data could not furnish enough information to determine the amount of throw.

The abutments are covered by lava boulders ranging from continuous boulder cover to shallow dark soils. Dark soils cover the basalts formation at the valley bottom. Resistivity profiling results indicate uniform characteristics of the bedrock between 4 m and 10 m below the dam-axis surface. The basalts forming the bedrock extend to a depth of about 9 m. Agglomerates occur at depths of 9 to 11 m below the valley bottom.

The lithostratification at the dam site obtained from the core-logs show that a basaltic lava flow was the first to be deposited. Fractures resulted from contraction during the cooling and crystallization of the lavas. The fractures in this zone are continuous, therefore described as open fractures. Quiescence of the volcanic activity allowed sufficient duration to enable processes of weathering to proceed. This resulted in the moderately and highly weathered zone (Fig 6.6).

Decomposition and disintegration occurred on the top surface resulting in the residual soils zone. The infiltrating waters carried the soils downward into the open fractures filling them as observed in the lower zone.

These were followed by deposition of volcanic debris of varying fragment sizes. These consolidated as an agglomerate bed with no joints or cracks of consequence. The surface weathering of the agglomerates is very slight indicating short time lapse before the deposition of a later basaltic lava; which forms the bedrock at the site. The relatively water retentive agglomerate bed might have inhibited downward water passage to deeper zones resulting in accumulation of water which facilitated weathering of the lower surface of the latter basalts. This resulted in the completely weathered zone and lenses of residual soils above the agglomerate zone.

The weathered zone above the agglomerates would have been the upper aquifer but the constituent materials were found to be only moist. It is envisaged that the infiltrating water flows on the surface of the agglomerates, since the layer dips downstream. The lower zone of moderately to highly weathered basalts, (Fig 6.6) is also a possible aquifer. The fractures at this depth are open (discussed earlier) and it is thought that the groundwater flows to deeper layers.

The drilling investigations did not strike any zone containing water. The information from the well data in the Kiserian area show that the main aquifers are struck at depths greater than 40 m. It is therefore, envisaged that the conductive zones extending to depths, greater than 44 m are possible aquifers.

CHAPTER 7

EVALUATION OF THE DAM SITE IN TERMS OF GEOLOGY

The investigations have shown that the dam site is made up of only one lithotype - the Ngong Basalts. However fresh basalts which compose the bedrock are overlain by overburden materials consisting of dark soils, boulderly rocks and weathered basalts. These contribute to varying overburden thickness at the site. Therefore the excavation depths to the foundation will vary from point to point. The removal of unreliable overburden material at the dam site may subject the foundation rock mass to rebound. The problem of rebound is dependent on the modulus of elasticity of the rocks concerned, the number of rock types involved and their permeability. Each rock type has a characteristic modulus of elasticity. At the Kiserian dam site, the foundation consists of one rock type and the aspect of differential rebound therefore is lessened. To counteract the heave, the dam should impose a load on the foundation equal to or slightly in excess of the load removed, (Bell, 1980). This aspect should be put into consideration during the design.

The stratigraphy at the dam site showed a weak zone of weathered material in the sequence of the basalt flow. This is of particular significance as regards the stability of the dam in respect to sliding. Weathered zones which are reduced to clays tend to be slippery under the foundation. Removal by erosion of the rock supporting the heel of the dam on a slippery part of the foundation; and presence of percolating water under the base of the dam may lead to collapse of the dam.

The investigations showed that the foundation bed is fractured to varying degrees. The presence of flat lying fractures may destroy much of the inherent shear strength of a rock mass. This may reduce the resistance of the foundation to horizontal forces, to one of sliding friction. In this case the continuity and roughness of fracture surfaces is a critical factor. At the Kiserian dam site the fractures were not continuous and they generally formed rough surfaces. However the keying of the dam some distance into the foundation is advisable. This can be done by building a key wall or by providing a cut-off at the heel of the dam. Another alternative would be a grout curtain keyed to the impervious agglomerate bed below the foundation. Another method of reducing sliding is to design the dam with a downward slope, to the base of the dam in the upstream direction of the valley.

Owing to the extensive fracturing of the basalts, the question of permeability of the foundation becomes of prime importance. Percolation of water through the foundation can remove filler materials which may be filling fractures which in turn can lead to differential settlement of the foundation. Percolation of water may also open fractures thus decreasing the strength of the rocks. Water tightness is essential to ensure that no water escapes. Any steady flow through a solid rock formation is bound to have some erosive action, which might gradually intensify the defective conditions causing the original leakage.

Another problem which might result from leakage of water between rock surface and dam structure is the uplift pressure. Uplift pressure acts against the base of the dam and is caused by water seeping beneath it, under hydrostatic head from the reservoir.

It might therefore be necessary to reduce the permeability of the foundation bed depending on the water pressure tests, (Appendix C). Seepage rates can be lowered by reducing the hydraulic gradient beneath the dam. This can be achieved by incorporating a cut-off into the design. An impervious earth fill against the lower part of the upstream face of the dam can also effectively reduce seepage.

Another aspect which is a fundamental factor in dam design is the pore water pressure. The pore water pressure within foundation materials is a variable force which acts in all directions and affects the engineering performance of the rocks. Variations in pore pressure cause changes in the state of stress in rock masses. Pore water in the stratified rocks of a dam foundation reduces the coefficient of friction between individual beds and between the foundation and the dam. Increase of pore pressure may lift beds and the dam itself and so decrease the shearing strength and resistance to sliding within the rock masses. Therefore an estimation of the pore water pressure is an essential factor. This should be done elsewhere and incorporated in the design of the dam.

Leakages from the reservoir are also associated with exposure of fractured underlying rocks or major defects in the geological structure such as faults. When filling the reservoir there is a possibility that the superficial material may be ruptured or partially removed exposing the underlying rocks. This may result in large and essentially localized flows taking place. Remedial measure to avert leakage problem is by sealing the reservoir lining in the first instance. Treatment such as cut-offs and blankets of impermeable material can control losses within acceptable amounts.

The formation of a reservoir will upset the groundwater regime and obstruct the water flowing downstream. At the dam site, the water table is below the foundation bed. Groundwater recharge will give rise to a changed hydrogeological environment as the water table rises. Some rocks which formerly were not within the zone of saturation may then become unstable and fail, as saturated material is weaker than unsaturated. This can lead to slumping and sliding on the flanks of the reservoir. In such instances, the impermeability of the reservoir floor is important. Seepage in such cases can be controlled by clay blankets or layers of silt.

The right abutment is covered by fractured basalts which may require treatment to prevent seepage. Flare of the dam at the right abutment would also provide large impervious contact.

Within the reservoir area, two faults were mapped which had a general NNE-SSW direction. Leakage along faults generally is not a serious problem as far as reservoirs are concerned, since the length of the flow path is usually too long. The fault mapped on the upstream section of the proposed extent of the embankment is at an angle (transversal) to the longitudinal axis of the dam. Considering that the fault is on the upstream section of the heel of the dam and not parallel to the longitudinal axis, it is thought not to be a major problem. The chances of the fault being re-activated to any measurable extent is slim, because the probability of a given fault moving in the short span of geological time represented by the dam structure is infinitely small.

The major fault mapped west of the dam site is away from the proposed extent of the dam embankment. However the reservoir might extend to the location of the fault. The present study does not furnish enough information to infer on its activity.

The main tributary flowing from the south is controlled by this fault, and the scarps on the valley sides seem to have been cut down by the stream. In places where the stream has meandered off the fault trend, the scarps have been eroded down. Hence no present activity of the fault is visible. Occurrence of fault in a river generally implies the material along the fault zone is highly altered. Pressure tests can determine the permeability of the fault zone and the results can be used to recommend on the necessary precautions. The hydrostatic pressure resulting from filling of the reservoir basin can cause removal of loose material from permeable fault zones and thereby accentuate leakage. Permeable fault zones can be grouted or if they are thin, excavated and filled with rolled clay.

Fault breaks occur in association of large and infrequent earthquakes, small shocks, and continuous slippage (fault creep). The nature of dam structures is such that, unless due allowance has been made in design, any movement of the foundation beds may lead to serious structural damage. Earthquakes impart acceleration to the dam which usually increase the effective loading on the dam. Usually an allowance of a horizontal acceleration of one-tenth that of gravity is made for earthquake shocks, (Creager, 1966). Vertical acceleration is neglected.

Although any dam site is subject to earthquake activity, the probability of having earthquakes in some areas is greater than others. The movements in Kiserian area are slight and infrequent. However allowance for seismic forces must be made even for dams founded on the most solid of rock formations, (Lomnitz, 1976).

CONCLUSIONS AND RECOMMENDATIONS8.1 Conclusions

The seismic refraction and resistivity methods have mapped the overburden/bedrock boundary of the dam foundation. Photo-interpretation, geological reconnaissance and core-logs have confirmed the rock formation at the Kiserian dam site.

The dam site is underlain by basalts of fairly uniform composition. Black cotton soils cover the basalts at the valley bottom, while the abutments are covered by continuous boulderly outcrops with shallow dark soils. The thickness of the overburden materials is more or less uniform and follows the surface topography across the dam-axis. The overburden materials on the valley bottom are mainly transported while those on the abutments are autochthonous.

Although the foundation bed at the dam site is uniform, and composed of one formation, it is fractured to varying degrees. The fracturing of the basalts in the bedrock did not show any continuity. However, horizontal, sub-vertical and vertical fractures join at some points constituting some limited openness. The right abutment contain highly fractured boulderly basalts exposed between BH1 and BH2. Seepage can occur in such zones which can exert excessive stress on the structure.

The use of shallow refraction investigation at the dam site was quite effective in mapping out the bedrock. Use of the seismic refraction and resistivity method has provided useful and adequate information to aid in the design of the dam.

During core-boring, advice on the depth to be drilled is valuable, when a crucial layer or zone is reached which needs recovery to unveil its extent.

8.2 Recommendations

It is apparent from the results that excavation of the dam foundation will take the shape of the surface topography. The overburden materials, composed of the black cotton soils and weathered boulderly basalts should be stripped.

The overburden/bedrock interface delineated by the core-logging would be the most appropriate depths to be excavated across the dam-axis. This would be to a depth of 2.4 m at the valley bottom, and a depth of 1.2 m at BH5 (left abutment). On the right abutment, the excavation depth at BH1 should be 2 m to 4 m in order to scale off the loose masses of rocks between BH1 and BH2.

Stripping along the valley bottom (longitudinal-axis of the dam) should be between 2.4 m to 5 m depending on the thickness of the residual soil layer and the unsound weathered rocks.

Grouting on the foundation is recommended in order to seal the open fractures and consolidate the basalt formation to make it act as a monolith under the structure. A cutoff is recommended at the heel of the dam so as to reduce uplift of the base of the dam and increase resistance to sliding. This would also reduce the danger of piping by increasing the length of the path of percolation. A "grout curtain" cut-off should be designed with regard to the results of water pressure tests at BH3 or BH7. This should be keyed on the impermeable agglomerate bed below or deeper.

REFERENCES

- ABEM, Instruction Manual, ABEM Terrameter SAS 300 System; Atlas Copco, Sweden.
- Bell, F.G., 1980. Engineering Geology and Geotechnics, Newnes-Butterworths.
- Berkey, C.P., 1929. Responsibilities of the geologist in Engineering projects. AIME Tech.Pub.;215:P.4.
- Chyba, J., 1986. Some improvements in the interpretation of Vertical Electrical Sounding Curve. Geoph.Prosp.34:913-922.
- Creager, W.P., Justin, J.D. and Hinds, J., 1966. Engineering for dams, Vol.1. General design; John Wiley & Sons Inc.
- Cummings, D. 1979. Computer Program: Determination of depths to an irregular interface in shallow seismic refraction surveys using a pocket calculator; Geoph.44:1987-1998.
- Dobrin M.B, 1976. Introduction to Geophysical Prospecting; Mcgraw-Hill Book Co.Inc.
- Fairburn, W.A., 1963. Geology of the North Machakos-Thika area, Report No 59; Geol.Surv.Kenya.
- Fawzia, A. and Hamid, O.A., 1986. Resistivity measurements for ground water investigations in the Umm Al-aish area of Northern Kuwait; Journ.of Hydrology 88:185-198
- Gardener, L.W; 1939. An aerial plan of mapping subsurface structure by refraction shooting Geoph. 4:247-259
- Gevaerts, E.A.R., 1964. Hydrogeology of the Nairobi area; Technical Report No.1, Water Development Dept.
- Grant, F.S. and West, G.F., 1965. Interpretation theory in Applied Geophysics; Mcgraw Hill Book Co.
- Gregory, J.W., 1921. The Rift Valleys and Geology of East Africa; London.

- Hagedoorn, J.G., 1959. The Plus-Minus method of interpreting seismic refraction sections; Geophy. Prosp. 7:158-182.
- Hatherly, P.J. and Neville, M.J., 1986. Experience with generalised reciprocal method of seismic refraction interpretation for shallow engineering site investigation; Geoph. 51:255-265.
- Hawkins, L.V., 1961. The reciprocal method of routine shallow seismic refraction investigations; Geoph. 26:806-819.
- Hunter, A.N., (Editor), 1965. Report on the Geology and Geophysics of the East African System; E.A. Comm. for Co-op in Geoph.
- Keller, G.V. and Frischknecht, F.G., 1982. Electrical methods in Geophysical Prospecting; Pergamon Press.
- Kunetz, G., 1966. Principles of direct current resistivity prospecting; Geexplor. Monogr., Ser. 1, No. 1.
- Legget, R.F., 1962. Geology and Engineering; Mcgraw Hill Book Co.
- Lomnitz, C. and Rosenbluth, E., Editors, 1976. Seismic Risk and Engineering Decisions; Elsevier Scientific Pub. Co.
- Loupekine, I.S., 1971. A catalogue of felt earthquakes in Kenya 1892-1969; Seismology Unit, Geol. Dept. Univer. of Nairobi.
- Matheson, F.J., 1966. Geology of Kajiado area. Report No. 70; Geol. Surv. of Kenya.
- Matias, M.J.S. and Habberjan, G.M., 1986. The effect of structure and anisotropy on resistivity measurements; Geoph. 51:964-971.
- McCann, C., 1977. Computer programming in "BASIC" for the interpretation of Gravity, Magnetic and Resistivity profiles; Geol. Dept., Univer. of Reading.
- McPhail, M.R., 1967. The mid point method of interpreting a refraction survey. Soc. Expl. Geophys.

- Musgrave, A.W., (Editor), 1967. Seismic Refraction Prospecting; Soc. of Expl. Geophysicists.
- Nimbus Instruments. Pocket-Seis Technical Manual; Engineering Seismograph ES-1A.
- O'Neil, D.J., 1975. Improved linear filter coefficients for application in apparent resistivity computations; Bul. Austr. Soc. Expl. Geoph. 6:104-109.
- Palmer, D., 1981. An introduction to the generalized reciprocal method of seismic refraction interpretation; Geoph. 46:1508-1518.
- Parasnis, D.S., 1979. Principles of Applied Geophysics; Chapman and Hall.
- Rijkwaterastat, 1980. Standard graphs for resistivity prospecting; European Assoc. of Geophysicists.
- Saggerson, H.L., 1961-67. Geological map of Nairobi area; Geol. Surv. of Kenya.
- Sikes, H.L., 1926. The structure of the eastern flank of the Rift Valley near Nairobi; Geogr. J. 68:385-402.
- _____, 1934. The underground water resources of Kenya colony: Kenya colony Protectorate, Crown agents for the colonies.
- _____, 1939. Notes on the geology of the country surrounding Nairobi; Geol. Surv. of Kenya.
- Slotnick, M. M.; 1950. A graphical method for the interpretation of refraction profile data. Geoph. 15:163-170.
- Soskei, J.L., 1958. The blind zone problem in Engineering Geophysics; Geoph. 24:359-365.
- Telford, W.M., Geldart, L.P., Sheriff, R.E. and Keys, D.A., 1980. Applied Geophysics; Cambridge University Press.
- Thornburgh, H.R., 1930. Wave-front diagram in Seismic Interpretation; Bull of the Amer. Assoc. of Petr. Geol: 14:185-200.

- Walters R.C.S., 1962. Dam Geology; Butterworths.
- Van Overmeeren, R.A., 1989. Aquifer boundaries explored by geoelectrical measurements in the coastal plain of Yemen. A case of equivalence; Geoph.54:34-48.
- Zohdy, A.A.R. 1980. Applications of Surface Geophysics to groundwater investigations: Techniques of Water resources investigations; U.S. Geol. Surv. Book 2.

APPENDICES

APPENDICES

APPENDIX A

SEISMIC REFRACTION DATA INTERPRETATION

The purpose of this section is to provide a detailed description of the seismic refraction data collected during the survey. The data were collected using a standard refraction survey technique, and the resulting travel time curves are shown in the following figures. The data were collected using a standard refraction survey technique, and the resulting travel time curves are shown in the following figures.

APPENDICES A

SEISMIC REFRACTION



APPENDIX A.1

THE PLUS MINUS METHOD OF SEISMIC REFRACTION
DATA INTERPRETATION.

The plus - minus method uses the principles of intercept time and delay time to determine the depth z of the refractor as discussed in section 5.1

Time-distance relations for a two-layer media which dips at an angle α , having respective speeds of v_1 and v_2 , are illustrated in Fig. A.1.

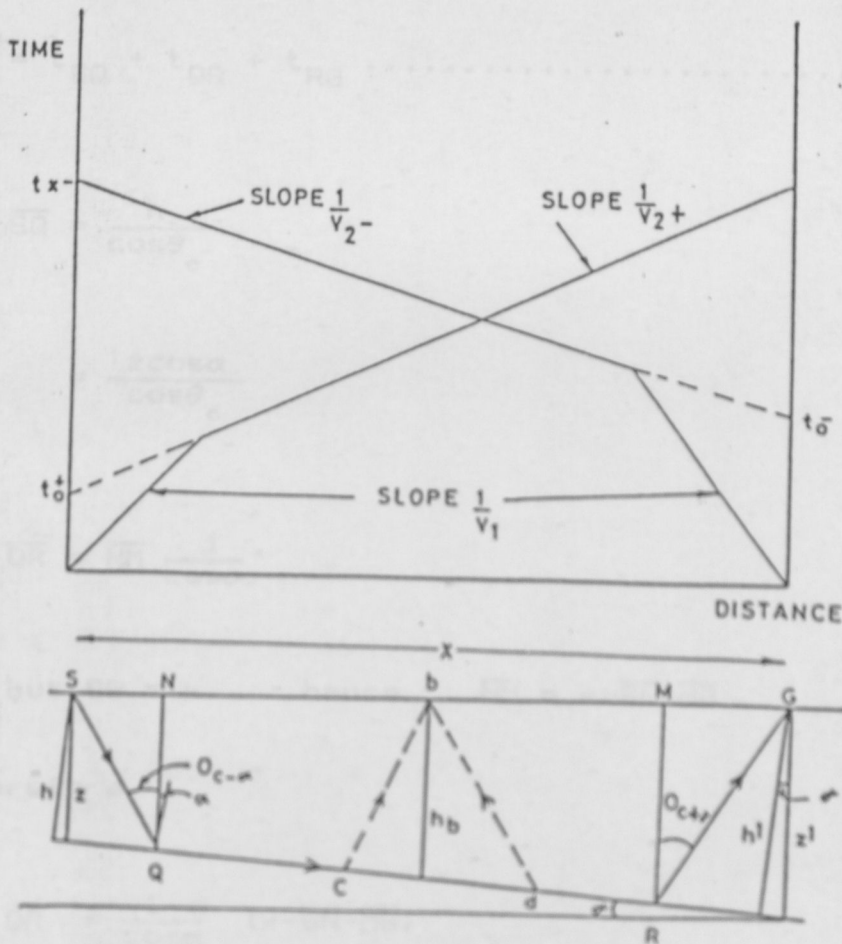


Fig A1 Raypaths and travel time curves for inclined interface.

A.1.2

The ray path for the first refracted arrival consists of three linear segments:

\overline{QR} along the sloping interface at speed v_2

\overline{SQ} and \overline{RG} in the upper medium making an angle θ_c with the normal to this boundary.

Shooting downdip, the total time t^+ from shot to detector is

$$t^+ = t_{SQ} + t_{QR} + t_{RG} \dots\dots\dots 1$$

$$\overline{SQ} = \frac{h}{\cos\theta_c}$$

$$= \frac{z \cos\alpha}{\cos\theta_c}$$

$$\overline{QR} = \overline{NM} \frac{1}{\cos\alpha}$$

but $SG = x$ hence $\overline{NM} = x - \overline{SN} - \overline{RG}$

Therefore,

$$\overline{QR} = \frac{1}{\cos\alpha} (x - \overline{SN} - \overline{RG})$$

A.1.3

$$= \frac{1}{\cos\alpha} \left[x - \frac{z \cos\alpha}{\cos\theta_c} \sin(i_c + \alpha) - \frac{z' \cos\alpha}{\cos\theta_c} \sin(\theta_c + \alpha) \right]$$

$$\overline{RG} = \frac{h'}{\cos\theta_c}$$

$$= z' \frac{\cos\alpha}{\cos\theta_c}$$

Therefore,

$$t^+ = \frac{1}{v_1} \left[\frac{z \cos\alpha}{\cos\theta_c} \right] + \frac{1}{v_1} \left[z' \frac{\cos\alpha}{\cos\theta_c} \right] + \frac{(\overline{GR})}{v_2 \cos\alpha}$$

$$\text{but } z' = z + \tan\alpha$$

Hence,

$$t^+ = \frac{x}{v_1} \sin(\theta_c + \alpha) + \frac{2z}{v_1} \cos\alpha \cos\theta_c \dots\dots\dots 2$$

similarly the updip time t^- is

$$t^- = \frac{x}{v_1} \sin(\theta_c + \alpha) + \frac{2z'}{v_1} \cos\alpha \cos\theta_c \dots\dots\dots 3$$

where z and z' are the depth to the interface at the updip and downdip ends respectively.

A.1.4

The updip velocity (v_2^-) and downdip velocity (v_2^+) are not true velocities and can be expressed as

$$v_2^+ = \frac{v_1}{\sin(\theta_c + \alpha)} \dots\dots\dots 4$$

$$v_2^- = \frac{v_1}{\sin(\theta_c - \alpha)} \dots\dots\dots 5$$

Equations 4 and 5 can be used to determine the critical angle θ_c and the angle of dip α , where

$$\sin(\theta_c + \alpha) = \frac{v_1}{v_2^+}$$

$$\sin(\theta_c - \alpha) = \frac{v_1}{v_2^-}$$

Therefore,

$$\theta_c + \alpha = \sin^{-1} \frac{v_1}{v_2^+} \dots\dots\dots 6$$

$$\theta_c - \alpha = \sin^{-1} \frac{v_1}{v_2^-} \dots\dots\dots 7$$

A.1.5

adding equations 6 and 7, we get

$$\theta_c = \frac{1}{2} \left(\sin^{-1} \frac{v_1}{v_2^+} + \sin^{-1} \frac{v_1}{v_2^-} \right) \dots\dots\dots 8$$

subtracting equation 7 from 6, we get

$$\alpha = \frac{1}{2} \left(\sin^{-1} \frac{v_1}{v_2^+} - \sin^{-1} \frac{v_1}{v_2^-} \right) \dots\dots\dots 9$$

The intercept time t_o , can be determined graphically from Fig.A.1, or numerically from the constant part of equations 2 and 3

where,

$$t_o^+ = \frac{2z}{v_1} \cos\alpha \cos\theta_c \dots\dots\dots 10$$

$$t_o^- = \frac{2z'}{v_1} \cos\alpha \cos\theta_c \dots\dots\dots 11$$

The perpendicular distance h to the interface can be determined by replacing $z' \cos\alpha$ with h'

A.1.6

$$t_o^- = \frac{2h'}{v_1} \cos\theta_c \dots\dots\dots 12$$

$$= \frac{2h'}{v_1} \sqrt{1 - \left[\frac{v_1}{v_2} \right]^2} \dots\dots\dots 13$$

$$h' = \frac{t_o^- v_1}{2 \cos\theta_c} \dots\dots\dots 14$$

$$\text{or } h' = \frac{t_o^- v_1}{2 \sqrt{1 - \frac{v_1^2}{v_2^2}}} \dots\dots\dots 15$$

The total travel time, t_x for the refraction path SQRG is the arithmetic mean of equations 2 and 3

Thus,

$$t_x = \frac{1}{2} (t^+ + t^-) \dots\dots\dots 16$$

$$= \frac{x}{v_2} \cos\alpha + \frac{\cos\theta_c}{v_1} (h + h') \dots\dots\dots 17$$

Considering a forward and reverse signal detected at point b

A.1.7

$$t_{SQcb} = t_1 = \frac{x_1}{v_1} \cos \alpha + \frac{\cos \theta_c}{v_1} (h + h_b) \dots \dots \dots 18$$

and

$$t_{GRdb} = t_2 = \frac{(x-x_1)}{v_2} \cos \alpha + \frac{\cos \theta_c}{v_1} (h_b + h_1) \dots \dots \dots 19$$

Difference caused by the ray traveling from (\overline{cdb}) instead of going straight on (\overline{cd}) , can be written as

$$t_b = (t_1 + t_2) - t_x \dots \dots \dots 20$$

but $t_b = 2h_b \frac{\cos \theta_c}{v_1}$ (from equation 12)

Hence, $h_b = \frac{t_b v_1}{2 \cos \theta_c} \dots \dots \dots 21$

Equation 20 is the plus time which is defined as the sum of the travel time t_1 , from the forward shotpoint and t_2 from the reverse shotpoint, minus the total travel time t_x between the shotpoints.

Equation 21 can give the depth of the refractor at any geophone position where the first arrivals from both forward and reverse shots have travelled through the same refractor.

APPENDIX A.2

SEISMIC REFRACTION DATA

Site: Kiserian Dam

Pr. S/W Sp. A-B

Date 23/11/87

x(m)	t ₁ (ms)	t ₂ (ms)
0.0	0.0	38.0
1.5	4.5	-
3.0	8.9	35.1
4.5	13.3	-
6.0	17.8	30.9
7.5	25.3	30.0
9.0	26.7	29.6
10.5	28.8	-
12.0	29.7	25.5
13.5	33.2	24.9
15.0	32.0	21.9
16.5	-	19.0
18.0	36.0	13.8
19.5	-	4.9
21.0	38.5	0.0
22.5		
24.0		
25.5		
27.0		
28.5		
30.0		

Pr. BH5 Sp. Z1-Z2

Date 24/11/87

x(m)	t ₁ (ms)	t ₂ (ms)
0.0	0.0	40.5
1.5	19.3	39.4
3.0	21.6	34.7
4.5	23.0	34.4
6.0	24.4	32.4
7.5	28.1	30.4
9.0	28.7	28.9
10.5	36.1	26.3
12.0	33.4	23.0
13.5	34.2	22.5
15.0	34.4	18.6
16.5	37.5	12.5
18.0	-	8.9
19.5	38.8	4.8
21.0	41.0	0.0
22.5		
24.0		
25.5		
27.0		
28.5		
30.0		

Pr. S/W Sp. V-W

Date 20/11/87

x(m)	t ₁ (ms)	t ₂ (ms)
0.0	0.0	47.0
1.5	18.0	-
3.0	23.9	44.8
4.5	26.1	-
6.0	32.3	42.8
7.5	35.5	-
9.0	27.5	40.0
10.5	-	-
12.0	30.6	38.0
13.5	31.4	-
15.0	33.0	33.6
16.5	-	-
18.0	35.5	27.5
19.5	-	-
21.0	39.6	25.0
22.5	37.5	-
24.0	38.3	24.0
25.5	-	14.2
27.0	44.0	8.2
28.5	-	-
30.0	47.0	0.0

SEISMIC REFRACTION DATA

Site: Kiserian Dam

Pr. BH1 Sp. D-J

Date 18/11/87

x(m)	t ₁ (ms)	t ₂ (ms)
0.0	0.0	49.9
1.5	5.2	-
3.0	9.8	46.2
4.5	13.2	45.9
6.0	15.2	41.6
7.5	22.1	35.8
9.0	24.0	35.8
10.5	26.6	34.0
12.0	31.5	-
13.5	30.2	33.3
15.0	32.5	32.8
16.5	-	30.4
18.0	34.8	28.3
19.5	-	26.9
21.0	37.2	23.2
22.5	43.6	18.4
24.0	44.9	11.5
25.5	47.5	5.4
27.0	49.0	0.0

Pr. BH1 Sp. F-G

Date 17/11/87

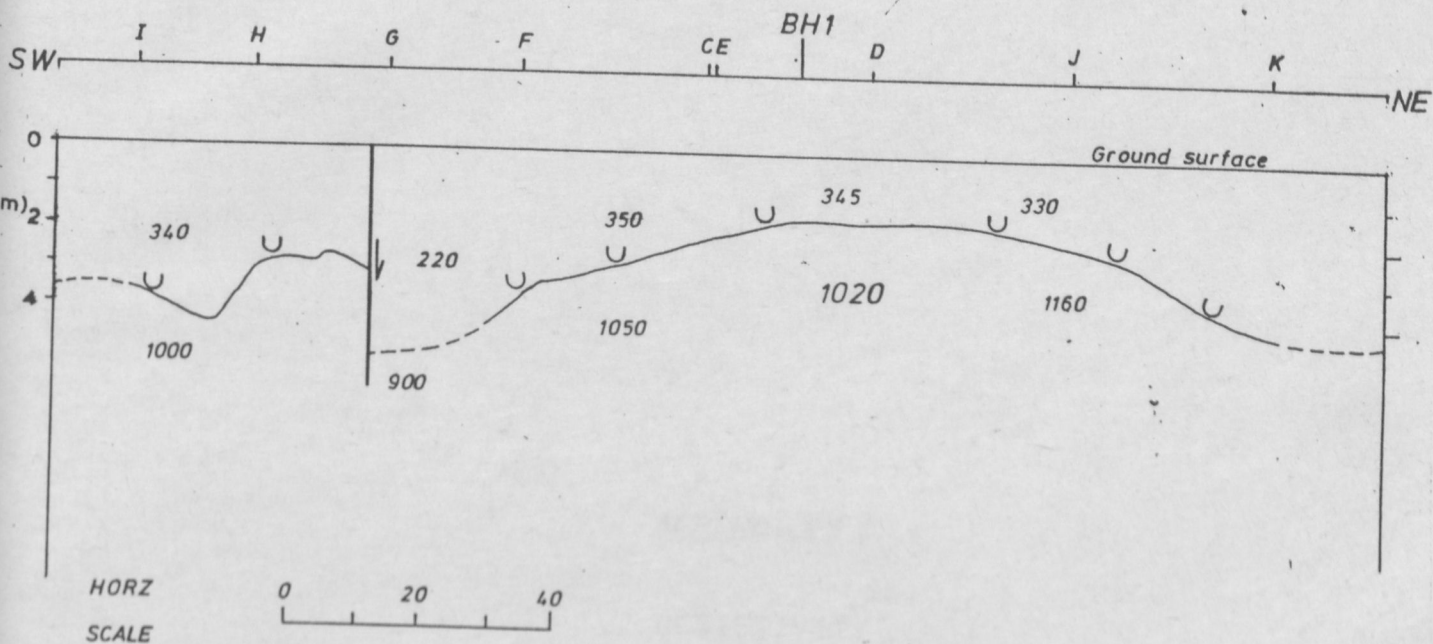
x(m)	t ₁ (ms)	t ₂ (ms)
0.0	0.0	33.3
1.5	7.0	35.5
3.0	18.3	34.5
4.5	20.6	33.5
6.0	24.5	32.6
7.5	26.6	29.6
9.0	29.3	20.4
10.5	29.7	26.2
12.0	31.5	16.3
13.5	29.3	12.8
15.0	33.3	9.3
16.5	34.6	0.0
18.0	-	-
19.5		
21.0		
22.5		
24.0		
25.5		
27.0		

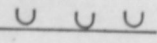
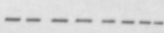
Pr. BH1 Sp. C-D

Date 12/11/87

x(m)	t ₁ (ms)	t ₂ (ms)
0.0	0.0	28.7
1.5	5.8	27.4
3.0	8.3	27.3
4.5	9.5	-
6.0	11.7	23.7
7.5	14.8	-
9.0	15.2	20.9
10.5	18.8	18.9
12.0	21.2	17.2
13.5	-	-
15.0	23.6	14.8
16.5	-	10.5
18.0	26.2	8.4
19.5	-	4.3
21.0	28.4	0.0
22.5		
24.0		
25.5		
27.0		

APPENDIX A.3
 INTERPRETED SEISMIC REFRACTION
 DEPTH SECTION ALONG BH1 PROFILE



-  Seismic refractor
-  Inferred Seismic refractor
- 1020 Layer Velocity (ms⁻¹)
- FE Spread position
-  Minor fault

50 1967

APPENDIX B.2
SCHEMATIC DIAGRAM
50 1967

APPENDICES B

RESISTIVITY

Station	Year	Resistivity	...
10	1964	100	
20	1965	110	
30	1966	120	
40	1967	130	
50	1968	140	
60	1969	150	
70	1970	160	
80	1971	170	
90	1972	180	
100	1973	190	
110	1974	200	
120	1975	210	
130	1976	220	
140	1977	230	
150	1978	240	
160	1979	250	
170	1980	260	
180	1981	270	
190	1982	280	
200	1983	290	
210	1984	300	
220	1985	310	
230	1986	320	
240	1987	330	
250	1988	340	
260	1989	350	
270	1990	360	
280	1991	370	
290	1992	380	
300	1993	390	
310	1994	400	
320	1995	410	
330	1996	420	
340	1997	430	
350	1998	440	
360	1999	450	
370	2000	460	
380	2001	470	
390	2002	480	
400	2003	490	
410	2004	500	
420	2005	510	
430	2006	520	
440	2007	530	
450	2008	540	
460	2009	550	
470	2010	560	
480	2011	570	
490	2012	580	
500	2013	590	
510	2014	600	
520	2015	610	
530	2016	620	
540	2017	630	
550	2018	640	
560	2019	650	
570	2020	660	
580	2021	670	
590	2022	680	
600	2023	690	
610	2024	700	
620	2025	710	
630	2026	720	
640	2027	730	
650	2028	740	
660	2029	750	
670	2030	760	
680	2031	770	
690	2032	780	
700	2033	790	
710	2034	800	
720	2035	810	
730	2036	820	
740	2037	830	
750	2038	840	
760	2039	850	
770	2040	860	
780	2041	870	
790	2042	880	
800	2043	890	
810	2044	900	
820	2045	910	
830	2046	920	
840	2047	930	
850	2048	940	
860	2049	950	
870	2050	960	
880	2051	970	
890	2052	980	
900	2053	990	
910	2054	1000	
920	2055	1010	
930	2056	1020	
940	2057	1030	
950	2058	1040	
960	2059	1050	
970	2060	1060	
980	2061	1070	
990	2062	1080	
1000	2063	1090	
1010	2064	1100	
1020	2065	1110	
1030	2066	1120	
1040	2067	1130	
1050	2068	1140	
1060	2069	1150	
1070	2070	1160	
1080	2071	1170	
1090	2072	1180	
1100	2073	1190	
1110	2074	1200	
1120	2075	1210	
1130	2076	1220	
1140	2077	1230	
1150	2078	1240	
1160	2079	1250	
1170	2080	1260	
1180	2081	1270	
1190	2082	1280	
1200	2083	1290	
1210	2084	1300	
1220	2085	1310	
1230	2086	1320	
1240	2087	1330	
1250	2088	1340	
1260	2089	1350	
1270	2090	1360	
1280	2091	1370	
1290	2092	1380	
1300	2093	1390	
1310	2094	1400	
1320	2095	1410	
1330	2096	1420	
1340	2097	1430	
1350	2098	1440	
1360	2099	1450	
1370	2100	1460	
1380	2101	1470	
1390	2102	1480	
1400	2103	1490	
1410	2104	1500	
1420	2105	1510	
1430	2106	1520	
1440	2107	1530	
1450	2108	1540	
1460	2109	1550	
1470	2110	1560	
1480	2111	1570	
1490	2112	1580	
1500	2113	1590	
1510	2114	1600	
1520	2115	1610	
1530	2116	1620	
1540	2117	1630	
1550	2118	1640	
1560	2119	1650	
1570	2120	1660	
1580	2121	1670	
1590	2122	1680	
1600	2123	1690	
1610	2124	1700	
1620	2125	1710	
1630	2126	1720	
1640	2127	1730	
1650	2128	1740	
1660	2129	1750	
1670	2130	1760	
1680	2131	1770	
1690	2132	1780	
1700	2133	1790	
1710	2134	1800	
1720	2135	1810	
1730	2136	1820	
1740	2137	1830	
1750	2138	1840	
1760	2139	1850	
1770	2140	1860	
1780	2141	1870	
1790	2142	1880	
1800	2143	1890	
1810	2144	1900	
1820	2145	1910	
1830	2146	1920	
1840	2147	1930	
1850	2148	1940	
1860	2149	1950	
1870	2150	1960	
1880	2151	1970	
1890	2152	1980	
1900	2153	1990	
1910	2154	2000	
1920	2155	2010	
1930	2156	2020	
1940	2157	2030	
1950	2158	2040	
1960	2159	2050	
1970	2160	2060	
1980	2161	2070	
1990	2162	2080	
2000	2163	2090	
2010	2164	2100	
2020	2165	2110	
2030	2166	2120	
2040	2167	2130	
2050	2168	2140	
2060	2169	2150	
2070	2170	2160	
2080	2171	2170	
2090	2172	2180	
2100	2173	2190	
2110	2174	2200	
2120	2175	2210	
2130	2176	2220	
2140	2177	2230	
2150	2178	2240	
2160	2179	2250	
2170	2180	2260	
2180	2181	2270	
2190	2182	2280	
2200	2183	2290	
2210	2184	2300	
2220	2185	2310	
2230	2186	2320	
2240	2187	2330	
2250	2188	2340	
2260	2189	2350	
2270	2190	2360	
2280	2191	2370	
2290	2192	2380	
2300	2193	2390	
2310	2194	2400	
2320	2195	2410	
2330	2196	2420	
2340	2197	2430	
2350	2198	2440	
2360	2199	2450	
2370	2200	2460	
2380	2201	2470	
2390	2202	2480	
2400	2203	2490	
2410	2204	2500	
2420	2205	2510	
2430	2206	2520	
2440	2207	2530	
2450	2208	2540	
2460	2209	2550	
2470	2210	2560	
2480	2211	2570	
2490	2212	2580	
2500	2213	2590	
2510	2214	2600	
2520	2215	2610	
2530	2216	2620	
2540	2217	2630	
2550	2218	2640	
2560	2219	2650	
2570	2220	2660	
2580	2221	2670	
2590	2222	2680	
2600	2223	2690	
2610	2224	2700	
2620	2225	2710	
2630	2226	2720	
2640	2227	2730	
2650	2228	2740	
2660	2229	2750	
2670	2230	2760	
2680	2231	2770	
2690	2232	2780	
2700	2233	2790	
2710	2234	2800	
2720	2235	2810	
2730	2236	2820	
2740	2237	2830	
2750	2238	2840	
2760	2239	2850	
2770	2240	2860	
2780	2241	2870	
2790	2242	2880	
2800	2243	2890	
2810	2244	2900	
2820	2245	2910	
2830	2246	2920	
2840	2247	2930	
2850	2248	2940	
2860	2249	2950	
2870	2250	2960	
2880	2251	2970	
2890	2252	2980	
2900	2253	2990	
2910	2254	3000	
2920	2255	3010	
2930	2256	3020	
2940	2257	3030	
2950	2258	3040	
2960	2259	3050	
2970	2260	3060	
2980	2261	3070	
2990	2262	3080	
3000	2263	3090	
3010	2264	3100	
3020	2265	3110	
3030	2266	3120	
3040	2267	3130	
3050	2268	3140	
3060	2269	3150	
3070	2270	3160	
3080	2271	3170	
3090	2272	3180	
3100	2273	3190	
3110	2274	3200	
3120	2275	3210	
3130	2276	3220	
3140	2277	3230	
3150	2278	3240	
3160	2279	3250	
3170	2280	3260	
3180	2281	3270	
3190	2282	3280	
3200	2283	3290	
3210	2284	3300	
3220	2285	3310	
3230	2286	3320	
3240	2287	3330	
3250	2288	3340	
3260	2289	3350	
3270	2290	3360	
3280	2291	3370	
3290	2292	3380	
3300	2293	3390	
3310	2294	3400	
3320	2295	3410	
3330	2296	3420	
3340	2297	3430	
3350	2298	3440	
3360	2299	3450	
3370	2300	3460	
3380	2301	3470	
3390	2302	3480	
3400	2303	3490	

APPENDIX B.1

GEOMETRICAL CONSTANTS (K) FOR SCHLUMBERGER ARRAY

AB/2 (m)	MN/2 (m)	0.5	5	10	25	50	100
1.6	7.26						
2	11.8						
2.5	18.8						
3.2	31.4						
4	49.5						
5	77.8						
6.3	124						
8	200						
10	313						
13	530		5m				
16	803	72.6					
20	1260	118					
25	1960	188		10m			
32	3220	314	145				
40	5030	495	236				
50	7850	788	377				
63	12500	1240	608		25m		
80	20100	2000	990	363			
100	31400	3130	1560	589			
130	53100	5300	2640	1020		50m	
160	80400	8030	4010	1570	726		
200	126000	12600	6270	2470	1180		
250		19600	9800	3890	1880		100m
320		32200	16100	6370	3140	1450	
400		50300	25100	10000	4950	2360	
500		78500	39300	15700	7780	3770	
630		125000	62300	24900	12400	6080	
800			101000	40200	20000	9900	
1000			157000	62800	31300	15600	

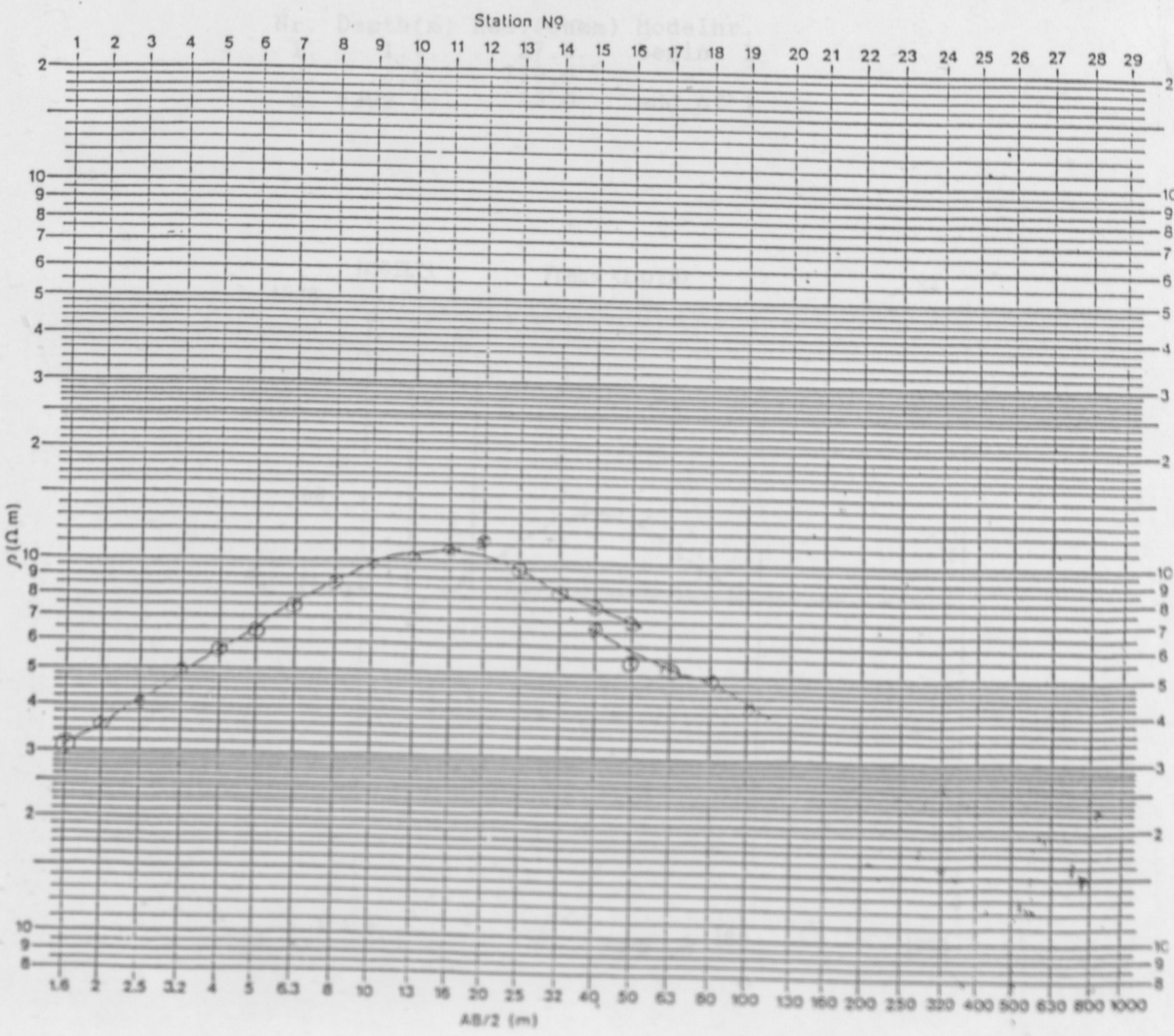
GEOMETRICAL CONSTANTS K
(Schlumberger array)

$$K = \pi \frac{(AB/2)^2 - (MN/2)^2}{MN}$$

$$\rho = K \frac{\Delta V}{I}$$

LOCATION: KISERIAN DAM SITE	DATE: 19/1/88
OPERATOR: : ABUUYU	V.E.S / SPREAD NO
MAXIMUM AB/2 100 m. AB AZIMUTH SW-NE	S7
REMARKS: MN/2 changed from 0.5m to 10m, at $\frac{AB}{2} = 40m$	

MN/2	AB/2	K	$\Delta V / I$	ρ	MN/2	AB/2	K	$\Delta V / I$	ρ	MN/2	AB/2	K	$\Delta V / I$	ρ
0.5	1.6	7.26	4.27	31.00	0.5	32	3220	0.0256	82.4					
"	2	11.8	2.99	35.28	"	40	5030	0.01503	76.46					
"	2.5	18.8	2.18	40.90	"	50	7850	0.00881	69.16					
"	3.2	31.4	1.59	49.910	"	40	236	0.280	66.08					
"	4.0	49.5	1.143	56.58	"	50	377	0.1436	54.13					
"	5.0	77.8	0.823	64.42	"	63	608	0.0868	52.77					
"	6.3	124	0.597	74.02	"	80	990	0.0496	49.1					
"	8.0	200	0.432	86.4	"	100	1560	0.0266	41.44					
"	10	313	0.308	96.4										
"	13	530	0.194	102.8										
"	16	503	0.135	105.4										
"	20	1260	0.0881	111.0										
"	25	1960	0.048	94.05										



APPENDIX B.4

COMPUTER MODEL AND CURVE FOR VES S7

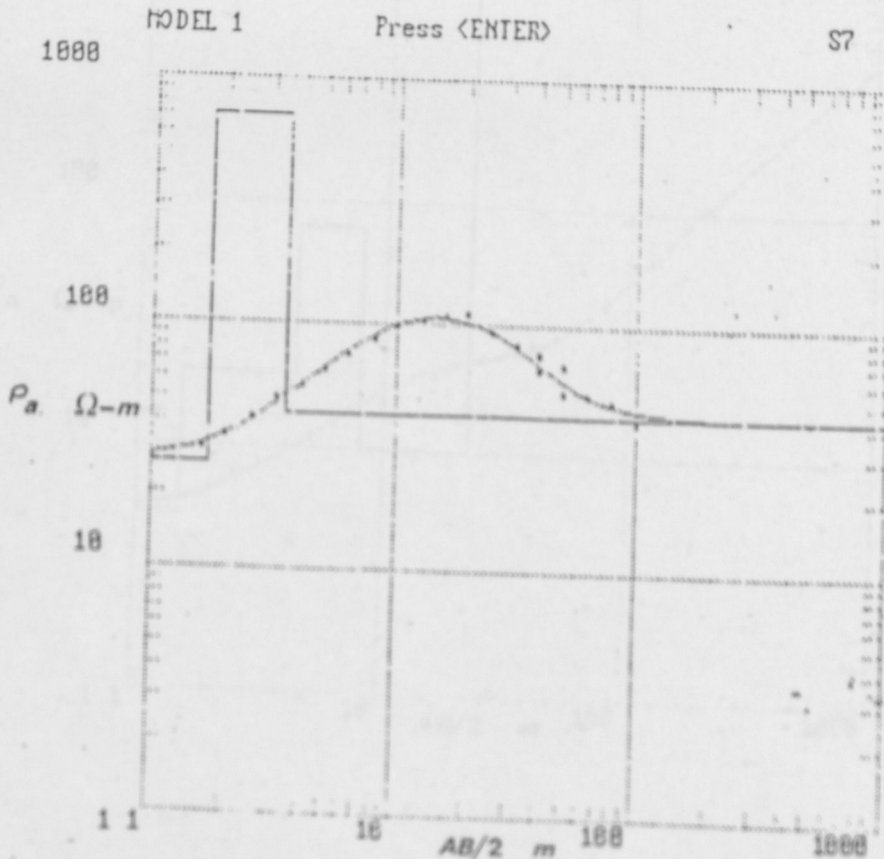
File number 14: S7

Measured apparent resistivities.

Nr.	L/2	Pa	Nr.	L/2	Pa
1.	1.6	31.0	12.	20.0	111.0
2.	2.0	35.3	13.	25.0	94.1
3.	2.5	41.0	14.	32.0	82.4
4.	3.2	49.9	15.	40.0	76.9
5.	4.0	56.6	16.	40.0	66.0
6.	5.0	64.4	17.	50.0	69.2
7.	6.3	74.0	18.	50.0	54.1
8.	8.0	86.4	19.	63.0	52.8
9.	10.0	96.4	20.	80.0	49.1
10.	13.0	102.8	21.	100.0	41.5
11.	16.0	108.4			

Resistivity model(s).

Nr.	Depth(m)	Res.(ohmm)	Modelnr.
1.	1.7	27.0	begin 1
2.	3.5	710.0	
3.	9999.0	43.0	end of 1



APPENDIX B.5

COMPUTER MODEL AND CURVE FOR VES S15

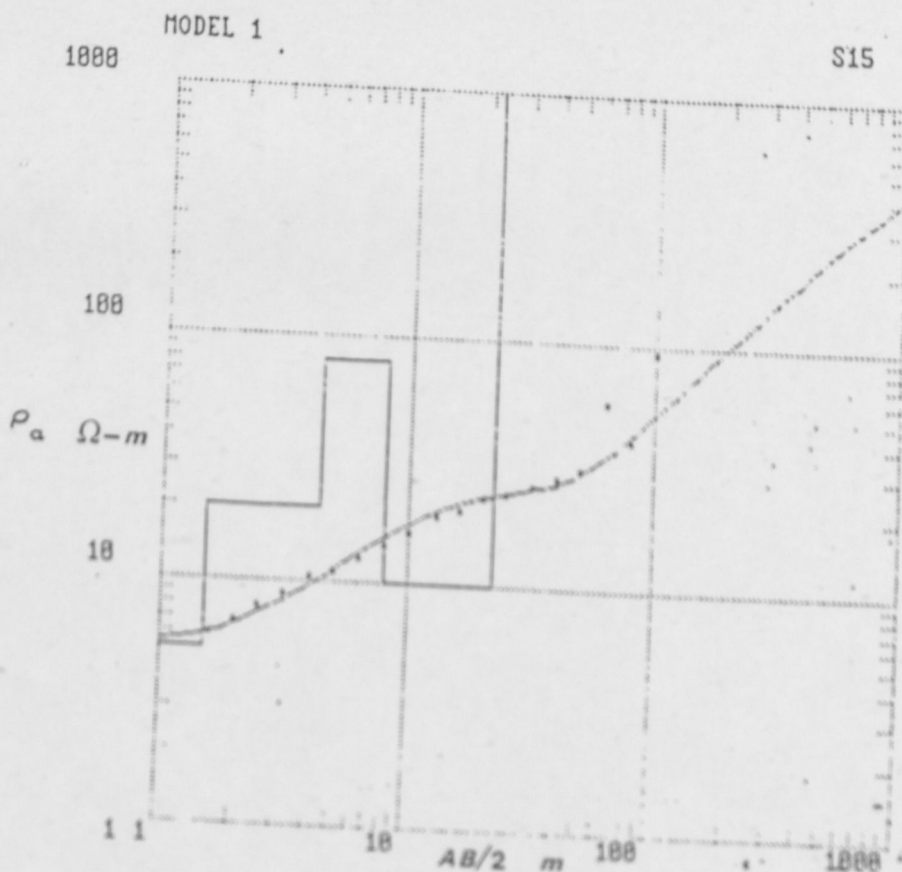
File number 22: S15

Measured apparent resistivities.

Nr.	L/2	Pa	Nr.	L/2	Pa
1.	1.6	5.99	11.	16.0	20.1
2.	2.0	6.81	12.	20.0	22.6
3.	2.5	7.86	13.	25.0	23.6
4.	3.2	8.98	14.	32.0	25.8
5.	4.0	10.5	15.	40.0	27.8
6.	5.0	11.2	16.	40.0	27.0
7.	6.3	12.6	17.	50.0	30.5
8.	8.0	14.2	18.	63.0	57.2
9.	10.0	16.2	19.	80.0	40.6
10.	13.0	18.8	20.	100.0	93.6

Resistivity model(s).

Nr.	Depth(m)	Res.(ohmm)	Modelnr.
1.	1.5	5.20	begin 1
2.	4.4	20.0	
3.	8.0	80.0	
4.	22.0	10.0	
5.	9999.0	1500.0	end of 1



APPENDIX C

GEO-HYDRAULICS

PACKER (PUMPING-IN) TESTS

Packer pressure 5.0 Bars Diameter of hole 86 mm.

Depth of section 4.50 to 7.00 m.		Date 13-1-83				
Bottom of casing 4.5 m.		Borehole No. 2				
Init. ground water lev. 4.85 m.		Packer type SINGLE				
Gauge ht above ground		Type of rock BASALT				
Gauge Pressure	Time (min)	0	5	10	15	Average flow q (l/min)
1.0	Flowmeter dipstick (1)	9306.4	9306.4	9306.4	9306.4	0.0
	Water take (1)	0.0	0.0	0.0	0.0	
1.5	Flowmeter dipstick (1)	9307.7	9307.9	9307.9	9307.9	0.013
	Water take (1)	0.2	0.0	0.0	0.0	
2.0	Flowmeter dipstick (1)	9308.3	9308.3	9309.1	9309.1	0.053
	Water take (1)	0.5	0.0	0.0	0.0	
1.5	Flowmeter dipstick (1)	9309.3	9309.6	9309.6	9309.6	0.02
	Water take (1)	0.2	0.1	0.0	0.0	
4.0	Flowmeter dipstick (1)	9300.5	9300.6	9300.6	9300.6	0.007
	Water take (1)	0.1	0.0	0.0	0.0	

Depth of section 7.00 to 9.00 m. Date 13-1-83
 Bottom of casing 4.5 m. Borehole No. 2
 Init. ground water lev. 5.2 m. Packer type SINGLE
 Gauge ht above ground 0.10 m. Type of rock BASALT

Gauge Pressure	Time (min)	0	5	10	15	Average flow q (l/min)
1.5	Flowmeter dipstick (1)	9291.5	9292.3	9292.6	9292.6	0.073
	Water take (1)	0.3	0.3	0.0	0.0	
2.0	Flowmeter dipstick (1)	9293.4	9293.7	9293.7	9293.7	0.02
	Water take (1)	0.3	0.0	0.0	0.0	
3.0	Flowmeter dipstick (1)	9294.4	9294.9	9295.2	9295.2	0.053
	Water take (1)	0.5	0.3	0.0	0.0	
2.0	Flowmeter dipstick (1)	9297.1	9297.7	9297.9	9298.3	0.027
	Water take (1)	0.6	0.0	0.4	0.0	
1.5	Flowmeter dipstick (1)	9299.6	9299.7	9301.3	9301.3	0.047
	Water take (1)	0.1	0.0	0.0	0.0	

Depth of section 9.00 to 11.00 m. Date 15-1-88
 Bottom of casing 4.5 m. Borehole No. 2
 Init. ground water lev. 8.6 m. Packer type SINGLE
 Gauge ht above ground 0.10 m. Type of rock BASALT

Gauge Pressure	Time (min)	0	5	10	15	Average flow q (l/min)
1.5	Flowmeter dipstick (1)	9392.4	9392.9	9392.9	9392.9	0.007
	Water take (1)	0.1	0.0	0.0	0.0	
3.0	Flowmeter dipstick (1)	9394.1	9400.1	9409.9	9410.0	1.10
	Water take (1)	3.6	7.2	0.7	0.0	
4.0	Flowmeter dipstick (1)	9341.8	9353.3	9435.7	9475.5	8.93
	Water take (1)	46.5	50.9	32.6	0.0	
3.0	Flowmeter dipstick (1)	9485.1	9487.5	9511.1	9524.4	2.62
	Water take (1)	12.4	13.6	13.5	0.0	
1.5	Flowmeter dipstick (1)	9527.7	9527.8	9527.8	9527.8	0.073
	Water take (1)	0.1	0.0	0.0	0.0	

PACKER (PUMPING-IN) TESTS

Packer pressure 5.0 Bars Diameter of hole 86 mm.

Depth of section 11.0 to 13.0 m.		Date 19-1-83				
Bottom of casing 4.5 m.		Borehole No. 2				
Init. ground water lev. 6.35 m.		Packer type SINGLE				
Gauge ht above ground		Type of rock WEATHERED BASALT				
Gauge Pressure	Time (min)	0	5	10	15	Average flow q (l/min)
2.0	Flowmeter dipstick (1)	9553.3	9554.3	9555.9	9556.7	0.233
	Water take (1)	1.6	1.1	0.5	0.0	
3.0	Flowmeter dipstick (1)	9572.2	9573.9	9574.4	9574.4	0.130
	Water take (1)	0.7	0.5	0.6	0.0	
4.0	Flowmeter dipstick (1)	9561.3	9561.3	9561.3	9561.3	0.267
	Water take (1)	2.4	1.2	0.4	0.0	
3.0	Flowmeter dipstick (1)	9565.4	9566.9	9566.9	9566.1	0.10
	Water take (1)	0.5	0.8	0.2	0.0	
2.0	Flowmeter dipstick (1)	9567.8	9568.2	9568.9	9569.2	0.093
	Water take (1)	0.0	0.0	0.0	0.0	

Depth of section 13.0 to 15.0 m. Date 20-1-83
 Bottom of casing 4.5 m. Borehole No. 2
 Init. ground water lev. 7.20 m. Packer type SINGLE
 Gauge ht above ground

Gauge Pressure	Time (min)	0	5	10	15	Average flow q (l/min)
2.0	Flowmeter dipstick (1)	9510.5	9511.4	9511.7	9510.9	0.097
	Water take (1)	2.2	2.3	1.2	0.0	
3.0	Flowmeter dipstick (1)	9510.5	9510.3	9510.2	9510.4	0.267
	Water take (1)	1.8	0.9	0.4	0.0	
4.0	Flowmeter dipstick (1)	9510.5	9510.8	9510.3	9510.3	0.137
	Water take (1)	0.3	0.2	0.7	0.0	
3.0	Flowmeter dipstick (1)	9510.2	9510.8	9510.3	9510.1	0.207
	Water take (1)	0.6	1.1	1.4	0.0	
2.0	Flowmeter dipstick (1)	9511.3	9511.8	9512.2	9512.5	0.140
	Water take (1)	0.5	1.0	0.6	0.0	

Depth of section 5.0 to 7.0 m. Date 21-1-88
 Bottom of casing 5.0 m. Borehole No. 3
 Init. ground water lev. 8.5 m. Packer type SINGLE
 Gauge ht above ground 0.3 m. Type of rock WEATHERED BASALT

Gauge Pressure	Time (min)	0	5	10	15	Average flow q (l/min)
1.0	Flowmeter dipstick (1)					0.0
	Water take (1)	0.0	0.0	0.0	0.0	
1.5	Flowmeter dipstick (1)					0.0
	Water take (1)	0.0	0.0	0.0	0.0	
2.0	Flowmeter dipstick (1)					0.0
	Water take (1)	0.0	0.0	0.0	0.0	
1.5	Flowmeter dipstick (1)					0.0
	Water take (1)	0.0	0.0	0.0	0.0	
1.0	Flowmeter dipstick (1)					0.0
	Water take (1)	0.0	0.0	0.0	0.0	

PACKER (PUMPING-IN) TESTS

Packer pressure 5.0 Bars Diameter of hole 86 mm.

Depth of section 7.00 to 10.60 m		Date 24-2-88				
Bottom of casing 5.0 m		Borehole No. 3				
Init. ground water lev. 0.40 m		Packer type SINGLE				
Gauge ht above ground 0.30 m		Type of rock WEATHERED BASALT / AGGLOMERATE				
Gauge Pressure	Time (min)	0	5	10	15	Average flow q (l/min)
1.5	Flowmeter dipstick (1)	—	—	—	—	0.0
	Water take (1)	0.0	0.0	0.0	—	0.0
2.0	Flowmeter dipstick (1)	—	—	—	—	0.0
	Water take (1)	0.2	0.0	0.0	—	0.0
2.5	Flowmeter dipstick (1)	—	—	—	—	0.013
	Water take (1)	0.19	0.0	0.0	—	0.0
2.0	Flowmeter dipstick (1)	—	—	—	—	0.0
	Water take (1)	0.0	0.0	0.0	—	0.0
1.5	Flowmeter dipstick (1)	—	—	—	—	0.0
	Water take (1)	0.0	0.0	0.0	—	0.0

Depth of section 10.00 to 13.40 m Date 25-1-88
 Bottom of casing 5.0 m Borehole No. 3
 Init. ground water lev. 0.50 m Packer type SINGLE
 Gauge ht above ground 0.30 m Type of rock AGGLOMERATE

Gauge Pressure	Time (min)	0	5	10	15	Average flow q (l/min)
1.5	Flowmeter dipstick (1)	—	—	—	—	0.0
	Water take (1)	0.0	0.0	0.0	—	0.0
2.0	Flowmeter dipstick (1)	—	—	—	—	0.0
	Water take (1)	0.0	0.0	0.0	—	0.0
2.5	Flowmeter dipstick (1)	—	—	—	—	0.0
	Water take (1)	0.0	0.0	0.0	—	0.0
2.0	Flowmeter dipstick (1)	—	—	—	—	0.0
	Water take (1)	0.0	0.0	0.0	—	0.0
1.5	Flowmeter dipstick (1)	—	—	—	—	0.0
	Water take (1)	0.0	0.0	0.0	—	0.0

Depth of section 13.40 to 16.10 m Date 28-2-88
 Bottom of casing 5.0 m Borehole No. 3
 Init. ground water lev. 0.50 m Packer type SINGLE
 Gauge ht above ground 0.30 m Type of rock AGGLOMERATE / RES. SOILS

Gauge Pressure	Time (min)	0	5	10	15	Average flow q (l/min)
2.0	Flowmeter dipstick (1)	—	—	—	—	0.0
	Water take (1)	0.0	0.0	0.0	—	0.0
3.0	Flowmeter dipstick (1)	—	—	—	—	0.0
	Water take (1)	0.0	0.0	0.0	—	0.0
3.5	Flowmeter dipstick (1)	—	—	—	—	0.0
	Water take (1)	0.5	0.0	0.0	—	0.0
3.0	Flowmeter dipstick (1)	—	—	—	—	0.0
	Water take (1)	0.0	0.0	0.0	—	0.0
2.0	Flowmeter dipstick (1)	—	—	—	—	0.0
	Water take (1)	0.0	0.0	0.0	—	0.0

PACKER (PUMPING-IN) TESTS

Packer pressure 5.0 Bars Diameter of hole 86 mm.

Depth of section 16.10 to 19.00 m		Date 27-1-88				
Bottom of casing 5.0 m		Borehole No. 3				
Init. ground water lev. 0.50 m		Packer type SINGLE				
Gauge ht above ground 0.30 m		Type of rock RES. SOILS / WEATH. BASALT				
Gauge Pressure	Time (min)	0	5	10	15	Average flow q (l/min)
3.0	Flowmeter dipstick (1)	—	—	—	—	0.0
	Water take (1)	0.0	0.0	0.0	—	0.0
3.5	Flowmeter dipstick (1)	—	—	—	—	0.009
	Water take (1)	0.44	0.0	0.0	—	0.0
4.0	Flowmeter dipstick (1)	—	—	—	—	0.023
	Water take (1)	0.25	0.0	0.0	—	0.0
3.5	Flowmeter dipstick (1)	—	—	—	—	0.0
	Water take (1)	0.0	0.0	0.0	—	0.0
3.0	Flowmeter dipstick (1)	—	—	—	—	0.0
	Water take (1)	0.0	0.0	0.0	—	0.0

Depth of section 19.00 to 21.60 m Date 3-2-88
 Bottom of casing 5.0 m Borehole No. 3
 Init. ground water lev. 0.50 m Packer type SINGLE
 Gauge ht above ground 0.30 m Type of rock WEATHERED BASALTS

Gauge Pressure	Time (min)	0	5	10	15	Average flow q (l/min)
—	Flowmeter dipstick (1)	—	—	—	—	0.058
	Water take (1)	0.45	0.0	0.0	—	0.023
—	Flowmeter dipstick (1)	—	—	—	—	0.068
	Water take (1)	0.28	0.0	0.0	—	0.009
—	Flowmeter dipstick (1)	—	—	—	—	0.009
	Water take (1)	0.29	0.0	0.0	—	0.0
—	Flowmeter dipstick (1)	—	—	—	—	0.0
	Water take (1)	0.0	0.0	0.0	—	0.0

Depth of section 21.60 to 26.0 m Date 5-2-88
 Bottom of casing 5.0 m Borehole No. 3
 Init. ground water lev. 0.70 m Packer type SINGLE
 Gauge ht above ground 0.30 m Type of rock BASALT

Gauge Pressure	Time (min)	0	5	10	15	Average flow q (l/min)
—	Flowmeter dipstick (1)	—	—	—	—	0.0
	Water take (1)	0.0	0.0	0.0	—	0.0
—	Flowmeter dipstick (1)	—	—	—	—	0.0
	Water take (1)	0.0	0.0	0.0	—	0.0
—	Flowmeter dipstick (1)	—	—	—	—	0.15
	Water take (1)	0.17	0.0	0.0	—	0.0
—	Flowmeter dipstick (1)	—	—	—	—	0.0
	Water take (1)	0.0	0.0	0.0	—	0.0
—	Flowmeter dipstick (1)	—	—	—	—	0.0
	Water take (1)	0.0	0.0	0.0	—	0.0

PACKER (PUMPING-IN) TESTS

Packer pressure 5.0 Bars Diameter of hole 86 mm.

Depth of section 7.00 to 10.00 m. Date 15-2-88
 Bottom of casing 7.00 m. Borehole No. 6
 Init. ground water lev. 1.65 m. Packer type SINGLE
 Gauge ht above ground 0.15 m. Type of rock WEATHERED BASALT / AGG.

Gauge Pressure	Time (min)	0	5	10	15	Average flow q (l/min)
1.5	Flowmeter dipstick (1)	-	-	-	-	0.0
	Water take (1)	0.0	0.0	0.0	-	0.0
2.0	Flowmeter dipstick (1)	-	-	-	-	0.0
	Water take (1)	0.0	0.0	0.0	-	0.0
2.5	Flowmeter dipstick (1)	-	-	-	-	0.0
	Water take (1)	0.0	0.0	0.0	-	0.0
2.0	Flowmeter dipstick (1)	-	-	-	-	0.0
	Water take (1)	0.0	0.0	0.0	-	0.0
1.5	Flowmeter dipstick (1)	-	-	-	-	0.0
	Water take (1)	0.0	0.0	0.0	-	0.0

Depth of section 10.00 to 12.00 m. Date 15-2-88
 Bottom of casing 7.00 m. Borehole No. 6
 Init. ground water lev. 1.65 m. Packer type SINGLE
 Gauge ht above ground 0.15 m. Type of rock AGGLOMERATE

Gauge Pressure	Time (min)	0	5	10	15	Average flow q (l/min)
2.0	Flowmeter dipstick (1)	-	-	-	-	0.0
	Water take (1)	0.0	0.0	0.0	-	0.0
2.5	Flowmeter dipstick (1)	-	-	-	-	0.0
	Water take (1)	0.0	0.0	0.0	-	0.0
3.0	Flowmeter dipstick (1)	-	-	-	-	0.0
	Water take (1)	0.0	0.0	0.0	-	0.0
2.5	Flowmeter dipstick (1)	-	-	-	-	0.0
	Water take (1)	0.0	0.0	0.0	-	0.0
2.0	Flowmeter dipstick (1)	-	-	-	-	0.0
	Water take (1)	0.0	0.0	0.0	-	0.0

Depth of section 12.00 to 14.00 m. Date 16-2-88
 Bottom of casing 7.00 m. Borehole No. 6
 Init. ground water lev. 1.65 m. Packer type SINGLE
 Gauge ht above ground 0.15 m. Type of rock AGGLOMERATE

Gauge Pressure	Time (min)	0	5	10	15	Average flow q (l/min)
2.5	Flowmeter dipstick (1)	-	-	-	-	0.0
	Water take (1)	0.0	0.0	0.0	-	0.0
3.0	Flowmeter dipstick (1)	-	-	-	-	0.011
	Water take (1)	0.17	0.0	0.0	-	0.011
4.0	Flowmeter dipstick (1)	-	-	-	-	0.035
	Water take (1)	0.25	0.17	0.11	-	0.035
3.0	Flowmeter dipstick (1)	-	-	-	-	0.0
	Water take (1)	0.0	0.0	0.0	-	0.0
2.5	Flowmeter dipstick (1)	-	-	-	-	0.0
	Water take (1)	0.0	0.0	0.0	-	0.0

PACKER (PUMPING-IN) TESTS

Packer pressure 5.0 Bars Diameter of hole 86 mm.

Depth of section 14.00 to 17.00 m. Date 17-2-88
 Bottom of casing 7.00 m. Borehole No. 6
 Init. ground water lev. 1.65 m. Packer type SINGLE
 Gauge ht above ground 0.15 m. Type of rock AGGLOMERATE / RES. SLT

Gauge Pressure	Time (min)	0	5	10	15	Average flow q (l/min)
2.5	Flowmeter dipstick (1)	-	-	-	-	0.0
	Water take (1)	0.0	0.0	0.0	-	0.0
3.0	Flowmeter dipstick (1)	-	-	-	-	0.0
	Water take (1)	0.0	0.0	0.0	-	0.0
4.0	Flowmeter dipstick (1)	-	-	-	-	0.0
	Water take (1)	0.0	0.0	0.0	-	0.0
3.0	Flowmeter dipstick (1)	-	-	-	-	0.0
	Water take (1)	0.0	0.0	0.0	-	0.0
2.5	Flowmeter dipstick (1)	-	-	-	-	0.0
	Water take (1)	0.0	0.0	0.0	-	0.0

Depth of section 17.00 to 20.00 m. Date 17-2-88
 Bottom of casing 7.00 m. Borehole No. 6
 Init. ground water lev. 1.65 m. Packer type SINGLE
 Gauge ht above ground 0.15 m. Type of rock RES. SLT / WEATHERED BASALT

Gauge Pressure	Time (min)	0	5	10	15	Average flow q (l/min)
3.0	Flowmeter dipstick (1)	-	-	-	-	0.0
	Water take (1)	0.0	0.0	0.0	-	0.0
4.0	Flowmeter dipstick (1)	-	-	-	-	0.019
	Water take (1)	0.19	0.09	0.0	-	0.019
6.0	Flowmeter dipstick (1)	-	-	-	-	0.015
	Water take (1)	0.11	0.17	0.05	-	0.015
4.0	Flowmeter dipstick (1)	-	-	-	-	0.0
	Water take (1)	0.0	0.0	0.0	-	0.0
3.0	Flowmeter dipstick (1)	-	-	-	-	0.0
	Water take (1)	0.0	0.0	0.0	-	0.0

Depth of section 20.00 to 23.00 m. Date 15-2-88
 Bottom of casing 7.00 m. Borehole No. 6
 Init. ground water lev. 1.65 m. Packer type SINGLE
 Gauge ht above ground 0.15 m. Type of rock WEATHERED BASALT

Gauge Pressure	Time (min)	0	5	10	15	Average flow q (l/min)
3.0	Flowmeter dipstick (1)	-	-	-	-	0.0
	Water take (1)	0.0	0.0	0.0	-	0.0
4.0	Flowmeter dipstick (1)	-	-	-	-	0.0
	Water take (1)	0.0	0.0	0.0	-	0.0
6.0	Flowmeter dipstick (1)	-	-	-	-	0.0
	Water take (1)	0.11	0.0	0.0	-	0.0
4.0	Flowmeter dipstick (1)	-	-	-	-	0.0
	Water take (1)	0.0	0.0	0.0	-	0.0
3.0	Flowmeter dipstick (1)	-	-	-	-	0.0
	Water take (1)	0.0	0.0	0.0	-	0.0

PACKER (PUMPING-IN) TESTS

Packer pressure 5.0 Bars Diameter of hole 86 mm.

Depth of section 23.0 to 26.0 m Date 18-2-88
 Bottom of casing 7.0 m Borehole No. 6
 Init. ground water lev. 1.65 m Packer type SINGLE
 Gauge ht above ground 0.15 m Type of rock WEATHERED BASALT

Gauge Pressure	Time (min)	Time (min)				Average flow q (l/min)
		0	5	10	15	
3.5	Flowmeter dipstick (1)	-	-	-	-	0.0
	Water take (1)	-	0.0	0.0	0.0	0.0
4.0	Flowmeter dipstick (1)	-	-	-	-	0.005
	Water take (1)	-	0.03	0.0	0.0	0.005
6.0	Flowmeter dipstick (1)	-	-	-	-	0.013
	Water take (1)	-	0.14	0.04	0.0	0.013
4.0	Flowmeter dipstick (1)	-	-	-	-	0.0
	Water take (1)	-	0.0	0.0	0.0	0.0
3.5	Flowmeter dipstick (1)	-	-	-	-	0.0
	Water take (1)	-	0.0	0.0	0.0	0.0

Depth of section 26.0 to 28.7 m Date 19-2-88
 Bottom of casing 7.0 m Borehole No. 6
 Init. ground water lev. 1.65 m Packer type SINGLE
 Gauge ht above ground 0.15 m Type of rock WEATHERED BASALT

Gauge Pressure	Time (min)	Time (min)				Average flow q (l/min)
		0	5	10	15	
3.5	Flowmeter dipstick (1)	-	-	-	-	0.0
	Water take (1)	-	0.0	0.0	0.0	0.0
4.0	Flowmeter dipstick (1)	-	-	-	-	0.025
	Water take (1)	-	0.20	0.14	0.03	0.025
6.0	Flowmeter dipstick (1)	-	-	-	-	0.035
	Water take (1)	-	0.29	0.17	0.07	0.035
4.0	Flowmeter dipstick (1)	-	-	-	-	0.049
	Water take (1)	-	0.13	0.6	0.0	0.049
3.5	Flowmeter dipstick (1)	-	-	-	-	0.0
	Water take (1)	-	0.0	0.0	0.0	0.0

Depth of section 5.0 to 7.0 m Date 14-12-87
 Bottom of casing 4.0 m Borehole No. 7
 Init. ground water lev. 2.4 m Packer type SINGLE
 Gauge ht above ground 0.20 m Type of rock BASALT

Gauge Pressure	Time (min)	Time (min)				Average flow q (l/min)
		0	5	10	15	
1.0	Flowmeter dipstick (1)	-	-	-	-	0.0
	Water take (1)	-	0.0	0.0	0.0	0.0
1.5	Flowmeter dipstick (1)	-	-	-	-	0.0
	Water take (1)	-	0.0	0.0	0.0	0.0
2.0	Flowmeter dipstick (1)	-	-	-	-	0.0
	Water take (1)	-	0.0	0.0	0.0	0.0
1.5	Flowmeter dipstick (1)	-	-	-	-	0.0
	Water take (1)	-	0.0	0.0	0.0	0.0
1.0	Flowmeter dipstick (1)	-	-	-	-	0.003
	Water take (1)	-	0.0	0.05	0.0	0.003

PACKER (PUMPING-IN) TESTS

Packer pressure 5.0 Bars Diameter of hole 86 mm.

Depth of section 7.0 to 9.0 m Date 15-12-87
 Bottom of casing 4.0 m Borehole No. 7
 Init. ground water lev. 1.65 m Packer type SINGLE
 Gauge ht above ground 0.20 m Type of rock BASALT

Gauge Pressure	Time (min)	Time (min)				Average flow q (l/min)
		0	5	10	15	
1.5	Flowmeter dipstick (1)	-	-	-	-	0.0
	Water take (1)	-	0.0	0.0	0.0	0.0
2.0	Flowmeter dipstick (1)	-	-	-	-	0.0
	Water take (1)	-	0.0	0.0	0.0	0.0
2.5	Flowmeter dipstick (1)	-	-	-	-	0.0
	Water take (1)	-	0.0	0.0	0.0	0.0
2.0	Flowmeter dipstick (1)	-	-	-	-	0.0
	Water take (1)	-	0.0	0.0	0.0	0.0
1.5	Flowmeter dipstick (1)	-	-	-	-	0.0
	Water take (1)	-	0.0	0.0	0.0	0.0

Depth of section 9.0 to 12.0 m Date 17-12-87
 Bottom of casing 4.0 m Borehole No. 7
 Init. ground water lev. 1.65 m Packer type SINGLE
 Gauge ht above ground 0.20 m Type of rock WEATHERED BASALT / AGG.

Gauge Pressure	Time (min)	Time (min)				Average flow q (l/min)
		0	5	10	15	
1.5	Flowmeter dipstick (1)	-	-	-	-	0.0
	Water take (1)	-	0.0	0.0	0.0	0.0
2.0	Flowmeter dipstick (1)	-	-	-	-	0.0
	Water take (1)	-	0.0	0.0	0.0	0.0
2.5	Flowmeter dipstick (1)	-	-	-	-	0.0
	Water take (1)	-	0.0	0.0	0.0	0.0
2.0	Flowmeter dipstick (1)	-	-	-	-	0.0
	Water take (1)	-	0.0	0.0	0.0	0.0
1.5	Flowmeter dipstick (1)	-	-	-	-	0.0
	Water take (1)	-	0.0	0.0	0.0	0.0

Depth of section 12.0 to 14.0 m Date 18-12-87
 Bottom of casing 4.0 m Borehole No. 7
 Init. ground water lev. 5.7 m Packer type SINGLE
 Gauge ht above ground 0.20 m Type of rock AGGLOMERATES

Gauge Pressure	Time (min)	Time (min)				Average flow q (l/min)
		0	5	10	15	
2.5	Flowmeter dipstick (1)	-	-	-	-	0.0
	Water take (1)	-	0.0	0.0	0.0	0.0
3.0	Flowmeter dipstick (1)	-	-	-	-	0.0
	Water take (1)	-	0.0	0.0	0.0	0.0
4.0	Flowmeter dipstick (1)	-	-	-	-	0.213
	Water take (1)	-	2.4	0.8	0.0	0.213
3.0	Flowmeter dipstick (1)	-	-	-	-	0.0
	Water take (1)	-	0.0	0.0	0.0	0.0
2.5	Flowmeter dipstick (1)	-	-	-	-	0.0
	Water take (1)	-	0.0	0.0	0.0	0.0

PACKER (PUMPING-IN) TESTS						
Packer pressure 5.0 Bars		Diameter of hole 86 mm.				
Depth of section 14.0 to 16.0 m.		Date 18-12-87				
Bottom of casing 4.0 m.		Borehole No. 7				
Init. ground water lev. 3.30 m.		Packer type SINGLE				
Gauge ht above ground 0.20 m.		Type of rock AGGLOMERATES/RES. SOILS				
Gauge Pressure	Time (min)	0	5	10	15	Average flow q (l/min)
3.0	Flowmeter dipstick (1)	9059.6	9059.6	9059.6	9059.6	0.0
	Water take (1)	0.0	0.0	0.0	0.0	
3.5	Flowmeter dipstick (1)	9059.7	9059.7	9059.7	9059.7	0.013
	Water take (1)					
4.0	Flowmeter dipstick (1)	9060.0	9060.0	9060.0	9060.0	0.007
	Water take (1)	0.0	0.0	0.0	0.0	
3.5	Flowmeter dipstick (1)	—	—	—	—	0.0
	Water take (1)	0.0	0.0	0.0	0.0	
3.0	Flowmeter dipstick (1)	—	—	—	—	0.0
	Water take (1)	0.0	0.0	0.0	0.0	
Depth of section 16.0 to 18.0 m.		Date 21-12-87				
Bottom of casing 4.0 m.		Borehole No. 7				
Init. ground water lev. 4.20 m.		Packer type SINGLE				
Gauge ht above ground 0.20 m.		Type of rock RESIDUAL SOILS				
Gauge Pressure	Time (min)	0	5	10	15	Average flow q (l/min)
4.0	Flowmeter dipstick (1)	9063.3	9063.3	9063.3	9063.3	0.120
	Water take (1)	1.3	0.0	0.0	0.0	
6.0	Flowmeter dipstick (1)	9064.5	9064.5	9064.5	9064.5	—
	Water take (1)	2.9	0.0	0.0	0.0	
10.0	Flowmeter dipstick (1)	9065.7	9065.7	9065.7	9065.7	—
	Water take (1)	1.1	0.0	0.0	0.0	
6.0	Flowmeter dipstick (1)	9064.1	9064.1	9064.1	9064.1	0.0
	Water take (1)	0.0	0.0	0.0	0.0	
4.0	Flowmeter dipstick (1)	9063.2	9063.2	9063.2	9063.2	0.0
	Water take (1)	0.0	0.0	0.0	0.0	
Depth of section 18.0 to 20.3 m.		Date 21-12-87				
Bottom of casing 4.0 m.		Borehole No. 7				
Init. ground water lev. 4.55 m.		Packer type SINGLE				
Gauge ht above ground 0.20 m.		Type of rock RESIDUAL SOILS				
Gauge Pressure	Time (min)	0	5	10	15	Average flow q (l/min)
4.0	Flowmeter dipstick (1)	9066.6	9066.6	9066.6	9066.6	0.0
	Water take (1)	0.0	0.0	0.0	0.0	
6.0	Flowmeter dipstick (1)	9066.9	9066.9	9066.9	9066.9	0.0
	Water take (1)	0.0	0.0	0.0	0.0	
10.0	Flowmeter dipstick (1)	9068.7	9068.7	9068.7	9068.7	0.0
	Water take (1)	0.0	0.0	0.0	0.0	
6.0	Flowmeter dipstick (1)	9066.3	9066.3	9066.3	9066.3	0.0
	Water take (1)	0.0	0.0	0.0	0.0	
4.0	Flowmeter dipstick (1)	9065.4	9065.4	9065.4	9065.4	0.0
	Water take (1)	0.0	0.0	0.0	0.0	

PACKER (PUMPING-IN) TESTS						
Packer pressure 5.0 Bars		Diameter of hole 86 mm.				
Depth of section 20.3 to 23.5 m.		Date 22-12-87				
Bottom of casing 4.0 m.		Borehole No. 7				
Init. ground water lev. 6.25 m.		Packer type SINGLE				
Gauge ht above ground 0.20 m.		Type of rock WEATHERED BASALTS				
Gauge Pressure	Time (min)	0	5	10	15	Average flow q (l/min)
4.0	Flowmeter dipstick (1)	9076.5	9076.5	9076.5	9076.5	0.0
	Water take (1)	0.0	0.0	0.0	0.0	
6.0	Flowmeter dipstick (1)	9076.6	9076.6	9076.6	9076.6	0.0
	Water take (1)	0.0	0.0	0.0	0.0	
10.0	Flowmeter dipstick (1)	9076.4	9076.4	9076.4	9076.4	0.0
	Water take (1)	0.0	0.0	0.0	0.0	
6.0	Flowmeter dipstick (1)	9074.5	9074.5	9074.5	9074.5	0.0
	Water take (1)	0.0	0.0	0.0	0.0	
4.0	Flowmeter dipstick (1)	9074.2	9074.2	9074.2	9074.2	0.0
	Water take (1)	0.0	0.0	0.0	0.0	
Depth of section 23.5 to 26.5 m.		Date 5-1-88				
Bottom of casing 4.0 m.		Borehole No. 7				
Init. ground water lev. 8.26 m.		Packer type SINGLE				
Gauge ht above ground 0.20 m.		Type of rock WEATHERED BASALT				
Gauge Pressure	Time (min)	0	5	10	15	Average flow q (l/min)
3.0	Flowmeter dipstick (1)	9076.4	9076.4	9076.4	9076.4	0.033
	Water take (1)	0.0	0.0	0.0	0.0	
4.0	Flowmeter dipstick (1)	9077.1	9077.1	9077.1	9077.1	0.027
	Water take (1)	0.0	0.0	0.0	0.0	
6.0	Flowmeter dipstick (1)	9077.9	9077.9	9077.9	9077.9	0.020
	Water take (1)	0.0	0.0	0.0	0.0	
4.0	Flowmeter dipstick (1)	9078.4	9078.4	9078.4	9078.4	0.0
	Water take (1)	0.0	0.0	0.0	0.0	
3.0	Flowmeter dipstick (1)	9077.2	9077.2	9077.2	9077.2	0.0
	Water take (1)	0.0	0.0	0.0	0.0	
Depth of section 26.5 to 29.5 m.		Date 7-1-88				
Bottom of casing 4.0 m.		Borehole No. 7				
Init. ground water lev. 3.74 m.		Packer type SINGLE				
Gauge ht above ground 0.20 m.		Type of rock WEATHERED BASALTS				
Gauge Pressure	Time (min)	0	5	10	15	Average flow q (l/min)
4.0	Flowmeter dipstick (1)	9076.3	9076.3	9076.3	9076.3	0.0
	Water take (1)	0.0	0.0	0.0	0.0	
6.0	Flowmeter dipstick (1)	9076.7	9076.7	9076.7	9076.7	0.04
	Water take (1)	0.0	0.0	0.0	0.0	
10.0	Flowmeter dipstick (1)	9076.5	9076.5	9076.5	9076.5	0.03
	Water take (1)	0.0	0.0	0.0	0.0	
6.0	Flowmeter dipstick (1)	9072.4	9072.4	9072.4	9072.4	0.0
	Water take (1)	0.0	0.0	0.0	0.0	
4.0	Flowmeter dipstick (1)	9072.4	9072.4	9072.4	9072.4	0.0
	Water take (1)	0.0	0.0	0.0	0.0	

WEATHERING GRADES

APPENDIX D

WEATHERING GRADES

HIGHLY WEATHERED - (H.W): More than half of the rock material is decomposed or disintegrated to a soil. Fresh or discolored rock is present either as a discontinuous framework or as concretions.

COMPLETELY WEATHERED - If all rock material is decomposed and/or disintegrated to soil, the original mass structure is still largely intact.

RESIDUAL SOIL - If all rock material is converted to soil. The mass structure and material fabric are destroyed. There is large change in volume, and the soil has not been transported significantly.

APPENDIX D

WEATHERING GRADES

- FRESH - (F): No visible signs of weathering.
- SLIGHTLY WEATHERED - (SF): Discolouration indicating weathering of rock material and discontinuity surfaces. The rock surfaces are discoloured by weathering and are some what weaker than in its fresh condition.
- MODERATELY WEATHERED - (M.W.): Less than half of the rock material is decomposed to soil-fresh or discoloured rock is present either as a continuous framework or as corestones.
- HIGHLY WEATHERED - (H.W): More than half of the rock material is decomposed or disintegrated to a soil. Fresh or discoloured rock is present either as a dis-continuous framework or as corestones.
- COMPLETELY WEATHERED - (C.W): All rock material is decomposed and/or disintegrated to soil. The original mass structure is still largely intact.
- RESIDUAL SOILS - (R.S): All rock material is converted to soil. The mass structure and material fabric are destroyed. There is large change in volume, but the soil has not been transported (autochtony).